DISSERTATION

Impact of Interferon-γ on neocortical inhibition

Der Einfluss von Interferon-γ auf die Inhibition im Neocortex

zur Erlangung des akademischen Grades
Medical Doctor - Doctor of Philosophy (MD/PhD)

vorgelegt der Medizinischen Fakultät
Charité – Universitätsmedizin Berlin

von

Gabriel Martin Salvator Janach

Erstbetreuer: Prof. Dr. med. Ulf Strauß
Datum der Promotion: 29. November 2024

Table of contents

List of tables iii

List of figures iv

Abbreviations v

Abstract vi

1 Introduction 10

1.1 IFN-γ - a multifaceted cytokine 10

1.2 IFN-γ and CNS function 11

1.3 Effects of type I and II IFNs on neocortical I_h and excitability 11

1.4 Research question 13

2 Materials and Methods 14

2.1 Interferon and kinase blockers 14

2.2 Animals and slice preparation 14

2.3 Electrophysiological data acquisition 15

2.4 Evoked, spontaneous, and miniature IPSCs 16

2.5 Pressure application of GABA 17

2.6 Paired pulse recordings 18

2.7 Peak-scaled non-stationary noise analysis 19

2.8 Single channel recordings and $GABA_A$ receptor driving force 21

2.9 Statistical analysis 21

3 Synopsis of Major Results 23

3.1 IFN-γ increases IPSC amplitudes in late juvenile rats 23

3.2 IFN-γ increases sIPSC amplitudes in adult rats 25

3.3 IFN-γ increases mIPSC amplitudes in female rats 26

3.4 IFN-γ selectively impacts inhibitory transmission via a postsynaptic mechanism 27

3.5 IFN-γ increases postsynaptic $GABA_AR$ number 29

3.6 The IFN-γ related increase in mIPSC amplitudes is PKC-dependent 31

3.7 IFN-γ leaves $GABA_AR$ single channel conductance unchanged 33
3.8 IFN-γ does not affect chloride homeostasis under resting conditions 35
4 Discussion 38
4.1 Summary of results 38
4.2 Intracellular signaling and isoform specificity 39
4.3 IFN-γ, PKC activation and altered inhibition due to changes in synaptic $GABA_AR$ quantity in the context of health and disease 40
4.3.1 Sickness behavior 40
4.3.2 Epilepsy 40
4.3.3 Depression 41
4.4 Pharmacological implications 41
4.5 Future directions 42
4.6 Strengths and limitations 43
5 Conclusion 44
6 References 45
7 Statutory Declaration 54
8 Declaration of Contribution 55
9 Printing Copy of Publication 1 56
10 Printing Copy of Publication 2 69
11 Curriculum Vitae 85
12 Complete List of Publications 86
13 Acknowledgements 87

List of tables

Table 1: Composition of bath and pipette solutions. 22
Table 2: Synopsis of major results.....37

List of figures

Figure 1: Type I and II IFNs overlap in I_h attenuation but differ in their effects on excitability. 12
Figure 2: Current responses to pressure applied GABA of two layer 5 pyramidal neurons under different experimental conditions. 18
Figure 3: Exemplary relations between parameters from mIPSCs used in peak-scaled NSNA. 20
Figure 4: Single channel current disappearance over time. 21
Figure 5: IFN-γ increases the amplitude of evoked IPSCs in neocortical layer 5 pyramidal neurons 23
Figure 6: IFN-γ increases the amplitude of spontaneous IPSCs in neocortical layer 5 pyramidal neurons of late juvenile rats. 24
Figure 7: IFN-γ increases mIPSC amplitude in neocortical layer 5 neurons. 25
Figure 8: IFN-γ increases the amplitude of spontaneous IPSCs in neocortical layer 5 pyramidal neurons of adult rats. 26
Figure 9: Acute application of IFN-γ augments mIPSC amplitudes in layer 5 pyramidal neurons of female rats. 27
Figure 10: IFN-γ acutely increases postsynaptic GABAergic current responses in neocortical layer 5 pyramidal neurons without impacting presynaptic properties. 28
Figure 11: IFN-γ acutely increases plasma membrane localization and postsynaptic number of $GABA_AR$s without affecting synaptic $GABA_AR$ conductance. 30
Figure 12: Increase of inhibition upon acute application of IFN-γ depends on PKC mediated $GABA_AR$ phosphorylation. 32
Figure 13: $GABA_AR$ single channel conductance is comparable with and without IFN-γ in neocortical layer 5 pyramidal neurons. 34
Figure 14: Acute application of IFN-γ does not alter $[Cl^-]_i$ or DF_{GABA} in neocortical layer 5 pyramidal neurons. 36

Abbreviations

ACSF ..... artificial cerebrospinal fluid
Akt ..... protein kinase B
Cl^- ..... chloride
CNQX 6-cyano-7-nitroquinoxaline-2,3-dione
CNS ..... central nervous system
CSF ..... cerebrospinal fluid
DAP-5 ..... D-(-)-2-amino-5-phosphonopentanoic acid
$DF_{GABA(A)}$ ..... $GABA_A$ receptor driving force
E/I balance ..... excitation-inhibition balance
E_{Cl-} ..... chloride reversal potential
eIPSC ..... evoked inhibitory postsynaptic current
E_{rev} ..... reversal potential
F-I slope ..... slope of frequency current relationship
FLIM ..... fluorescence lifetime imaging microscopy
GABA ..... gamma-aminobutyric acid, gamma-aminobutyric acid
$GABA_AR$ ..... $GABA_A$ receptor
IFN ..... interferon
I_h ..... hyperpolarization-activated current
KCC2 ..... chloride potassium symporter 5
MHC ..... major histocompatibility complex
mIPSC ..... miniature inhibitory postsynaptic current
MQAE ..... N-(Ethoxycarbonylmethyl)-6-methoxyquinolinium bromide
NSNA ..... non-stationary noise analysis
P ..... postnatal day
PI3K ..... phosphatidylinositol 3-kinases
PKC ..... protein kinase C
PPR ..... paired pulse ratio
PSC ..... postsynaptic current
R_s ..... series resistance
sACSF ..... high sucrose artificial cerebrospinal fluid
sIPSC ..... spontaneous inhibitory postsynaptic current
STAT1 ..... signal transducer and activator of transcription 1
TTX ..... tetrodotoxin
V_{hold} ..... command voltage in whole-cell recordings
V_{mem} ..... membrane voltage
V_p ..... command voltage in cell-attached recordings

Abstract

IFN-γ is a pro-inflammatory cytokine with wide-ranging properties from host defense and suppression of tumor growth to alteration of brain function. While low levels of IFN-γ in the CNS are essential for normal social behavior, many CNS diseases including infection, epilepsy, stroke and depression go along with elevated levels of IFN-γ. In addition, therapeutically applied recombinant IFN-γ leads to frequent CNS related adverse effects as headache and fatigue and IFN-γ rises in infectious disease have been associated to sickness behavior.

Previous studies on neocortical pyramidal neurons demonstrated corresponding effects of type I IFNs and IFN-γ upon the hyperpolarization activated cation current I_h but deviating effects upon neuronal excitability. Therefore, we here investigated whether acutely (20 - 45 min) elevated levels of IFN-γ (1.000 IU ml^{-1}) alter perisomatic inhibition in layer 5 pyramidal neurons in the primary somatosensory neocortex of late juvenile male Wistar rats.

By analysis of evoked, spontaneous, and miniature inhibitory postsynaptic currents, we revealed that elevated levels of IFN-γ indeed augment neocortical inhibition. The strengthening of inhibition is mediated at the postsynapse, as supported by unaltered paired pulse ratios and increased inhibitory postsynaptic current amplitudes in response to pressure applied GABA.

We found that the underlying mechanism of effect encloses a markable increase in synaptic $GABA_AR$ number, as demonstrated by peak-scaled non-stationary noise analysis of mIPSCs and $GABA_AR$ γ_2 subunit biotinylation. Changes in $GABA_AR$ single channel properties or decreased intracellular chloride levels unlikely contributed to the observed IFN-γ effect, since we could not find alterations in single channel currents of $GABA_ARs$ recorded in cell-attached mode, $GABA_AR$ driving force and in fluorescence lifetime imaging of intracellular chloride.

The pro-inhibitory effect of IFN-γ depends on functional protein kinase C (PKC), but not phosphoinositide 3-kinases, as shown by blocker experiments using Wortmannin and Calphostin C and increased serine phosphorylation of PKC motifs at $GABA_AR$ γ_2 subunits. The persistence of augmented inhibition due to acutely elevated IFN-γ in female and adult rats indicates that the effect is not sex dependent or restricted to late juvenile age.

Our results provide a molecular basis for further research on behavioral effects of pronounced IFN-γ release and its underlying mechanisms. Moreover, they can contribute

to the pathophysiological understanding of numerous CNS diseases and provide a link to future research on novel therapeutical approaches.

Zusammenfassung

IFN-γ ist ein proinflammatorisches Zytokin, das nicht nur der Wirtsabwehr und der endogenen Tumorkontrolle dient, sondern auch die Gehirnfunktion beeinflusst.
Während niedrige IFN-γ-Spiegel im ZNS essenziell für normales Sozialverhalten sind, gehen ZNS-Erkrankungen wie Infektionen, Epilepsie, Schlaganfall und Depression mit erhöhten IFN-γ-Spiegeln einher. Darüber hinaus führt die Therapie mit rekombinantem IFN-γ häufig zu ZNS-bezogenen Nebenwirkungen wie Kopfschmerzen und Müdigkeit, und IFN-γ-Anstiege im Rahmen von Infektionen wurden mit *sickness behavior* assoziiert.
Frühere Studien an neokortikalen Pyramidenzellen haben gezeigt, dass Typ-I-Interferone und IFN-γ den durch Hyperpolarisation aktivierten Kationenstrom I_h gleichsam reduzieren, dass aber ihre Auswirkungen auf die neuronale Erregbarkeit voneinander abweichen. Daran anknüpfend haben wir untersucht, ob kurzfristig (20 - 45 min) erhöhte IFN-γ-Spiegel (1.000 IU ml^{-1}), die Inhibition von Pyramidenzellen der Schicht 5 im primären somatosensorischen Neokortex von spät juvenilen männlichen Wistar-Ratten verändern.
Durch Analyse von elektrisch evozierten sowie spontanen und miniatur inhibitorischen postsynaptischen Strömen (e/s/m IPSCs) zeigten wir, dass erhöhte IFN-γ-Spiegel zu einer Verstärkung der Inhibition führen. Diese Verstärkung wird, entsprechend unveränderten *paired pulse ratios* und einem Amplitudenanstieg von IPSCs nach Präsynapsen-unabhängiger GABA-Applikation, über die Postsynapse vermittelt.
Der zugrundeliegende Wirkmechanismus beinhaltet einen deutlichen Anstieg der synaptischen $GABA_A$-Rezeptoranzahl. Dies konnten wir mittels *peak-scaled* nicht-stationärer Noiseanalyse von mIPSCs und der Biotinylierung von $GABA_AR$ γ2 Untereinheiten zeigen. Veränderungen der $GABA_AR$-Einzelkanaleigenschaften oder verringerte intrazelluläre Chloridspiegel trugen wahrscheinlich nicht zu der beobachteten IFN-γ-Wirkung bei, da wir keine Veränderungen der *cell-attached* aufgenommenen $GABA_AR$-Einzelkanalströme, der $GABA_AR$ *driving force* und in der Fluoreszenzlebensdauer-Mikroskopie von intrazellulärem Chlorid feststellen konnten.
Der pro-inhibitorische Effekt von IFN-γ hängt von einer funktionierenden Proteinkinase C (PKC), nicht aber Phosphoinositid-3-Kinasen ab, wie Blockerexperimente mit Wortmannin und Calphostin C sowie ein Anstieg der Serinphosphorylierungen von PKC-Motiven an $GABA_AR$ γ_2 Untereinheiten zeigten. Die Tatsache, dass die neokortikale Inhibition auch bei weiblichen und erwachsenen Ratten verstärkt wird, weist darauf hin,

dass der Effekt nicht geschlechtsabhängig oder auf das spät juvenile Alter beschränkt ist. Unsere Ergebnisse bieten eine molekulare Grundlage für die weitere Erforschung verhaltensverändernder IFN-γ-Wirkungen und ihrer zugrundeliegenden Mechanismen. Darüber hinaus können sie beim Verständnis der Pathophysiologie zahlreicher ZNS-Erkrankungen helfen und einen Anknüpfungspunkt für die zukünftige Erforschung neuer Therapieansätze bieten.

1 Introduction

1.1 IFN-γ - a multifaceted cytokine

IFN-γ, the only type II interferon, is commonly known as a pro-inflammatory cytokine involved in host defense. IFN-γ is primarily produced and secreted by natural killer cells, e.g. after pattern recognition receptor activation or binding of other cytokines, and T lymphocytes in response to specific pathogen recognition via T cell receptors (Ivashkiv, 2018). However, IFN-γ is also produced by resident CNS cells such as neurons, astrocytes, cerebral endothelial cells and microglia following different stimuli as traumatic injury or ageing (*reviewed in* Monteiro et al., 2017), suggestive of functions beyond pathogen defense.

After binding of IFN-γ homodimers to ubiquitously present (Bach et al., 1997) IFN-γ receptors, different signaling pathways can be activated. Whereas in the classical pathway, Janus kinase activity results in homodimerization of STAT1 and consecutive initiation of transcription (Gough et al., 2008), numerous alternative pathways exist. Alternative pathways include activation of PI3K, different isoforms of PKC and Akt (Gough et al., 2008; Green et al., 2017), putatively allowing for a more rapid modulation of cellular functions.

The consequences of IFN-γ receptor activation do not only comprise increased expression of chemokines, MHC-molecules and anti-pathogenic factors, long-lasting activation of macrophages, T cell response modulation and B cell class switch, but also suppression of tumor cell proliferation, regulation of autoinflammation and prolonged or transient alteration of CNS function (Monteiro et al., 2017; Ivashkiv, 2018).
To date, the origin of IFN-γ in the CNS has not been solved conclusively. While it has been shown that IFN-γ can be directly released by parenchymal CNS cells under various conditions (Monteiro et al., 2017) and that meningeal T-cells are able to express IFN-γ (Filiano et al., 2016), IFN-γ and/or IFN-γ producing immune cells may also enter the CNS from the periphery. Possible routes for this scenario include transit of peripheral immune cells or IFN-γ via the blood-brain or the blood-CSF barrier as well as passage via circumventricular organs (Clark et al., 2022). Access of peripheral IFN-γ via circumventricular organs seems particularly likely as it has been shown that an

intravenously administered protein with similar molecular weight as IFN-γ homodimers can enter the brain through the median eminence (Broadwell et al., 1983; Clark et al., 2022). However, it remains unclear under which conditions and to which extent baseline and elevated CNS IFN-γ levels, e.g. after CNS infection (Frei et al., 1988), neurotrauma (Lau and Yu, 2001) or stroke (Li et al., 2001), can be assigned to different sources.

1.2 IFN-γ and CNS function

Increased CNS levels of IFN-γ in non-infectious conditions (Monteiro et al., 2017), CNS related side effects - e.g. headaches and fatigue - in response to therapeutically applied IFN-γ (Miller et al., 2009) and a link between IFN-γ and sickness behavior (Kirsten et al., 2020) suggest a neuromodulatory role beyond its immunogenic properties. While the consequences of elevated IFN-γ in acute neurological conditions as stroke and neurotrauma are unclear, temporarily increased IFN-γ in meningitis leads to long-term behavioral changes (Too et al., 2014). Further, IFN-γ has been shown to account for depressive-like behavior after infection with Bacillus Calmette-Guérin (O'Connor et al., 2009) and intrathecal application of IFN-γ leads to anxiety- and depressive-like demeanor (Mandolesi et al., 2017).
On the contrary, maintenance of basal IFN-γ levels is pivotal for normal social behavior in mice (Filiano et al., 2016), implying an important role in mammalian brain function that may be negatively affected by acutely increased IFN-γ levels.

1.3 Effects of type I and II IFNs on neocortical I_h and excitability

Before my research, acute neuromodulatory effects of type I IFNs that are likewise important immunoregulatory cytokines, have been studied with a focus on IFN-β. Similarly to IFN-γ, type I IFNs have been linked to sickness behavior (Dantzer et al., 2008) and provoke CNS-related adverse effects when used as therapeutics (e.g. IFN-α in hairy cell leukemia or IFN-β in multiple sclerosis) (Bayas and Rieckmann, 2000; Tayal and Kalra, 2008). In detail, IFN-β is a type I interferon that acts via a different receptor complex and is - in contrast to IFN-γ - considered as an anti-inflammatory cytokine, but overlaps in signaling properties with IFN-γ (Chow and Gale, 2015; McNab et al., 2015). When directly applied to *ex vivo* rat brain slices, high levels (1.000 IU ml^{-1}) of IFN-β have been shown to acutely alter sub- and supra-threshold excitability of neocortical pyramidal neurons (Hadjilambreva et al., 2005; Reetz et al., 2014). Furthermore, IFN-α as well as IFN-β led

to attenuation of I_h (Stadler et al., 2014) that is involved in shaping of neuronal networks and modulation of synaptic transmission (Wahl-Schott and Biel, 2009). To decipher whether IFN-γ affects neocortical pyramidal neurons in a similar way, corresponding experiments were performed with IFN-γ. Interestingly, the same concentration of IFN-γ led to corresponding effects on I_h in neocortical layer 5 pyramidal neurons, but left sub- (according to steady input resistance) and supra-threshold excitability (according to steady F-I slope and rheobase values) unchanged (Janach et al., 2020).

Thus, likewise attenuation of I_h (Fig. 1A/B) suggested functional cross-talk between type I and type II IFNs, while the absence of sub- and supra-threshold (Fig. 1C/D) excitability changes pointed towards a deviation in the neuromodulatory effects of IFN-γ.

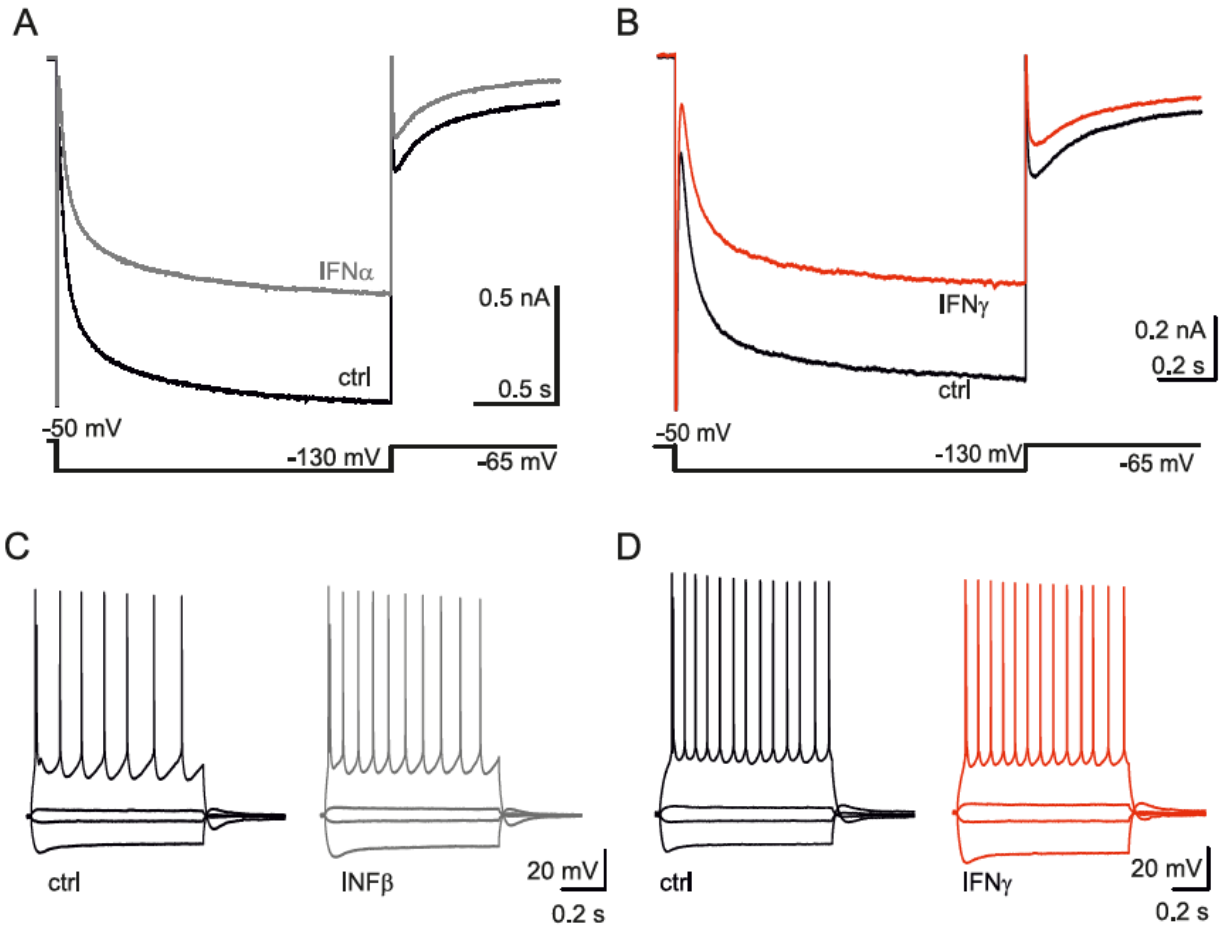

Figure 1: Type I and II IFNs overlap in I_h attenuation but differ in their effects on excitability. **A/B**: Exemplary recordings of offline leak subtracted I_h in response to the voltage steps displayed beyond the current traces under the influence of IFN-α (a type I IFN) and IFN-γ. Both, type I and type II IFNs led to attenuation of maximum I_h amplitude (Stadler et al., 2014; Janach et al., 2020). Note, that while the example in A was recorded under the influence of IFN-α, likewise attenuation occurred under the influence of IFN-β (Stadler et al., 2014). **C/D**: Exemplary recordings of voltage

responses to rectangular current injections of -300, -50, 50 and 450 pA (C) or -300, -50, 50 and 250 pA (D) before and after the application of IFN-β and IFN-γ respectively. While the type I IFN IFN-β led to an increase in supra-threshold excitability illustrated by a comparatively increased action potential frequency in response to the same current injection (C) and increased sub-threshold excitability according to increased input resistance (not displayed here) (Hadjilambreva et al., 2005; Reetz et al., 2014), these effects remained absent under the influence of IFN-γ (D) (measurement of input resistance not shown). All recordings shown were performed in layer 5 pyramidal neurons of the primary somatosensory rat neocortex. Figure compiled for this thesis by: Gabriel Janach. A was adapted from (Stadler et al., 2014), Fig. 2A; B and D were adapted from (Janach et al., 2020), Fig. 3A and 2A respectively; C was adapted from (Reetz et al., 2014), Fig. 2G.

1.4 Research question

To better understand the effect of elevated IFN-γ in the CNS and potentially counteract adverse effects of recombinant IFN-γ as well as behavioral alterations after infection and neuroinflammation, a detailed understanding of IFN-γ effects on CNS function is necessary. In my studies, I focused upon acute effects of IFN-γ, as this putatively parallels the rise in CNS infection or after therapeutic application of IFN-γ and cerebral increase of IFN-γ levels seems to alter behavior with a relatively fast time-course of < 12 h (Mandolesi et al., 2017). These observations are in line with previous reports on rapid neuromodulation by type I IFNs that intersect with IFN-γ signaling and CNS effects (see section 1.3) on a single cell (Hadjilambreva et al., 2005; Reetz et al., 2014; Stadler et al., 2014) and network level (Stadler et al., 2014). Furthermore, the investigation of relatively short-term effects allows for untangling IFN-γ effects from that of other, consecutively released cytokines (e.g. TNF-α or IL-6) (Boehm et al., 1997; Ivashkiv, 2018). At the beginning of my research work, the overlap in I_h attenuation conditional upon type I IFNs or IFN-γ and the lack of excitability changes after the application of IFN-γ (Fig. 1 and section 1.3) gave rise to the assumption that IFN-γ increases neuronal inhibition and therewith prevents the excitability changes following type I IFN elevation. This hypothesis was reinforced by pilot experiments on action potential independent inhibitory postsynaptic currents (mIPSCs) from Olivia Reetz that revealed an amplitude increase after acute application of IFN-γ (Janach et al., 2020). Therefore, I concentrated on the question whether IFN-γ does indeed alter inhibitory neurotransmission in the neocortex and if so, what the underlying mechanisms of action are.

2 Materials and Methods

This chapter comprises extended information on materials and the relevant methods I used. Information on techniques that were exclusively used by co-authors can be found in the corresponding sections of the attached publications. According to the Charité requirements for good scientific practice, I am citing the underlying publications (Janach et al., 2020; Janach et al., 2022) also in the corresponding subsections. Information on equipment, programs and manufacturers/suppliers is solely provided in the attached publications and not restated in this thesis.

2.1 Interferon and kinase blockers

I used Chinese hamster ovary or Escherichia coli derived recombinant IFN-γ at a final concentration of 1.000 IU ml^{-1} in all experiments involving IFN-γ. This concentration is in the range of what has been observed in the CSF after viral meningitis (Frei et al., 1988). Further, in previous experiments on IFN-β, 1.000 IU ml^{-1} (applied for 30 min) showed maximum effects on membrane characteristics of neocortical pyramidal neurons (Hadjilambreva et al., 2005). Following reconstitution in sterile double-distilled water, I stored aliquots of 100.000 IU IFN-γ at –20°C and added it to the ACSF prior to individual experiments (Janach et al., 2020; Janach et al., 2022).

Whereas in my longitudinal experiments the application period of IFN-γ ranged from 20 - 45 min (Janach et al., 2020; Janach et al., 2022), it ranged from 15 - 60 min in cell-attached recordings of preincubated neurons (Janach et al., 2022).

I diluted the PI3K inhibitor Wortmannin and the PKC inhibitor Calphostin C in dimethyl sulfoxide and applied them at a final concentration of 100 nM each (Janach et al., 2020; Janach et al., 2022).

During the experiments involving Wortmannin I ensured protection from light due to its light sensitivity. In Calphostin C experiments, I exposed the diluted Calphostin C to ordinary white light during pre-incubation and bath application, because inhibition of PKC by Calphostin C is light-dependent (Bruns et al., 1991).

2.2 Animals and slice preparation

We obtained male and female specific pathogen-free (SPF) Wistar rats from Janvier labs or from the Charité central animal facility and performed all procedures in agreement with

the European Communities Council Directive of September 22nd, 2010 (2010/63/EU) under the licenses T 0212/14 and T-CH 0034/20 (Janach et al., 2020; Janach et al., 2022). I prepared acute 300 - 400 µm thick (for immunohistochemistry and fluorescence-lifetime imaging a slice thickness of 50 or 250 µm was used respectively) coronal brain slices containing primary somatosensory cortex (S1) from postnatal day (P) 10 - 84 rats as described in (Janach et al., 2022, section 2.2). Notably, I carried out most experiments on brain slices from rats P21 (average age for each series stated below figures in according publications) or older, rendering an impact of undeveloped GABAergic transmission less likely (Miller, 1988; Del Rio et al., 1992; Le Magueresse and Monyer, 2013). In brief, I rapidly removed the brain after isoflurane anesthesia and decapitation and cut in 2°C carbogenated (i.e. enriched with 95% O_2 and 5% CO_2 to assure constant oxygenation of brain slices and maintain pH balance) sACSF (Table 1) using a vibratome. To recover, I stored the slices for 30 min in 33 ± 1 °C sACSF, then kept them at room temperature in a holding solution containing 2-[4-(2-hydroxyethyl)piperazin-1-yl]ethanesulfonic acid (20 mM) (Table 1) to prevent tissue swelling and increase pH buffering capacity (MacGregor et al., 2001). I performed electrophysiological experiments after ≥ 30 min storage in the holding solution.

2.3 Electrophysiological data acquisition

I performed patch clamp recordings on layer 5 pyramidal neurons in the primary somotasosensory cortex (S1). After transfer to the recording chamber, I constantly perfused the slices with carbogenated 32 ± 2°C ACSF (Table 1) as described in (Janach et al., 2020; Janach et al., 2022, section 2.3).

Besides cell selection due to location (S1, layer 5) and typical morphology (pyramidal shape and apical dendrite) as visualized by infrared differential interference contrast video microscopy, we further characterized a subset of neurons by responses to current injections and *post hoc* visualization (examples displayed in Janach et al., 2022, Fig. S2). In whole-cell experiments, selection of layer 5 pyramidal cells was corroborated by relatively high capacitance values (mean capacitance 196.2 ± 12.4 pF, n = 101), determined in response to square voltage pulses (20 ms, 10 mV) (Janach et al., 2020; Janach et al., 2022). The membrane capacitance corresponds with the (clamped) membrane surface of studied neurons and typically shows higher values in comparison to interneurons and layer 2/3 pyramidal neurons.

In most whole-cell experiments, I tolerated a change ≤ 25 % in series resistance (R_s). Besides the pipette resistance, R_s encloses the access resistance between the pipette and the cell membrane, being affected by e.g. moving organelles that may clog parts of the pipette tip, flapping cell membrane or leak current. Accordingly, the accuracy of voltage clamp is affected by R_s changes, leading to seemingly altered transmembrane current amplitudes. Therefore, it is important to keep R_s relatively stable in paired long-term experiments when measuring postsynaptic current (PSC) amplitudes. The relative stability (ΔR_s ≤ 25 %) of my individual recordings was corroborated by comparable R_s values in all experimental series analyzed for mean PSC amplitudes (Janach et al., 2020; Janach et al., 2022). During the patch clamp experiments for (Janach et al., 2022) I switched from lead glass pipettes to borosilicate glass pipettes (Janach et al., 2022), as personal experience revealed tighter seals and more stable R_s values when using borosilicate glass. I gathered R_s values from current responses to square voltage pulses (20 ms, 3 or 10 mV) (Janach et al., 2020; Janach et al., 2022). In case of mIPSC recordings for peak-scaled non-stationary noise analysis (NSNA), I tolerated only a 10 % R_s change (Janach et al., 2022), because R_s alterations may lead to inaccurate channel number estimations (Heinemann and Conti, 1992). Further details on data acquisition can be found in the according publications (Janach et al., 2020; Janach et al., 2022, section 2.3).

2.4 Evoked, spontaneous, and miniature IPSCs

Recording of evoked, spontaneous, and miniature IPSCs permits analysis of current amplitudes and - in the case of s/mIPSCs - event frequency. While eIPSCs evoked by electrical stimulation result in presynaptic vesicle release from interneuronal axons, sIPSCs and mIPSCs are part of spontaneous network activity. sIPSCs originate from either action potential dependent or action potential independent spontaneous presynaptic vesicle release, whereas mIPSCs are exclusively due to action potential independent presynaptic vesicle release.

For the recording of e/s/mIPSCs I blocked ionotropic glutamate receptors via 10 - 20 µM 6-cyano-7-nitroquinoxaline-2,3-dione (CNQX) and 25 µM D-(-)-2-amino-5-phosphonopentanoic acid (DAP-5) (Janach et al., 2020) to minimize interference with excitatory transmission. In addition, I blocked voltage-sensitive sodium channels using

1µM tetrodotoxin (TTX) in the case of mIPSCs to prevent action potential propagation (Janach et al., 2022).

For details regarding the recording and analysis of IPSCs, refer to materials and methods sections of the according publications (Janach et al., 2020; Janach et al., 2022, section 2.9). Composition of the pipette solutions used is given in Table 1.

Note that the increase in electrochemical chloride driving force due to 10 mV more negative V_{hold} and 12 mM more Cl^- in the pipette solution, as well as the blockage of shunting potassium currents via cesium in (Janach et al., 2022) compared to (Janach et al., 2020) may explain the difference in averaged mIPSC amplitude values between the publications. I made these changes in (Janach et al., 2022) to enhance mIPSC quality and increase mIPSC amplitudes for peak-scaled NSNA.

2.5 Pressure application of GABA

Direct pressure application of neurotransmitters evokes postsynaptic currents that are independent of presynaptic vesicle release. Therefore, contribution of the postsynapse to a change in e/s/mIPSC amplitudes can be investigated discretely.

For pressure ejection experiments, I locally applied GABA diluted in ACSF. I tested different GABA concentrations, electrolyte configurations and command voltages to accomplish consistent responses that are large enough for precise analysis of current amplitudes but still enable a reasonable clamp (examples shown in Fig. 2) with the result of 100 µM GABA, 50 mM intracellular Cl^- and a command voltage of –70 mV. During the process of establishing the pressure ejection method I experimented with a variety of pipette tip diameters to achieve an ideal balance between infrequent clogging of the pipette and negligible tissue swelling. The resulting tip of the ejection pipette had an approximate resistance of 0.5 MΩ when the pipette was filled with ACSF. After positioning the pipette tip 5 - 10 µm from the soma, I kept pressure and duration of application constant during individual experiments. I monitored tissue swelling and pipette positioning visually and discontinued experiments in case of alterations (Janach et al., 2022). Composition of the pipette solution used can be found in Table 1.

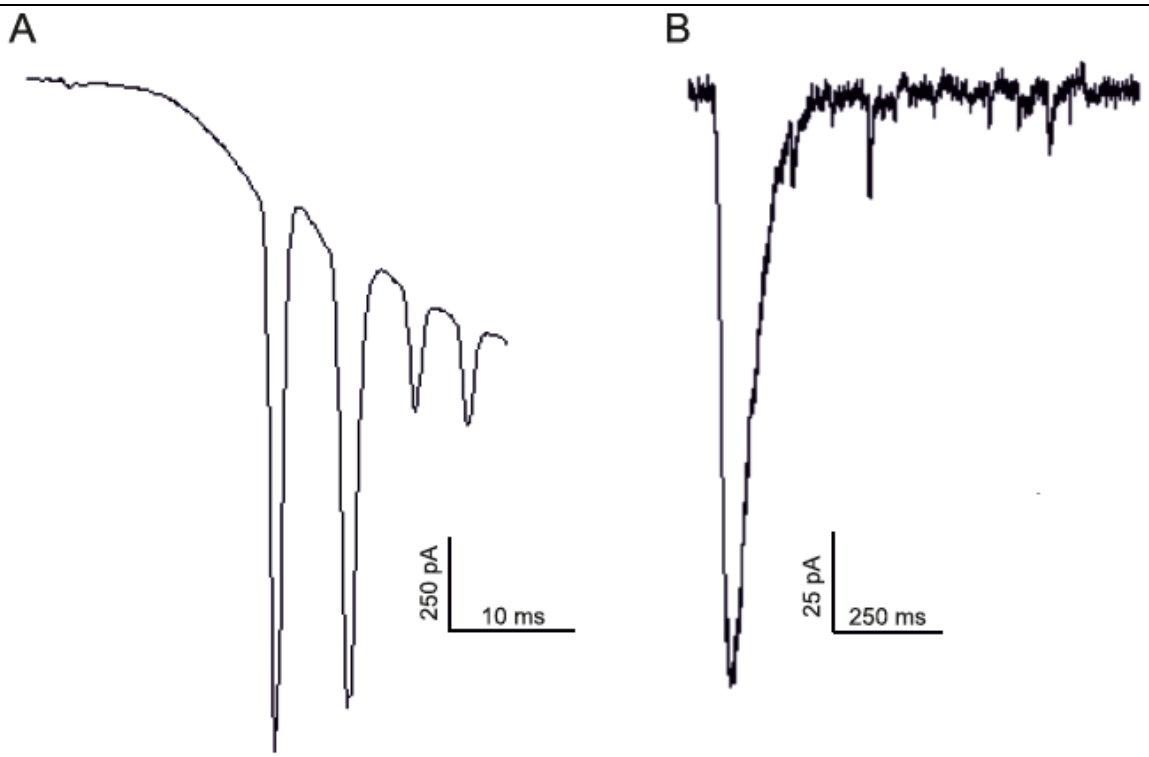

Figure 2: Current responses to pressure applied GABA of two layer 5 pyramidal neurons under different experimental conditions.

A: Response to pressure application of 1 mM GABA, equimolar intra- and extracellular chloride concentration (chloride reversal potential, E_{Cl-} ~ 0 mV) and command voltage of –60 mV. In this example the membrane voltage most likely depolarized to a value beyond action potential threshold due to unclamped ionic currents. **B**: Response to pressure application of 100 µM GABA, 50 mM intracellular Cl^- (E_{Cl-} ~ –25 mV) at a command voltage of –70 mV. Here, I reduced the concentration of GABA and the concentration gradient of Cl^- to decrease the amplitude of Cl^- currents. Further, I increased the difference between command voltage and action potential threshold to lower the probability of action potential generation. For both exemplary recordings I applied GABA in ACSF for 3 ms with 0.3 bar pressure. Note that current is inwardly directed (corresponding to an outflow of negatively charged Cl^- ions from the cytosol) because electrolyte configurations result in an E_{Cl-} that is more depolarized than the command voltage. Under physiological conditions E_{Cl-} is roughly equivalent to or more hyperpolarized than resting membrane voltage of developed neurons, resulting in shunting inhibition or hyperpolarization when $GABA_A$Rs open. Figure compiled for this thesis on the basis of my term report in module 23 (‘Wissenschaftliches Arbeiten’, sixth semester).

2.6 Paired pulse recordings

For paired pulse experiments, I evoked two consecutive eIPSCs with a frequency of 10 (inter-stimulus interval = 100 ms) or 20 Hz (inter-stimulus interval = 50 ms) and calculated

the paired pulse ratio (PPR) as amplitude of second eIPSC divided by amplitude of first eIPSC. The reference point for current measurement was the holding current prior to the eIPSC stimulation artifact (Janach et al., 2022). When comparing the two conditions (control *vs.* application of IFN-γ) I averaged 20 consecutive PPRs respectively. Changes in PPR may indicate alterations in presynaptic properties including release probability of presynaptic vesicles, local presynaptic calcium concentration and the size of the readily releasable pool (Regehr, 2012). I chose an interval of 10 s between individual paired pulse stimuli, as neither IPSC amplitude rundown nor PPR alterations were observed previously at this frequency in rat visual cortex (Imbrosci et al., 2013). Note that in this experimental series, R_s significantly increased from $R_{s\text{-}ctrl}$ = 11.1 ± 0.1 MΩ to $R_{s\text{-}IFN\text{-}\gamma}$ = 13 ± 0.1 MΩ (Janach et al., 2022). However, changes in R_s should not affect the ratio of consecutively evoked current responses. Further details on recording of paired pulse responses can be found in (Janach et al., 2022, section 2.5), whereas the pipette solution used is documented in Table 1.

2.7 Peak-scaled non-stationary noise analysis

Peak-scaled non-stationary noise-analysis (NSNA) (*reviewed in* Hartveit and Veruki, 2007) is based on variance in channel openings and closings during PSC decay. In contrast to biotinylation experiments that quantify protein levels, peak-scaled NSNA allows for estimation of functional synaptic receptor numbers and unitary channel current amplitudes.

Details on acquisition and selection of mIPSCs for peak-scaled NSNA can be found in (Janach et al., 2022, section 2.10). Prior to analysis of mIPSCs I tested the data for time stability to investigate the possibility of electrotonic filtering and synchronous presynaptic release. Therefore, I correlated chronological event number of mIPSCs selected for NSNA with peak amplitudes, 10 - 90 % rise times and decay time constants from monoexponential fits in each experimental condition using Spearman's rank-order correlation test. If significant correlation ($P < 0.05$) indicated lack of time stability in one condition, I excluded the respective experiment from analysis. Further, I only considered experiments without significant correlation between rise and decay time (that would point towards electrotonic filtering (Hartveit and Veruki, 2007)) and without significant negative correlation between rise / decay time and amplitude (that would point towards IPSC summation due to synchronous presynaptic release and/or electrotonic filtering (de

Koninck and Mody, 1994)) for peak-scaled NSNA (Janach et al., 2022). Examples for correlation can be found in Fig. 3.

After determination of mean current and variance values of binned mIPSCs, I plotted the data and fitted it with the parabolic function $\sigma^2 = iI - I^2/N$ to determine the average number of channels, open at the peak of an mIPSC (N) and the weighted mean unitary channel current (i). In the given formula σ^2 is the variance and I is the average current. I calculated chord conductance as i / (V_{mem} - E_{rev}) for a temperature of 32° C (Janach et al., 2022).

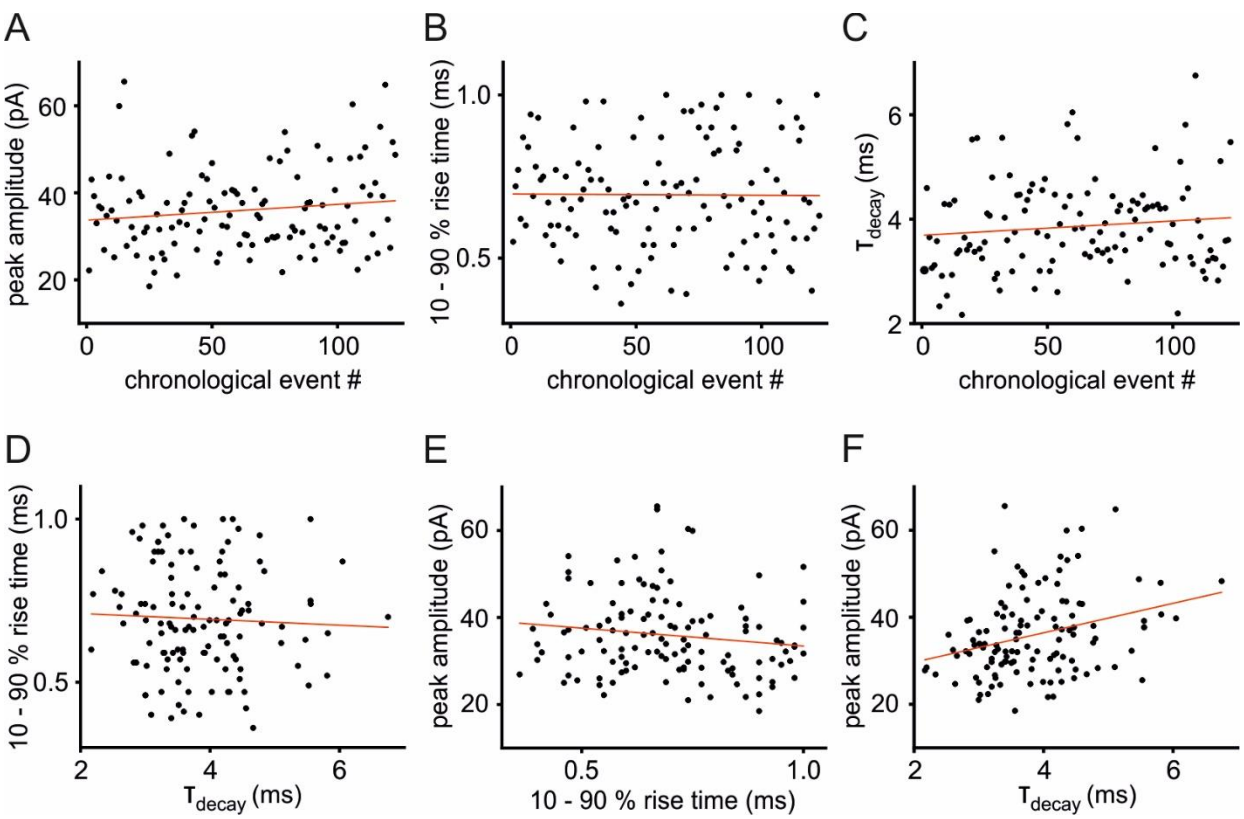

Figure 3: Exemplary relations between parameters from mIPSCs used in peak-scaled NSNA.

A - C: Time stability was given, as there was no significant correlation between chronological event number and mIPSC peak amplitude, 10 - 90 % rise time or decay time. **D / E**: No significant correlation between 10 - 90 % rise time and decay time or mIPSC peak amplitude and 10 - 90 % rise time could be detected. **F**: For the experimental condition shown, I found a positive correlation between mIPSC peak amplitude and decay time. However, this is contrary to the anticipated correlation in case of electrotonic filtering (Gill et al., 2006). Figure compiled for this thesis by: Gabriel Janach.

2.8 Single channel recordings and $GABA_A$ receptor driving force

Cell-attached recordings of single ion channels permit calculation of single channel conductance and electrochemical driving force devoid of interference with intracellular signaling during IFN-γ application, because the neuronal membrane remains intact.
For cell-attached recordings of $GABA_AR$ currents I used inverted command voltages ($-V_p$) between –80 and +80 mV. Further details on acquisition and analysis of single channel currents, as well as calculation of $DF_{GABA(A)}$ can be found in (Janach et al., 2022, sections 2.11 and 3.5). Composition of pipette solution is documented in Table 1.
Interestingly in most long-term cell-attached recordings (21/25), single channel currents vanished after 10 - 20 minutes (example in Fig. 4) although seal resistance remained stable throughout (Janach et al., 2022). This may be attributed to endocytosis or lateral diffusion from the patch (Herring et al., 2003; Luca et al., 2017; Janach et al., 2022).

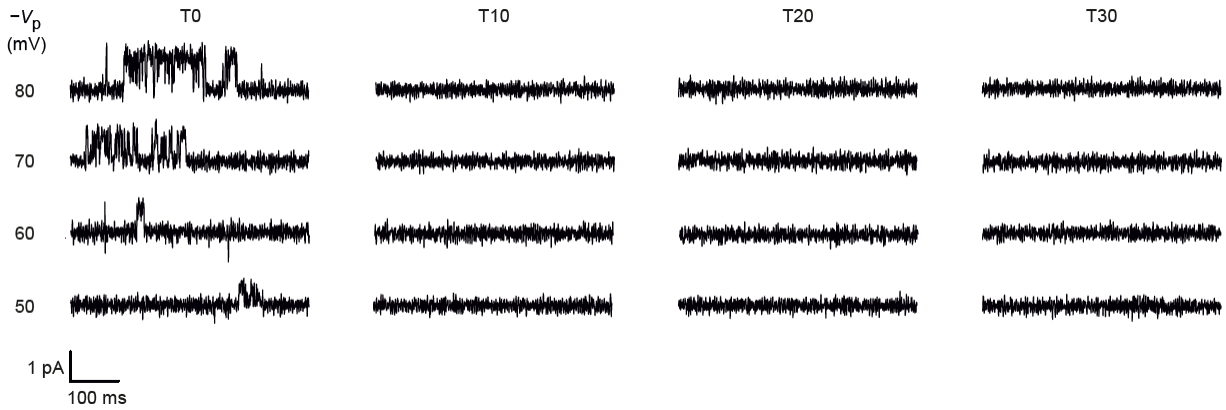

Figure 4: Single channel current disappearance over time.
Exemplary current traces from a long-term cell-attached recording. After seal stabilization (T0) clear channel openings can be observed at different $-V_p$ values. 10 (T10), 20 (T20) and 30 (T30) minutes after, no change in baseline noise could be registered, although the seal resistance remained stable (T0 = 22.6 GΩ, T10 = 24.2 GΩ, T20 = 24.3 GΩ, T30 = 26.1GΩ). For all given $-V_p$ values and time points I recorded a minimum duration of 10 sec. Figure from (Janach et al., 2022).

2.9 Statistical analysis

To compare likely normally distributed samples (P > 0.05 in Shapiro-Wilk test) in longitudinal experimental series, I used paired t-tests. When normal distribution was

unlikely ($P < 0.05$ in Shapiro-Wilk test), I used Wilcoxon signed-rank tests. To compare the means of independent samples, I used two-sample t-tests ($P > 0.05$ in Shapiro-Wilk test for all independent conditions). For the analysis of cumulative probabilities, I used two-sample Kolmogorov-Smirnov tests. I set the significance level to 5% and report all data as mean ± standard error of the mean (SEM) (Janach et al., 2020; Janach et al., 2022).

Table 1: Composition of bath and pipette solutions.

	sACSF	holding	ACSF	e / s / mIPSC2	mIPSC1	PE	PPR	CA
NaCl	85	92	119	4			4	120
CsCl				140				
KCl	2.5	2.5	2.5		130	44	40	5
K-gluconate						86	86	
$MgCl_2$	7		1.3	1	1	2	2	10
$MgSO_4$		2						
$CaCl_2$	0.5	2	2.5		1	1	1	0.5
NaH_2PO_4	1	1.2	1					
$NaHCO_3$	26	30	26					
Na-phosphocreatine					10			
Glucose	10	25	10					10
Sucrose	50							
HEPES		20		10	10	10	10	10
Sodium ascorbate		5						
Sodium pyruvate		3						
Thiourea		2						
EGTA				0.1	11	11	11	5
GTP				0.3	0.3	0.5	0.5	
Mg^{2+}-ATP				2	2		2	
Na^{2+}-ATP						2		
QX-314				5			5	
TEA								20
4-AP								5
GABA								0.001
V_{hold}				–70 / –60 / –70	–60	–70	–70	

Table 1: All values are given in mM, except for V_{hold} given in mV. Abbreviations: sACSF = high sucrose artificial cerebrospinal fluid for slicing, holding = holding solution for storage, ACSF = artificial cerebrospinal fluid for recording, e / s / mIPSC2 = pipette solution for eIPSCs / sIPSCs in (Janach et al., 2020) and mIPSCs in (Janach et al., 2022), mIPSC1 = pipette solution for mIPSCs in (Janach et al., 2020), PE = pipette solution for pressure ejection experiments, PPR = pipette solution for paired pulse experiments, CA = pipette solution for cell-attached recordings.

3 Synopsis of Major Results

Here, I recipatulate and link major results from (Janach et al., 2020) and (Janach et al., 2022). I delineated some of the results from (Janach et al., 2020), that were not acquired by myself, in the introduction (section 1.3). In part, I include results that were not acquired by me (refer to page 55 for a detailed summary of personal contributions) in this chapter, due to their contextual relevance.

3.1 IFN-γ increases IPSC amplitudes in late juvenile rats

The overlap in modulation of I_h between type I IFNs (Stadler et al., 2014) and IFN-γ (Janach et al., 2020), as well as the divergence in excitability changes after the application of IFN-β (a type I IFN) and IFN-γ (Hadjilambreva et al., 2005; Janach et al., 2020) suggested a potential role of GABAergic inhibition (section 1.3 and Janach et al., 2020). Therefore, we recorded IPSCs that involve pre- and postsynapse in layer 5 pyramidal neurons of S1 in late juvenile male Wistar rats. In all three experimental series (eIPSCs, sIPSCs, mIPSCs) application of 1.000 IU ml^{-1} IFN-γ for 20 - 40 min led to a significant increase in IPSC amplitudes (Fig. 5 - 7; Table 2).

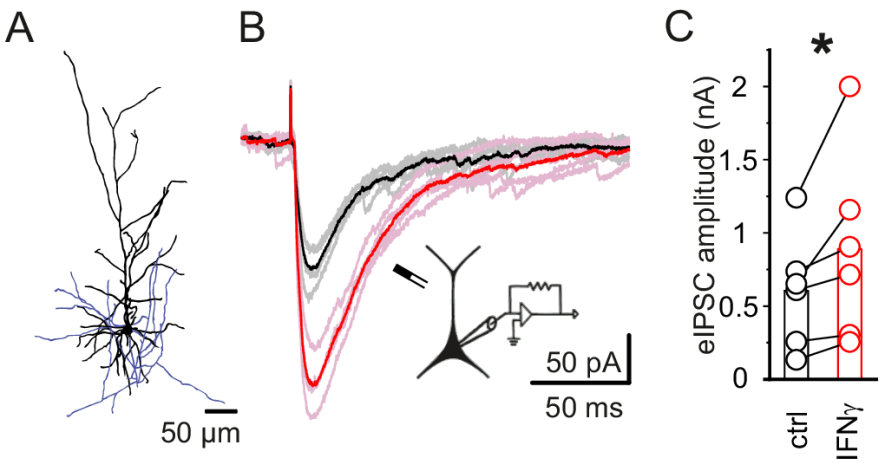

Figure 5: IFN-γ increases the amplitude of evoked IPSCs in neocortical layer 5 pyramidal neurons.

Electrically evoked IPSCs were recorded in the presence of CNQX and DAP5 to block ionotropic glutamate receptors.

A: Exemplary layer 5 pyramidal neuron stained with biocytin and reconstructed to ensure neuronal identity when electrophysiological characterization was impaired by recording conditions. Soma and dendrites are represented in black, the axon in blue. **B**: Example traces of IPSCs evoked

before (*grey*) and after 30 minutes of IFNγ application (1.000 IU ml^{-1}; *rose*). Averaged traces are shown in black (before IFN-γ application) and red (after IFN-γ application). A scheme of the experimental setup, including the apicolaterally positioned bipolar stimulation electrode, is depicted below. **C**: Maximum amplitudes of all eIPSCs increased under the influence of IFN-γ. Analysis of eIPSC amplitudes was performed before and 20 to 40 minutes after the application of IFN-γ.

Figure and figure legend modified from (Janach et al., 2020). For further details see Fig. 4 in (Janach et al., 2020).

Event frequency of spontaneous or miniature IPSCs was not consistently altered, but markedly increased in a few individual experiments (Fig. 6B *right* and Fig. 7B *right*). The occasional increase in event frequency may be indicative of a partial persistence of nitric oxide dependent IPSC frequency increase due to IFN-γ as observed in early postnatal development (Döhne et al., 2022).

Interestingly, the increase in eIPSC amplitudes (48 % mean increase) was considerably stronger than that of s/mIPSCs (14.6 % / 20 % mean increase). This discrepancy may be attributed to the segregation of evoked and spontaneous inhibitory neurotransmission (Horvath et al., 2020) and/or the putative activation of transiently increased extrasynaptic $GABA_A$Rs, as further discussed in (Janach et al., 2022, section 4.1).

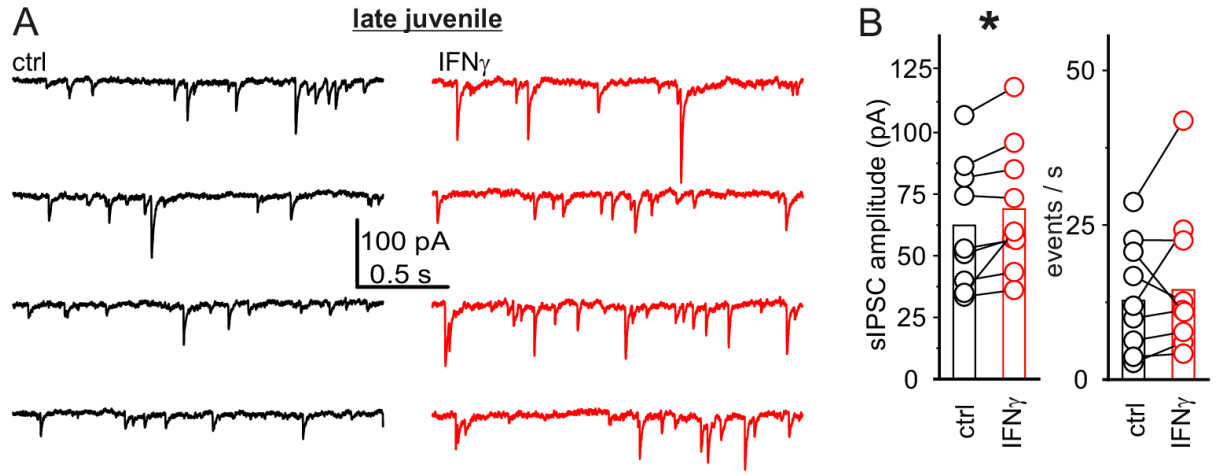

Figure 6: IFN-γ increases the amplitude of spontaneous IPSCs in neocortical layer 5 pyramidal neurons of late juvenile rats.

Spontaneous IPSCs were measured in the presence of CNQX and DAP5 to block ionotropic glutamate receptors.

A: Example traces of sIPSCs of late juvenile rats before (*black*) and after application of IFN-γ (1.000 IU ml^{-1}; 20 minutes; *red*). **B**: IFN-γ application (20 to 30 minutes) increased sIPSC

amplitudes of pyramidal neurons of late juvenile rats (*left*) but left sIPSC frequency (*right*) unchanged.

Figure and figure legend modified from (Janach et al., 2020). For further details see Fig. 5 in (Janach et al., 2020).

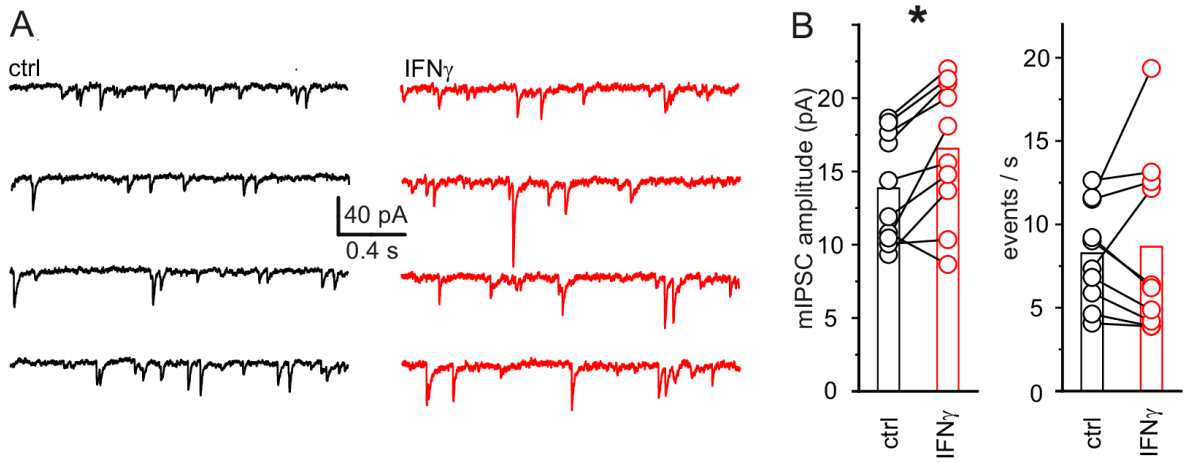

Figure 7: IFN-γ increases mIPSC amplitude in neocortical layer 5 neurons.

A: Example traces of mIPSCs recorded in the presence of CNQX, DAP5 and TTX before (*black*) and upon application of IFN-γ (1.000 IU ml^{-1}; 20 minutes; *red*). **B**: Mean mIPSC amplitudes (*left*) increased upon application of IFN-γ, while mIPSC frequency (*right*) remained unaltered.

Figure and figure legend modified from (Janach et al., 2020). For further details see Fig. 6 in (Janach et al., 2020).

3.2 IFN-γ increases sIPSC amplitudes in adult rats

Although the biggest part of inhibitory circuitry forms in the postnatal period up to P21 (Miller, 1988; Del Rio et al., 1992; Le Magueresse and Monyer, 2013), an age that complies with our late juvenile cohort, further developmental changes in inhibitory transmission (Luhmann and Prince, 1991) and neocortical $GABA_AR$ density (Xia and Haddad, 1992) occur later on. Therefore, we recorded sIPSCs under the influence of 1.000 IU ml^{-1} IFN-γ (20 - 30 min) in adult male rats to assess potential alterations of the IFN-γ effect. In adult male rats, IFN-γ increased sIPSC amplitudes in a similar extent as in late juvenile rats (Fig. 8; Table 2), arguing for a comparable impact of IFN-γ onto neocortical inhibition in the adult rat brain. Further, our analysis of sIPSCs in adult rats revealed a strong increase in baseline sIPSC frequency compared to late juvenile rats. These results may be delineated in a future publication.

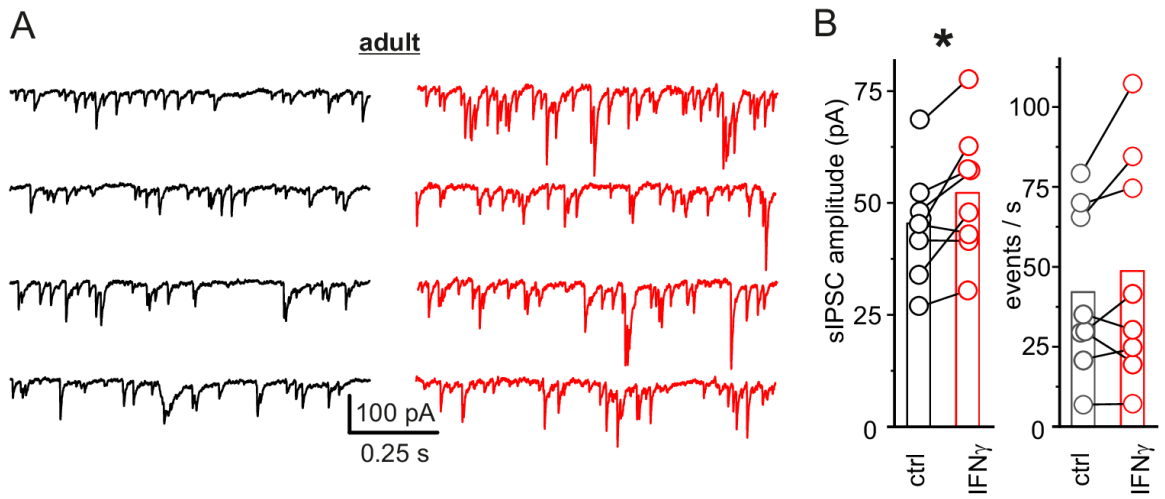

Figure 8: IFN-γ increases the amplitude of spontaneous IPSCs in neocortical layer 5 pyramidal neurons of adult rats.

Spontaneous IPSCs were measured in the presence of CNQX and DAP5 to block ionotropic glutamate receptors.

A: Example traces of sIPSCs of adult rats before (*black*) and after application of IFN-γ (1.000 IU ml^{-1}; 20 minutes; *red*). **B**: IFN-γ application (20 to 30 minutes) increased sIPSC amplitudes of pyramidal neurons of adult rats (*left*) but left sIPSC frequency (*right*) unchanged.

Figure and figure legend modified from (Janach et al., 2020). For further details see Fig. 5 in (Janach et al., 2020).

3.3 IFN-γ increases mIPSC amplitudes in female rats

As subunit expression of $GABA_A$Rs varies depending on the stage of the estrous cycle (Lovick, 2006) and not only pharmacokinetics, but also pharmacodynamics often differ between male and female individuals (Farkouh et al., 2020), we investigated whether synaptic inhibition onto layer 5 pyramidal neurons is similarly affected by IFN-γ in female rats. Recording and analysis of mIPSCs before and after 25 - 35 min of continuous application of 1.000 IU ml^{-1} IFN-γ (Fig. 9; Table 2) indicated a likewise (male: 20.7 % vs. female: 25.3 %) increase in current amplitudes (Janach et al., 2022), suggestive of a sex-independent mechanism of action.

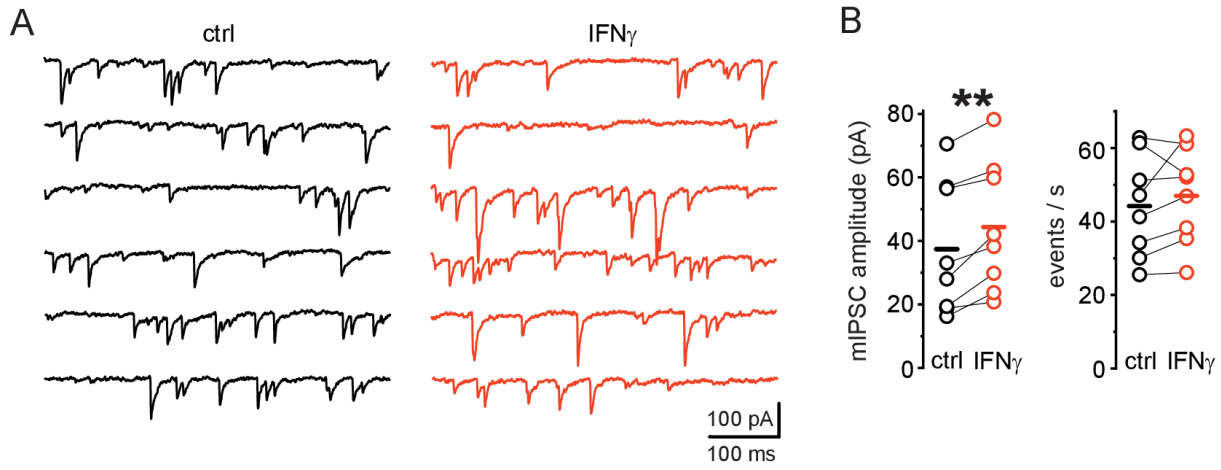

Figure 9: Acute application of IFN-γ augments mIPSC amplitudes in layer 5 pyramidal neurons of female rats.

A: Example traces of mIPSCs before and after 25 minutes of persistent IFN-γ (1.000 IU ml^{-1}) application. **B**: Average mIPSC amplitudes (*left*) increased, whereas event frequency remained unchanged (*right*) after persistent application of IFN-γ as shown in respective population data plots.

Figure and figure legend modified from (Janach et al., 2022). For further details see Fig. 6 in (Janach et al., 2022).

3.4 IFN-γ selectively impacts inhibitory transmission via a postsynaptic mechanism

To study the mechanism by which IFN-γ strengthens neocortical inhibition onto layer 5 pyramidal neurons, we first segregated pre- and postsynapse as potential targets of IFN-γ.

Replacement of presynaptic GABA release by pressure application of 100 µM GABA before and 20 - 35 min after persistent IFN-γ application (1.000 IU ml^{-1}) revealed an increase in IPSC amplitudes and charge transfer (Fig. 10 A/B; Table 2) (Janach et al., 2022). The mean increase in IPSC amplitudes after pressure application of GABA (49 %) (Janach et al., 2022) corresponded to the mean increase in eIPSC amplitudes (48 %) (Janach et al., 2020), pointing towards a pro-inhibitory modulation of postsynaptic, but not presynaptic properties. This assumption was further supported by unchanged PPRs (inter-stimulus intervals: 50 and 100 ms) after 25 - 40 min of persistent IFN-γ application (Fig. 10C/D; Table 2) (Janach et al., 2022).

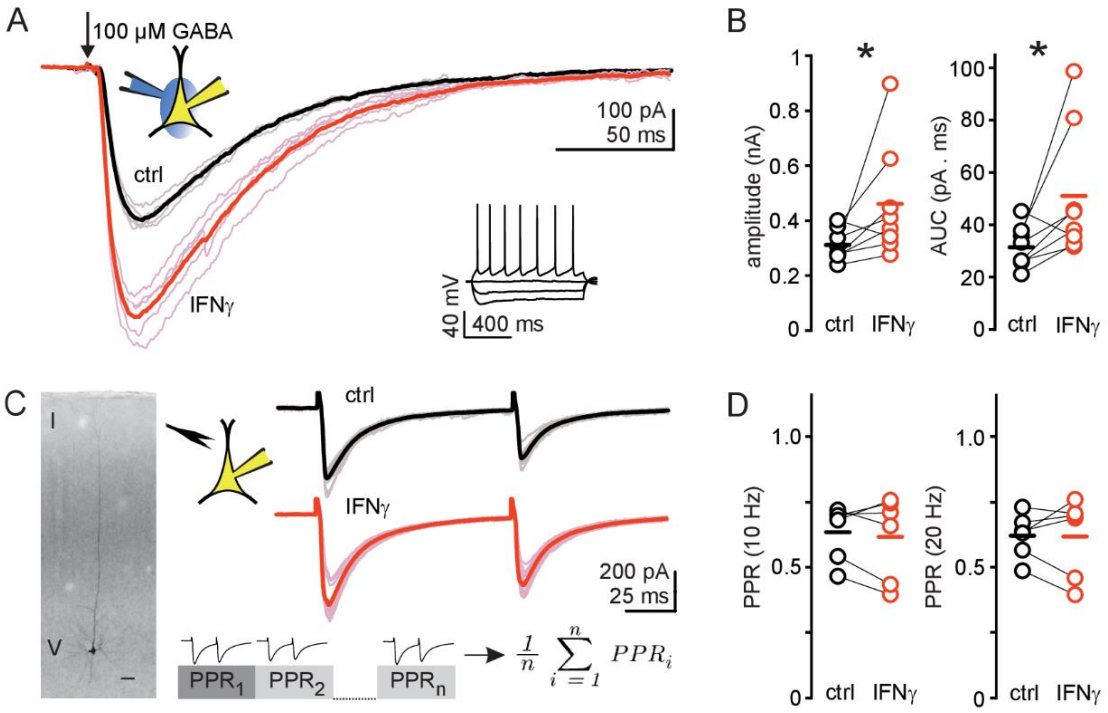

Figure 10: IFN-γ acutely increases postsynaptic GABAergic current responses in neocortical layer 5 pyramidal neurons without impacting presynaptic properties.

A: Five individual current responses (*thin lines*) to GABA (100 µM, pressure applied for 3 ms, *arrow*) before and 30 minutes after start of IFN-γ application are averaged (*bold lines*). Responses appear as negative deflections (efflux of Cl^- ions) due to experimentally elevated $[Cl^-]_i$ (see 2.11). Insets illustrating pressure ejection (*top*) and current-clamp characterization of the recorded layer 5 pyramidal neuron (*bottom right*). **B**: IFN-γ increases averaged current amplitude and charge transfer (integrated area under the curve, AUC), as depicted in respective population data. **C**: *Left*: Visualization of biocytin-filling confirming the identity of a layer 5 pyramidal neuron, located approximately 950 µm from the pia mater (scale bar = 50 µm). *Right*: Example traces of current responses to electrical stimulations with 100 ms inter-pulse interval (10 Hz) before and with 40 minutes of IFN-γ application (stimulation artifact truncated). Although 20 consecutive responses (*thin lines*) were averaged (*bold lines*) for clarity, paired pulse ratios (PPR) were calculated for every trace and averaged subsequently (bottom scheme). Inset depicts the somatic whole-cell configuration with apicolateral position of stimulating electrode. **D**: IFN-γ did not alter PPR at 100 ms (*left*) or 50 ms (*right*) inter-pulse intervals (population data).

Figure from (Janach et al., 2022), figure legend modified from (Janach et al., 2022). For further details see Fig. 1 in (Janach et al., 2022).

3.5 IFN-γ increases postsynaptic $GABA_AR$ number

The strength of synaptic inhibition on the level of the postsynapse is determined by multiple factors including synaptic $GABA_AR$ quantity, $GABA_AR$ single channel properties and $GABA_AR$ driving force.

Synaptic $GABA_AR$ quantity is linked to the amplitude of IPSCs because $GABA_ARs$ at the postsynaptic membrane are likely saturated after presynaptic GABA vesicle release (Otis et al., 1994; Nusser et al., 1997). To assess the quantity of membrane-bound $GABA_AR$ γ_2 subunits, Marta Rosário performed cell surface biotinylation of neocortical tissue. These experiments revealed a significant increase in $GABA_AR$ γ_2 protein levels (Fig. 11A/B; Table 2) upon 30 min of IFN-γ application (1.000 IU ml^{-1}) (Janach et al., 2022). We chose the γ_2 subunit for these experiments because it is predominantly embedded in synaptic $GABA_ARs$ at mature synapses (Schweizer, 2003) and essential for the synaptic clustering of $GABA_ARs$ (Thomson and Jovanovic, 2010). The result suggests an increase in synaptic $GABA_ARs$ underlying the augmentation of postsynaptic inhibition due to IFN-γ. However, elevated protein quantity of membrane-bound subunits does not prove correct assembly, function, and synaptic localization of $GABA_ARs$.

To tackle these imponderabilities, we analyzed mIPSCs using peak-scaled NSNA that allows for the determination of average synaptic receptor number open at the peak of an mIPSC and chord conductance of synaptic receptors (see section 2.7 in this thesis and (Janach et al., 2022, section 2.10)). Indeed, peak-scaled NSNA showed an increase in postsynaptic $GABA_AR$ number (Fig. 11C - G; Table 2) that was comparable to the average increase in mIPSC amplitudes (23.5 % vs. 20.7 %) after 20 - 35 min of persistent IFN-γ application (1.000 IU ml^{-1}) (Janach et al., 2022). In conjunction with the results from surface biotinylation experiments, this finding renders elevated synaptic $GABA_AR$ number as cause for the IFN-γ related augmentation of postsynaptic inhibition likely.

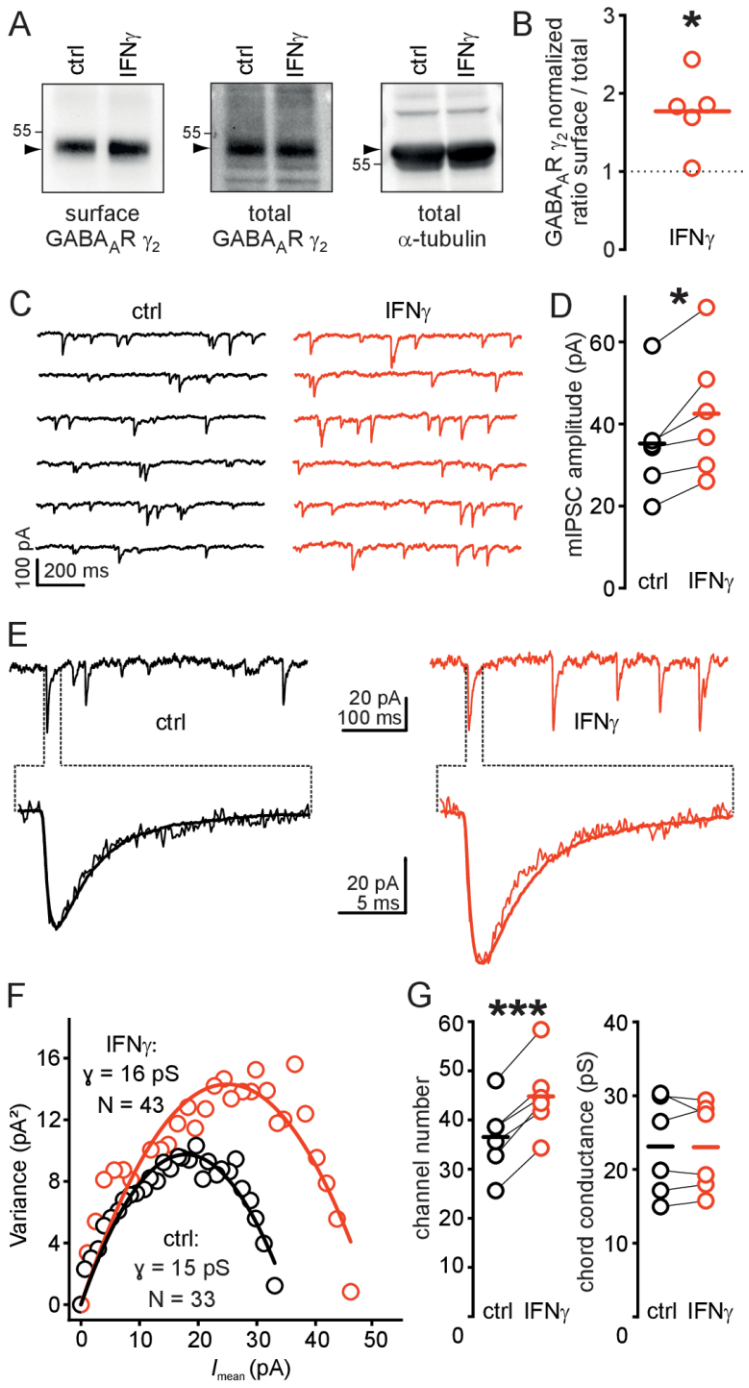

Figure 11: IFN-γ acutely increases plasma membrane localization and postsynaptic number of GABA$_A$Rs without affecting synaptic GABA$_A$R conductance.

A/B: IFN-γ promotes plasma membrane localization of GABA$_A$R γ$_2$ subunits. **A**: Levels of surface expressed (biotinylated) and total GABA$_A$R γ$_2$ compared in animal-matched control and IFN-γ stimulated neocortical samples. **B**: Quantification of IFN-γ induced increase in surface / total ratio of γ$_2$ subunit containing GABA$_A$Rs normalized to respective controls. **C/D**: IFN-γ increased mIPSC amplitudes in neocortical layer 5 pyramidal neurons that underwent non-stationary noise analysis (NSNA – E-G). **C**: Consecutive example traces of mIPSCs recorded held at –70 mV without and

with IFN-γ (applied for 25 minutes). **D**: Population data on paired comparison of mIPSC amplitudes. **E-G**: IFN-γ increased synaptic $GABA_AR$ number without affecting conductance as revealed by NSNA. **E**: Sections of mIPSC recordings before and under the influence of IFN-γ. Extended mIPSCs are superimposed with the respective peak-scaled average mIPSC waveform. Note the increase in mIPSC deviance from the averaged waveform during decay under influence of IFN-γ. **F**: Current-variance plots for the experiment in C. While comparable slope values in the initial part of parabolic fits account for roughly unchanged synaptic channel conductance, mean current and variance increases after 30 minutes of persistent IFN-γ application. **G**: Population data on IFN-γ effects on channel numbers (*left*) and chord conductance (*right*).
Figure from (Janach et al., 2022), figure legend modified from (Janach et al., 2022). For further details see Fig. 2 in (Janach et al., 2022).

3.6 The IFN-γ related increase in mIPSC amplitudes is PKC-dependent

Due to the relatively fast onset of the IFN-γ induced effect, mediation via modulation of protein kinase activity is more likely than via transcriptional modification. In search of promising candidates, we focused on PI3K and PKC because both kinase families have been shown to be activated by IFN-γ in different cell types (Gough et al., 2008; Green et al., 2017) and to strengthen inhibitory neurotransmission as well as to elevate $GABA_AR$ quantity (Serantes et al., 2006; Vetiska et al., 2007; Terunuma et al., 2008). Furthermore, IFN-γ-dependent activation of PKC in layer 5 pyramidal neurons appeared likely, since the attenuation of I_h upon application of type I IFNs (Stadler et al., 2014) that is presumably PKC-dependent (Reetz and Strauss, 2013; Reetz et al., 2014) paralleled the IFN-γ effect onto I_h (Janach et al., 2020).

Pre-incubation of acute brain slices in 100 nM of the PI3K inhibitor Wortmannin, followed by mIPSC recording and 20 - 30 min co-application of 100 nM Wortmannin with 1.000 IU ml^{-1} IFN-γ (Fig. 12A/B; Table 2) did not block the IFN-γ effect on mIPSC amplitudes (Janach et al., 2022). In contrast, blockage of PKC via pre-incubation in 100 nM Calphostin C and subsequent mIPSC recordings before and after 20 - 30 min of co-application with 1.000 IU ml^{-1} IFN-γ (Fig. 12C/D; Table 2) prevented the augmentation of mIPSC amplitudes by IFN-γ (Janach et al., 2022). This indicates essential contribution of activated PKC to the observed effect.

As $GABA_AR$ phosphorylation at a multitude of subunits has been shown to affect receptor trafficking (Nakamura et al., 2015) and membrane-bound quantity of $GABA_AR$ γ_2 subunits increased after IFN-γ application (Janach et al., 2022), we aimed to explore whether IFN-

γ alters the PKC-associated serine phosphorylation state at $GABA_AR$ γ_2 subunits. Indeed, experiments conducted by Marta Rosário revealed that after incubation of cortical tissue in 1.000 IU ml^{-1} IFN-γ for 30 min, levels of PKC-substrate serine phosphorylation at $GABA_AR$ γ_2 subunits (Fig. 12E/F; Table 2) were increased (Janach et al., 2022). The change in phosphorylation state of $GABA_AR$ γ_2 subunits may be - putatively besides further PKC-related phosphorylation at other $GABA_AR$ subunits - explicative for increased synaptic $GABA_AR$ membrane presence. This assumption is corroborated by others' findings, linking PKC activation to increased synaptic efficacy (Field et al., 2021) and phosphorylation of $GABA_AR$ γ_{2L} subunits at a PKC-specific site to accumulation of $GABA_AR$s at inihibitory synapses (Meier and Grantyn, 2004).

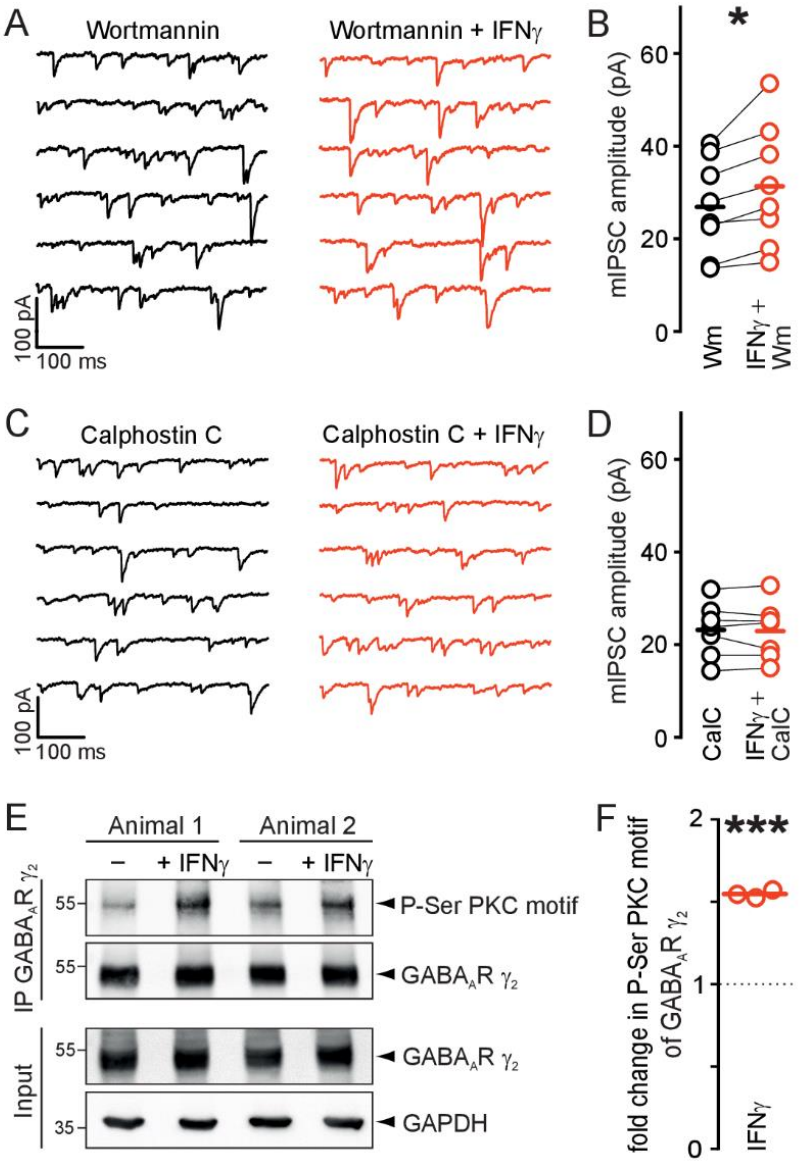

Figure 12: Increase of inhibition upon acute application of IFN-γ depends on PKC mediated $GABA_AR$ phosphorylation.

A/B: Augmentation of mIPSC amplitudes upon application of IFN-γ persists under blockade of PI3K. **A**: Example traces depict increased mIPSC amplitudes after 30 minutes of persistent IFN-γ (1.000 IU ml^{-1}) + Wortmannin (100 nM) application (*right*) following Wortmannin (100 nM) preincubation (*left*). **B**: Average mIPSC amplitudes increased after IFN-γ application despite PI3K blockade with Wortmannin.
C/D: Augmentation of mIPSC amplitudes upon application of IFN-γ is prevented by blockade of PKC. **C**: Current traces exemplify lack of change in mIPSC amplitudes after 20 minutes of persistent IFN-γ (1.000 IU ml^{-1}) + Calphostin C (100 nM) application (*right*) following Calphostin C (100 nM) preincubation (*left*). D: Blockade of PKC by Calphostin C prevented an increase in average mIPSC amplitudes by IFN-γ.
E/F: IFN-γ promotes phosphorylation of $GABA_AR$ γ_2 at PKC substrate sites. **E**: Immunoprecipitation of endogenous $GABA_AR$ γ_2 from animal-matched control or IFN-γ stimulated neocortical slices. Levels of PKC-substrate serine phosphorylation of $GABA_AR$ γ_2 immunoprecipitates was detected by Western blotting with an antibody directed against phosphorylated PKC substrate motifs. Representative images for two animals are shown. **F**: Fold change in PKC-directed serine phosphorylation on endogenous $GABA_AR$ γ_2 (P-Ser levels/total immunoprecipitated $GABA_AR$ γ_2).
Figure from (Janach et al., 2022), figure legend modified from (Janach et al., 2022). For further details see Fig. 4 in (Janach et al., 2022).

3.7 IFN-γ leaves $GABA_AR$ single channel conductance unchanged

Although the increase in synaptic $GABA_AR$ number determined by peak-scaled NSNA may directly explain the augmentation of mIPSC amplitudes (Janach et al., 2022), we investigated whether IFN-γ affects $GABA_AR$ single channel conductance. Chord conductance, calculated from unitary currents at –70 mV V_{hold} in peak-scaled NSNA remained stable (Fig. 11G; Table 2) after 20 - 35 min of IFN-γ (1.000 IU ml^{-1}) application. However, chord conductance calculations do not take voltage dependency as a common channel property into account and solely rely on one current amplitude at one given membrane voltage. To calculate slope conductance values, we recorded $GABA_AR$ single channel currents in cell-attached configuration. The few sufficient recordings from long-term cell-attached experiments (Fig. 13A - C; Table 2) were indicative of unchanged $GABA_AR$ slope conductance (Janach et al., 2022). Because longitudinal experiments were relatively inefficient (see also section 2.8), we conducted additional cell-attached recordings using a preincubation approach. These experiments did not show relevant changes in $GABA_AR$ slope conductance either (Fig. 13D - F; Table 2). Collectively, the

results from peak-scaled NSNA and cell-attached experiments argue against $GABA_AR$ single channel conductance alterations in response to acute application of IFN-γ (Janach et al., 2022).

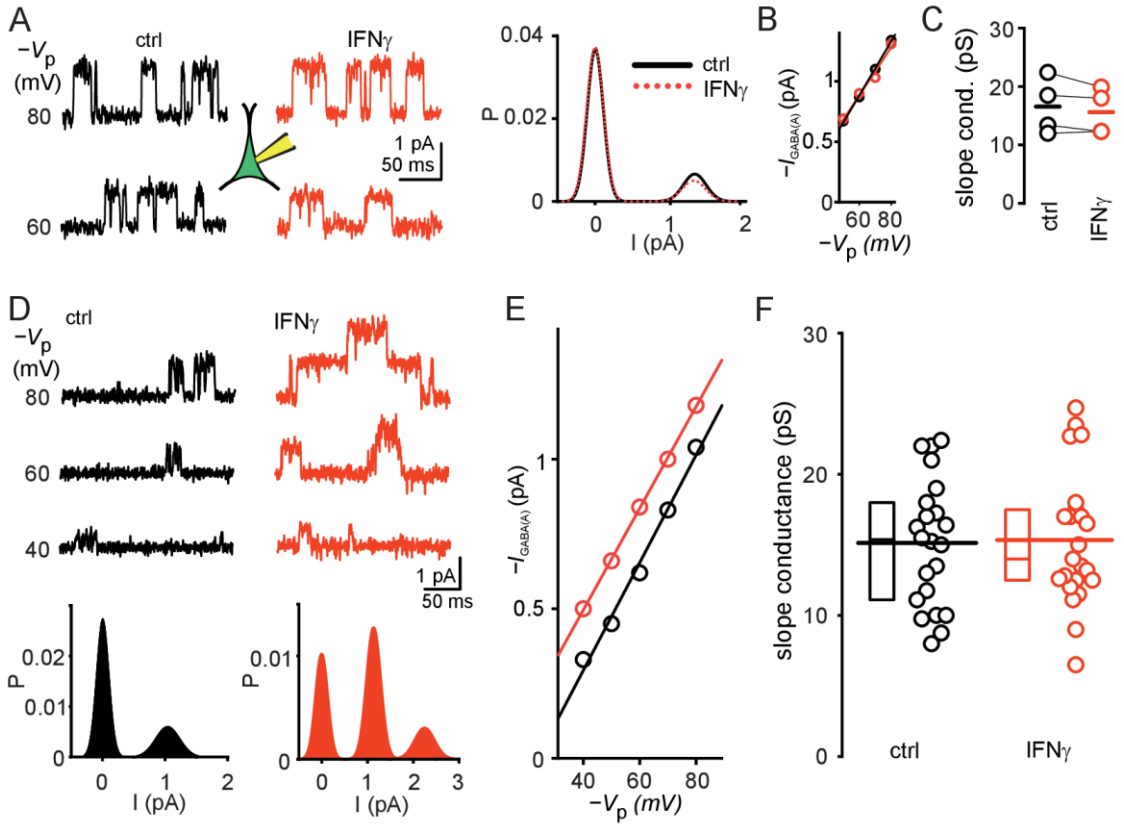

Figure 13: $GABA_AR$ single channel conductance is comparable with and without IFN-γ in neocortical layer 5 pyramidal neurons.

A-C: $GABA_AR$ single channel slope conductance remained unchanged in long-term cell-attached recordings. **A**: Single channel current amplitudes at 60 and 80 mV inverted command voltage ($-V_p$) in a long-term cell-attached recording (before and after 20 minutes of persistent IFN-γ application) remained comparable (*left*). Inset depicts scheme of somatic cell-attached configuration. Probability histogram (*right*) shows consistent single channel current amplitude distributions at 80 mV $-V_p$ in both conditions. **B**: $GABA_AR$ conductance for the experiment displayed in A was similar after ongoing application of IFN-γ, as shown in respective slopes. **C**: Paired analysis of 4 long-term single channel recordings shows comparable $GABA_AR$ slope conductance after persistent application of IFN-γ for 20 - 30 minutes. **D**: *Top*: current traces of single channel openings in ACSF and after 60 minutes of preincubation with IFN-γ for different command voltages. Probability histograms (*bottom*) show current amplitude distribution for 80 mV ($-V_p$). Note that while one channel was detected in the control recording, there were two after IFN-γ preincubation. **E**: Slope conductance from the two experiments shown in D is comparable. Larger absolute single channel current values do not necessarily increase slope conductance, as

exemplified. **F**: 25% - 75% box plots and corresponding individual slope conductance values from cell-attached recordings in ACSF or after 20 - 60 minutes of preincubation with IFN-γ. Thin lines in the box plots indicate median, bold lines crossing box plots and individual data indicate average slope conductance values.
Note that current traces have been inverted because Cl^- influx appears outwardly directed in cell-attached configuration and vice versa. Pipette voltage is inverted for comprehensibility, because positive V_p hyperpolarizes the membrane in cell-attached recordings.
Unpaired experiments were age matched by use of alternating slices.
Figure from (Janach et al., 2022), figure legend modified from (Janach et al., 2022). For further details see Fig. 3 in (Janach et al., 2022).

3.8 IFN-γ does not affect chloride homeostasis under resting conditions

$GABA_AR$ driving force is determined by chloride homeostasis that is, in turn, primarily controlled by the chloride potassium symporter KCC2 after early postnatal development (Kaila et al., 2014). Interestingly, PKC has been shown to positively affect cell surface stability and activity of KCC2 (Lee et al., 2007; Kfir et al., 2020). Accordingly, IFN-γ may lead to changes in chloride levels and $DF_{GABA(A)}$, therewith augmenting postsynaptic inhbitory strength. To test this hypothesis, we recorded $GABA_AR$ single channel currents in the cell-attached mode using different approaches (longitudinal design and preincubation, also compare section 2.8; Fig. 14C - E; Table 2), and found no substantial change in $GABA_AR$ driving force (Janach et al., 2022). These results were corroborated by studies of putative alterations in intracellular chloride levels before and after application of 1.000 IU ml^{-1} IFN-γ using fluorescence lifetime imaging microscopy of the chloride indicator N-(Ethoxycarbonylmethyl)-6-methoxyquinolinium bromide (MQAE; refer to 2.13 in (Janach et al., 2022) for methodological details) under resting conditions. In these experiments that were conducted and analyzed by Max Böhm and Ulf Strauss, we did not observe any change in the rate of fluorescence decay (Fig. 14A/B; Table 2), indicating a constant level of intracellular chloride (Janach et al., 2022).
These results render a critical impact of acutely elevated IFN-γ on chloride homeostasis unlikely.

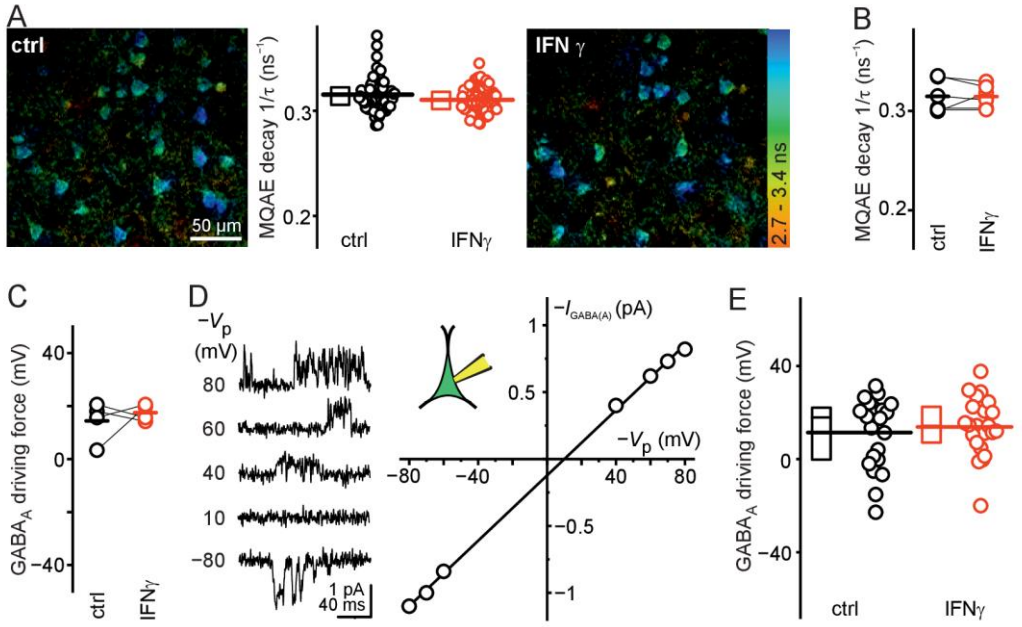

Figure 14: Acute application of IFN-γ does not alter $[Cl^-]_i$ or DF_{GABA} in neocortical layer 5 pyramidal neurons.

A: *Left and right* panel: one fifth of a fluorescence lifetime imaging microscopy image before and after 20 minutes of persistent superfusion with IFN-γ. Note the slight shift in the z-plane, leading to a different ROI number in time, reasoning an unpaired approach when comparing both conditions. The *middle* panel depicts 25% - 75% box plots and corresponding individual 1/τ data for neurons under each condition in this experiment. Mean values are indicated by bold lines crossing box plots and individual data. Median values are concealed, due to the overlap with average values. **B**: Population data illustrating averaged 1/τ (exemplified by bold lines in A) for each experiment before and after 20 minutes IFN-γ incubation. **C**: $DF_{GABA(A)}$ calculated from long-term single channel recordings was not altered upon 20 - 30 minutes of persistent IFN-γ application. **D**: *Left* panel: examples of $GABA_AR$ single channel currents at various pipette voltages. *Right* panel: corresponding I-V-plot. $DF_{GABA(A)}$ resembles $-V_p$ at $E_{GABA(A)}$ (x-intercept of the linear fit, here 10 mV). Inset displays somatic cell-attached configuration. **E**: 25% - 75% box plots and corresponding individual values of $DF_{GABA(A)}$ in control conditions or after 20 - 60 minutes of preincubation with IFN-γ. Bold lines crossing box plot and individual values indicate mean, whereas thin lines in box plot indicate median values (overlap of mean and median for IFN-γ).

Average values in paired and unpaired experiments slightly shifted towards a more depolarized $DF_{GABA(A)}$, rendering a decrease in intracellular Cl^- or HCO_3^- unlikely. Single channel current traces and V_p have been inverted for clarity, as in Fig. 13. Unpaired experiments were age matched by use of alternating slices.

Figure from (Janach et al., 2022), figure legend modified from (Janach et al., 2022). For further details see Fig. 5 in (Janach et al., 2022).

Table 2: Synopsis of major results.

	ctrl (mean ± SEM)	IFN-γ (mean ± SEM)	% increase	n	p-value
eIPSC amplitude	605 ± 160 pA	889 ± 263 pA	48 %	6	< 0.05
sIPSC amplitude (late juvenile)	62.4 ± 8.7 pA	69.5 ± 8.8 pA	14.6 %	9	< 0.05
sIPSC amplitude (adult)	45.4 ± 4.4 pA	52.2 ± 5.2 pA	15.7 %	8	< 0.05
mIPSC amplitude (2020)	13.8 ± 1.2 pA	16.5 ± 1.5 pA	20 %	10	< 0.01
GABA PE amplitude	311 ± 20 pA	461 ± 73 pA	49%	8	< 0.05
GABA PE AUC	31.4 ± 8 pA * ms	51 ± 25 pA * ms	62.2 %	8	< 0.05
PPR (10 Hz)	0.64 ± 0.04	0.63 ± 0.07	-	6	0.57
PPR (20 Hz)	0.62 ± 0.03	0.62 ± 0.06	-	6	0.94
$GABA_AR\ \gamma_2$ biotinylation	1 (normalized)	1.8 ± 0.2 - fold	-	5	< 0.05
mIPSC amplitude (2022)	35.2 ± 5.4 pA	42.5 ± 6.3 pA	20.7 %	6	< 0.05
NSNA channel number	36.5 ± 3.0	44.8 ± 3.2	23.5 %	6	< 0.001
mIPSC amplitude (Wortmannin)	26.9 ± 3.6 pA	31.3 ± 4.6 pA	16 %	8	< 0.05
mIPSC amplitude (Calphostin C)	23.2 ± 2.2 pA	22.9 ± 2.3 pA	-	7	0.65
PKC motif phosphorylation	1 (normalized)	1.55 ± 0.01 - fold	-	3	< 0.001
mIPSC amplitude (females)	37.4 ± 7.4 pA	44.4 ± 7.2 pA	25.3 %	8	< 0.01
NSNA conductance	23.1 ± 2.7 pS	23.0 ± 2.5 pS	-	6	0.89
cell attached cond. (longitudinal)	16.6 ± 2.4 pS	15.6 ± 2 pS	-	4	0.21
cell attached cond. (preincubation)	15.1 ± 1.0 pS	15.3 ± 1.0 pS	-	22 vs. 23	0.88
MQAE FLIM fluorescence decay	0.315 ± 0.006 ns^{-1}	0.315 ± 0.005 ns^{-1}	-	6	0.96
GABAAR DF (longitudinal)	14.4 ± 3.8 mV	17.5 ± 1.6 mV	-	4	0.57
GABAAR DF (preincubation)	11.4 ± 3.2 mV	13.8 ± 2.6 mV	-	22 vs. 23	0.56

Table 2: comparative representation of central results from (Janach et al., 2020) and (Janach et al., 2022). Newly introduced abbreviations: PE = pressure ejection, cond. = conductance, FLIM = fluorescence lifetime imaging microscopy.

4 Discussion

In the discussion here, I focus onto topics that have not been covered in the attached publication's discussion sections (Janach et al., 2020; Janach et al., 2022) and expand some of the subjects. Topics that we have covered in the according publications include: placing of results in context with existing research (Janach et al., 2020; Janach et al., 2022), putative reasons for the deviation of effect between type I IFNs and IFN-γ (Janach et al., 2020), putative microglial involvement in the mediation of IFN-γ effects (Janach et al., 2020; Janach et al., 2022), potential consequences of short-term increase in inhibitory synaptic transmission (Janach et al., 2020; Janach et al., 2022), possible pathophysiological consequences of increased IFN-γ levels (Janach et al., 2020; Janach et al., 2022) and the difference between amplitude increase in spontaneous and artificially evoked IPSCs (Janach et al., 2022).

4.1 Summary of results

We demonstrated a novel role for IFN-γ in modulating neocortical inhibition by showing that acute elevation of IFN-γ to 1.000 IU ml^{-1} augments synaptic inhibition onto layer 5 pyramidal neurons in late juvenile male and female rats as well as adult male rats. We investigated the underlying mechanism of action in late juvenile male rats. Our studies reveal that the augmentation of inhibition is based on a postsynaptic mechanism. In detail, short-term (20 - 45 min) application of 1.000 IU ml^{-1} IFN-γ led to an acute increase in functional synaptic $GABA_AR$s and membrane presence of the $GABA_AR$ γ_2 subunit that is present in most synaptic $GABA_AR$s (Thomson and Jovanovic, 2010). PKC block, but not PI3K block prevented the augmentation of synaptic inhibition, arguing for PKC-dependency. This was corroborated by an increase in serine phosphorylation of $GABA_AR$ γ_2 subunits at PKC substrate motifs. Analysis of $GABA_AR$ single channel recordings did not show altered conductance or $GABA_AR$ driving force. Further, intracellular chloride levels determined via MQAE FLIM remained stable. Therefore, changes in intracellular chloride levels under resting conditions or $GABA_AR$ single channel conductance unlikely contributed to the increase in synaptic inhibition.

4.2 Intracellular signaling and isoform specificity

While we discussed how PKC activity may increase synaptic inhibition (Janach et al., 2022, section 4.1), we did not debate hypotheses about the distinct pathway between IFN-γ and PKC activation as well as isoform specificity of the effect there. There are three classes of PKC isoenzymes, namely classical (α, βI, βII, γ), novel (δ, ε, η, θ) and atypical (ι, ζ) PKCs, differing in molecular structure, tissue distribution and function (Zeng et al., 2012).

Because we used the PKC inhibitor Calphostin C that inhibits classical, novel and atypical PKC isoforms (Keenan et al., 1997; Siddiqi and Mansbach, 2008), we cannot give clear evidence on the isoform(s) responsible. IFN-γ activates various isoforms of PKC, including PKCδ (Deb et al., 2003) and PKCε (Choudhury, 2004). However, the latter two isoforms are likely activated downstream of PI3K (Deb et al., 2003; Choudhury, 2004) and our results suggest that IFN-γ activates one or multiple PKC isoform(s), responsible for the increase in synaptic $GABA_AR$ number, independently of PI3K (Janach et al., 2022). This notion is compatible with PKCα and PKCβI/II activation by IFN-γ (Giroux et al., 2003; Nikodemova et al., 2007; Seo et al., 2009) and the proposition of activated classical PKC isoforms as modulators of lateral $GABA_AR$ diffusion, leading to increased synaptic inhibition (Bannai et al., 2015), although the latter was not linked to known phosphorylation sites at $GABA_AR$ γ_2 subunits. Classical PKC isoforms also seem to be promising candidates because, in contrast to PKCδ and PKCε that can be activated by type I IFNs as well as by IFN-γ (Wang et al., 1993; Deb et al., 2003; Choudhury, 2004; Yanase et al., 2012), classical PKCs have - to the best of my knowledge - not been shown to be activated by other IFNs than IFN-γ. This could clarify the deviation in effect between type I IFNs and IFN-γ - i.e. both IFN classes may activate novel PKCs (namely δ and ε), therewith modulating currents as I_h, whereas solely IFN-γ would activate classical PKCs, therewith additionally enhancing inhibitory synaptic neurotransmission.

These assumptions are based on reports regarding PKC activation in various body regions and are highly speculative, because kinase activation profiles by IFN-γ can vary upon different cell types (see e.g. Seo et al., 2009).

4.3 IFN-γ, PKC activation and altered inhibition due to changes in synaptic $GABA_AR$ quantity in the context of health and disease

4.3.1 Sickness behavior

CNS related side effects of therapeutically applied IFN-γ, e.g. fatigue (Miller et al., 2009), as well as consequences of elevated IFN-γ levels in CNS infection, e.g. depressive-like and sickness behavior (Kirsten et al., 2020), may be associated with increased synaptic inhibition. This assumption is underlined by reports on increased synaptic inhibition in the arcuate nucleus, that underlies an animal model of depression (Fang et al., 2021). Further, a connection between increased synaptic inhibition in layer 5 neocortical pyramidal neurons by enhanced $GABA_AR$ exocytosis and slow wave sleep has been revealed (Kurotani et al., 2008). Considering these findings, IFN-γ is a promising candidate for the mediation of sickness behavior including fatigue, reduced social interaction and depression, during the initial stages of immune response and after therapeutic application of IFN-γ.

4.3.2 Epilepsy

Post- and interictal elevation in CNS IFN-γ levels has been observed in humans (Gao et al., 2017) and IFN-γ has been shown to ameliorate epileptic seizures, putatively via augmentation of tonic inhibition due to increased layer I interneuron activity (Filiano et al., 2016). The activation of PKC by IFN-γ may contribute to the increase in tonic inhibition as PKC-dependent phosphorylation of different $GABA_AR$ subunits led to increased cell surface expression of extrasynaptic $GABA_ARs$ (Abramian et al., 2010). Additionally, enhancing the membrane presence of γ_2 subunit containing $GABA_ARs$, that is consistent with the effect we reported in (Janach et al., 2022), may compensate for reduced surface expression of γ_2 subunit containing $GABA_ARs$ as a pathomechanism of epilepsy (Tan et al., 2007). These findings are corroborated by improved outcomes in pilocarpine induced epilepsy when IFN-γ is co-applied intraperitoneally (Li et al., 2017), altogether arguing for an anti-epileptic role of IFN-γ. On the contrary, limbic seizures after infection with West Nile virus have been shown to be IFN-γ-dependent (Getts et al., 2007). Because the latter study compared IFN-$\gamma^{-/-}$ with wild type mice and basal levels of IFN-γ are essential for normal cortical connectivity (Filiano et al., 2016), it cannot be excluded that neurodevelopmental alterations due to the absence of IFN-γ contributed to the observed effect.

4.3.3 Depression

Whereas IFN-γ has been postulated to be involved in the pathogenesis of depression by interference with tryptophan metabolism (Widner et al., 2002; Myint et al., 2013) and anhedonic behavior in rats correlates with increased peripheral IFN-γ levels (Géa et al., 2019), it may also contribute to depression or depression-like conditions by increasing synaptic inhibition. This assumption is supported by a study linking enhanced inhibitory synaptic transmission in the arcuate nucleus to the persistence of an animal model of depression (Fang et al., 2021). In return, there is evidence that chronic depression may - at least in part - be explicable by a deficit in GABA and an imbalance of inhibitory and excitatory transmission, whereas antidepressant therapies can reverse the GABA deficit and therewith ameliorate depression (Kalueff and Nutt, 2007; Duman et al., 2019). This underlines the importance of a tightly controlled balance between excitation and inhibition and connects to studies showing that normal brain function neither prevails in the absence (Filiano et al., 2016) nor during elevation of IFN-γ (Miller et al., 2009).

However, further studies are needed to determine whether different parameters as concentration, duration and localization of CNS IFN-γ increase could explain its beneficial vs. pathogenic consequences in the above-mentioned conditions.

4.4 Pharmacological implications

In previous studies, a link between $GABA_AR$ phosphorylation by various kinases including PKC and the properties of inhibitory transmission had been stated (*reviewed in* Nakamura et al., 2015). While modulation of $GABA_AR$ properties is the underlying mechanism of action for various sedatives and anesthetics (Saari et al., 2011), regulation of inhibitory efficacy by $GABA_AR$ quantity is a less established concept in $GABA_AR$ pharmacology that may serve as a future therapeutic target (Vien et al., 2016). Our findings complement various reports on fast (< 15 min after application of PKC activators) changes in inhibitory neurotransmission due to altered $GABA_AR$ trafficking (Kittler et al., 2000; Kittler et al., 2005) and PKC activity (Terunuma et al., 2008), that is often investigated by directly aiming at intracellular molecules via the pipette solution in whole-cell experiments. Evidence on protein kinase activity changes following binding of transmembrane receptors and subsequent alterations in $GABA_AR$ trafficking refer to a time course of hours (Serantes et al., 2006; Vithlani et al., 2013). We show that the mechanistic

sequence from external receptor binding to significant alteration in synaptic inhibitory transmission due to altered $GABA_AR$ membrane presence can be efficacious in less than 30 minutes. This stresses the potential of relatively fast pharmacological intervention via PKC modulators that could e.g. significantly reduce the required dosage of well-established sedatives/anaesthetics and therewith their adverse effects, or act beneficial on some of the conditions discussed in section 4.3. Putatively, IFN-γ could even be considered as a neuromodulatory therapeutic with specific signaling profiles, far beyond the simple mechanism of action of many drugs that operate via more discrete pharmacodynamics. For this, a thorough understanding of its signaling properties in different CNS and body regions is necessary.

4.5 Future directions

Given the many functions of PKC isoforms (Zeng et al., 2012) and previous research on PKC activation in neocortical layer 5 pyramidal neurons (Reetz et al., 2014), as well as the variety of parallel signaling pathways following IFN-γR binding (Gough et al., 2008), IFN-γ presumably not only alters synaptic GABAergic transmission (Janach et al., 2020; Janach et al., 2022) and I_h (Janach et al., 2020), but also many other neuronal properties. This is important to consider, when reflecting upon clinical implications for the observed IFN-γ effect and attempts for its induction or antagonization. External modulation of GABAergic transmission or PKC activity in parallel to disease or therapy related elevation of CNS IFN-γ levels may destabilize E/I balance or alter cellular metabolism in an unforeseen manner. Thus, further experiments on the molecular, cellular, and behavioral consequences in three areas (elevated IFN-γ levels, PKC activation, increased functional synaptic $GABA_AR$ number in neocortical layer 5 pyramidal neurons) are necessary, prior to the establishment of a translational approach.

In detail, our research (1) focuses on one particular part of IFN-γ effects onto neuronal function. (2) Our studies leave a knowledge gap concerning specific PKC isoform(s) activated by IFN-γ. As different PKC isoforms comprise different functions (Zeng et al., 2012), this question should be resolved in order to establish a more accurate concept of the IFN-γ effect. (3) The impact of elevated synaptic $GABA_AR$ number onto neuronal transmission and subsequent psychopathological characteristics remain unclear. This question may be investigated in the context of conditions involving elevated CNS IFN-γ levels, using electrophysiological techniques and behavioral experiments. (4) It remains

to be defined, to which extent the increase in synaptic $GABA_AR$ number and inhibitory strength persists after more long-lasting elevation of CNS IFN-γ levels.
Once these questions are answered, detailed knowledge on detrimental and/or beneficial roles of IFN-γ elevation in the CNS could be applied in a therapeutic context - either by antagonism of the full or partial IFN-γ effect or artificial raise in CNS IFN-γ levels.

4.6 Strengths and limitations

In the two publications underlying this thesis (Janach et al., 2020; Janach et al., 2022) we assessed the effect of IFN-γ under precisely controlled conditions. Accurate adjustment and monitoring of experimental properties as composition of pipette and bath solutions, recording temperature, time of experiments, stimulus intensities and intervals allowed for high comparability between experiments. We used a paired approach in most experiments to minimize the impact of inter-neuronal or inter-individual differences and used at least two methods to answer most of our scientific questions. Further, the similarity of the pro-inhibitory effect of IFN-γ in female and adult male rats suggests that the observed effect is sex independent and persists in the adult brain.

Limitations of our studies have been discussed in (Janach et al., 2022, section 4.3) and partly overlap with the outlook delineated in section 4.5 of this thesis. In brief, we only studied the IFN-γ effect in one cell type of one brain region in one species, namely layer 5 pyramidal neurons in the somatosensory neocortex of Wistar rats. Although Wistar rats are an outbred line, they comprise a limited gene pool. Consequently, it is unclear to which extent the results can be generalized to other cell types, brain regions, strains, and species. Our experiments were limited to a relatively short application period without investigation of acute versus chronic long-term effects or behavioral consequences. Lastly, effects of cytokines that increase in response to IFN-γ and an involvement of microglia cannot be excluded on the basis of our experiments.

5 Conclusion

In this work we (1) recorded evoked, spontaneous and miniature IPSCs to assess alterations in synaptic inhibitory neurotransmission, (2) conducted paired pulse and pressure ejection experiments to segregate pre- vs. postsynaptic mediation of the effect, (3) assessed changes in synaptic $GABA_AR$ number via peak-scaled NSNA and molecular biological determination of membrane bound $GABA_AR$ γ_2 subunit quantity, (4) showed PKC-dependence of the effect via pharmacological inhibition and molecular biological evaluation of PKC motif phosphorylation, (5) examined $GABA_AR$ single channel conductance via peak-scaled NSNA and cell-attached recordings, and (6) evaluated changes in chloride homeostasis via MQAE FLIM and $GABA_AR$ driving force calculations.

We hereby revealed an acute augmentation of synaptic inhibitory neurotransmission following elevation of IFN-γ at layer 5 pyramidal neurons in the somatosensory neocortex of late juvenile and adult male Wistar rats as well as late juvenile female Wistar rats. This augmentation was due to a PKC-dependent increase in synaptic $GABA_ARs$.

The illumination of the pro-inhibitory property of IFN-γ and its mechanism of action may contribute to future research on pathogenic functions and therapeutic prospects of IFN-γ and PKC modulators.

6 References

Abramian, A.M., Comenencia-Ortiz, E., Vithlani, M., Tretter, E.V., Sieghart, W., Davies, P.A., Moss, S.J., 2010. Protein kinase C phosphorylation regulates membrane insertion of GABAA receptor subtypes that mediate tonic inhibition. The Journal of biological chemistry 285, 41795–41805.

Bach, E.A., Aguet, M., Schreiber, R.D., 1997. The IFN gamma receptor: a paradigm for cytokine receptor signaling. Annual review of immunology 15, 563–591.

Bannai, H., Niwa, F., Sherwood, M.W., Shrivastava, A.N., Arizono, M., Miyamoto, A., Sugiura, K., Lévi, S., Triller, A., Mikoshiba, K., 2015. Bidirectional Control of Synaptic GABAAR Clustering by Glutamate and Calcium. Cell reports 13, 2768–2780.

Bayas, A., Rieckmann, P., 2000. Managing the Adverse Effects of Interferon-β Therapy in Multiple Sclerosis. Drug-Safety 22, 149–159.

Boehm, U., Klamp, T., Groot, M., Howard, J.C., 1997. Cellular responses to interferon-gamma. Annual review of immunology 15, 749–795.

Broadwell, R.D., Balin, B.J., Salcman, M., Kaplan, R.S., 1983. Brain-blood barrier? Yes and no. Proceedings of the National Academy of Sciences 80, 7352–7356.

Bruns, R.F., Miller, F.D., Merriman, R.L., Howbert, J.J., Heath, W.F., Kobayashi, E., Takahashi, I., Tamaoki, T., Nakano, H., 1991. Inhibition of protein kinase C by calphostin C is light-dependent. Biochemical and biophysical research communications 176, 288–293.

Choudhury, G.G., 2004. A linear signal transduction pathway involving phosphatidylinositol 3-kinase, protein kinase Cepsilon, and MAPK in mesangial cells regulates interferon-gamma-induced STAT1alpha transcriptional activation. The Journal of biological chemistry 279, 27399–27409.

Chow, K.T., Gale, M., 2015. SnapShot: Interferon Signaling. Cell 163, 1808-1808.e1.

Clark, D.N., Begg, L.R., Filiano, A.J., 2022. Unique aspects of IFN-γ/STAT1 signaling in neurons. Immunological reviews 311, 187–204.

Dantzer, R., O'Connor, J.C., Freund, G.G., Johnson, R.W., Kelley, K.W., 2008. From inflammation to sickness and depression: when the immune system subjugates the brain. Nat Rev Neurosci 9, 46–56.

de Koninck, Y., Mody, I., 1994. Noise analysis of miniature IPSCs in adult rat brain slices: properties and modulation of synaptic GABAA receptor channels. Journal of neurophysiology 71, 1318–1335.

Deb, D.K., Sassano, A., Lekmine, F., Majchrzak, B., Verma, A., Kambhampati, S., Uddin, S., Rahman, A., Fish, E.N., Platanias, L.C., 2003. Activation of Protein Kinase Cδ by IFN-γ. The Journal of Immunology 171, 267–273.

Del Rio, J.A., Soriano, E., Ferrer, I., 1992. Development of GABA-immunoreactivity in the neocortex of the mouse. J. Comp. Neurol. 326, 501–526.

Della-Morte, D., Raval, A.P., Dave, K.R., Lin, H.W., Perez-Pinzon, M.A., 2011. Post-Ischemic Activation of Protein Kinase C Epsilon Protects the Hippocampus from Cerebral Ischemic Injury via Alterations in Cerebral Blood Flow. Neuroscience letters 487, 158–162.

Döhne, N., Falck, A., Janach, G.M.S., Byvaltcev, E., Strauss, U., 2022. Interferon-γ augments GABA release in the developing neocortex via nitric oxide synthase/soluble guanylate cyclase and constrains network activity. Front. Cell. Neurosci. 16, 413.

Duman, R.S., Sanacora, G., Krystal, J.H., 2019. Altered Connectivity in Depression: GABA and Glutamate Neurotransmitter Deficits and Reversal by Novel Treatments. Neuron 102, 75–90.

Fang, X., Jiang, S., Wang, J., Bai, Y., Kim, C.S., Blake, D., Weintraub, N.L., Lei, Y., Lu, X.-Y., 2021. Chronic unpredictable stress induces depression-related behaviors by suppressing AgRP neuron activity. Mol Psychiatry, 1–17.

Farkouh, A., Riedl, T., Gottardi, R., Czejka, M., Kautzky-Willer, A., 2020. Sex-Related Differences in Pharmacokinetics and Pharmacodynamics of Frequently Prescribed Drugs: A Review of the Literature. Advances in therapy 37, 644–655.

Field, M., Dorovykh, V., Thomas, P., Smart, T.G., 2021. Physiological role for GABAA receptor desensitization in the induction of long-term potentiation at inhibitory synapses. Nature communications 12, 2112.

Filiano, A.J., Xu, Y., Tustison, N.J., Marsh, R.L., Baker, W., Smirnov, I., Overall, C.C., Gadani, S.P., Turner, S.D., Weng, Z., Peerzade, S.N., Chen, H., Lee, K.S., Scott, M.M., Beenhakker, M.P., Litvak, V., Kipnis, J., 2016. Unexpected role of interferon-γ in regulating neuronal connectivity and social behaviour. Nature 535, 425–429.

Frei, K., Leist, T.P., Meager, A., Gallo, P., Leppert, D., Zinkernagel, R.M., Fontana, A., 1988. Production of B cell stimulatory factor-2 and interferon gamma in the central nervous system during viral meningitis and encephalitis. Evaluation in a murine model infection and in patients. The Journal of experimental medicine 168, 449–453.

Gao, F., Gao, Y., Zhang, S.-J., Zhe, X., Meng, F.-L., Qian, H., Zhang, B., Li, Y.-J., 2017. Alteration of plasma cytokines in patients with active epilepsy. Acta neurologica Scandinavica 135, 663–669.

Géa, L.P., Colombo, R., Rosa, E.D.d., Antqueviezc, B., Aguiar, É.Z.d., Hizo, G.H., Schmidt, G.B., Oliveira, L.F.d., Stein, D.J., Rosa, A.R., 2019. Anhedonic-like behavior correlates with IFNγ serum levels in a two-hit model of depression. Behavioural Brain Research 373, 112076.

Getts, D.R., Matsumoto, I., Müller, M., Getts, M.T., Radford, J., Shrestha, B., Campbell, I.L., King, N.J.C., 2007. Role of IFN-gamma in an experimental murine model of West Nile virus-induced seizures. Journal of neurochemistry 103, 1019–1030.

Gill, S.B., Veruki, M.L., Hartveit, E., 2006. Functional properties of spontaneous IPSCs and glycine receptors in rod amacrine (AII) cells in the rat retina. The Journal of physiology 575, 739–759.

Giroux, M., Schmidt, M., Descoteaux, A., 2003. IFN-gamma-induced MHC class II expression: transactivation of class II transactivator promoter IV by IFN regulatory factor-1 is regulated by protein kinase C-alpha. Journal of immunology (Baltimore, Md. : 1950) 171.

Gough, D.J., Levy, D.E., Johnstone, R.W., Clarke, C.J., 2008. IFNgamma signaling-does it mean JAK-STAT? Cytokine & growth factor reviews 19.

Green, D.S., Young, H.A., Valencia, J.C., 2017. Current prospects of type II interferon γ signaling and autoimmunity. Journal of Biological Chemistry 292, 13925–13933.

Hadjilambreva, G., Mix, E., Rolfs, A., Müller, J., Strauss, U., 2005. Neuromodulation by a cytokine: interferon-beta differentially augments neocortical neuronal activity and excitability. Journal of neurophysiology 93.

Hartveit, E., Veruki, M.L., 2007. Studying properties of neurotransmitter receptors by non-stationary noise analysis of spontaneous postsynaptic currents and agonist-evoked responses in outside-out patches. Nature protocols 2, 434–448.

Heinemann, S.H., Conti, F., 1992. [7] Nonstationary noise analysis and application to patch clamp recordings. In: Rudy, B. (Ed.) Ion channels, vol. 207. Acad. Press, San Diego, Calif., pp. 131–148.

Herring, D., Huang, R., Singh, M., Robinson, L.C., Dillon, G.H., Leidenheimer, N.J., 2003. Constitutive GABAA receptor endocytosis is dynamin-mediated and dependent on a dileucine AP2 adaptin-binding motif within the beta 2 subunit of the receptor. The Journal of biological chemistry 278, 24046–24052.

Horvath, P.M., Piazza, M.K., Monteggia, L.M., Kavalali, E.T., 2020. Spontaneous and evoked neurotransmission are partially segregated at inhibitory synapses. eLife 9.

Imbrosci, B., Neubacher, U., White, R., Eysel, U.T., Mittmann, T., 2013. Shift from phasic to tonic GABAergic transmission following laser-lesions in the rat visual cortex. Pflugers Archiv : European journal of physiology 465, 879–893.

Ivashkiv, L.B., 2018. IFNγ: signalling, epigenetics and roles in immunity, metabolism, disease and cancer immunotherapy. Nature reviews. Immunology 18, 545–558.

Janach, G.M.S., Böhm, M., Döhne, N., Kim, H.-R., Rosário, M., Strauss, U., 2022. Interferon-γ enhances neocortical synaptic inhibition by promoting membrane association and phosphorylation of GABAA receptors in a protein kinase C-dependent manner. Brain, behavior, and immunity 101, 153–164.

Janach, G.M.S., Olivia Reetz, Noah Döhne, Konstantin Stadler, Sabine Grosser, Egor Byvaltcev, Anja U. Bräuer, Ulf Strauss, 2020. Interferon-γ acutely augments inhibition of neocortical layer 5 pyramidal neurons. J Neuroinflammation 17, 1–12.

Kaila, K., Price, T.J., Payne, J.A., Puskarjov, M., Voipio, J., 2014. Cation-chloride cotransporters in neuronal development, plasticity and disease. Nature reviews. Neuroscience 15, 637–654.

Kalueff, A.V., Nutt, D.J., 2007. Role of GABA in anxiety and depression. Depression and anxiety 24, 495–517.

Keenan, C., Goode, N., Pears, C., 1997. Isoform specificity of activators and inhibitors of protein kinase C γ and δ. FEBS Letters 415, 101–108.

Kfir, A., Awasthi, R., Ghosh, S., Kundu, S., Paul, B., Lamprecht, R., Barkai, E., 2020. A Cellular Mechanism of Learning-Induced Enhancement of Synaptic Inhibition: PKC-Dependent Upregulation of KCC2 Activation. Sci Rep 10, 1–11.

Kirsten, T.B., Cabral, D., Galvão, M.C., Monteiro, R., Bondan, E.F., Bernardi, M.M., 2020. Zinc, but not paracetamol, prevents depressive-like behavior and sickness behavior, and inhibits interferon-gamma and astrogliosis in rats. Brain, behavior, and immunity 87.

Kittler, J.T., Chen, G., Honing, S., Bogdanov, Y., McAinsh, K., Arancibia-Carcamo, I.L., Jovanovic, J.N., Pangalos, M.N., Haucke, V., Yan, Z., Moss, S.J., 2005. Phospho-dependent binding of the clathrin AP2 adaptor complex to GABAA receptors regulates the efficacy of inhibitory synaptic transmission. Proceedings of the National Academy of Sciences of the United States of America 102.

Kittler, J.T., Delmas, P., Jovanovic, J.N., Brown, D.A., Smart, T.G., Moss, S.J., 2000. Constitutive Endocytosis of GABA A Receptors by an Association with the Adaptin AP2 Complex Modulates Inhibitory Synaptic Currents in Hippocampal Neurons. J. Neurosci. 20, 7972–7977.

Kurotani, T., Yamada, K., Yoshimura, Y., Crair, M.C., Komatsu, Y., 2008. State-Dependent Bidirectional Modification of Somatic Inhibition in Neocortical Pyramidal Cells. Neuron 57, 905–916.

Lau, L.T., Yu, A.C., 2001. Astrocytes produce and release interleukin-1, interleukin-6, tumor necrosis factor alpha and interferon-gamma following traumatic and metabolic injury. Journal of neurotrauma 18, 351–359.

Le Magueresse, C., Monyer, H., 2013. GABAergic interneurons shape the functional maturation of the cortex. Neuron 77, 388–405.

Lee, H.H.C., Walker, J.A., Williams, J.R., Goodier, R.J., Payne, J.A., Moss, S.J., 2007. Direct protein kinase C-dependent phosphorylation regulates the cell surface stability and activity of the potassium chloride cotransporter KCC2. The Journal of biological chemistry 282, 29777–29784.

Li, H.L., Kostulas, N., Huang, Y.M., Xiao, B.G., van der Meide, P., Kostulas, V., Giedraitas, V., Link, H., 2001. IL-17 and IFN-gamma mRNA expression is increased in the brain and systemically after permanent middle cerebral artery occlusion in the rat. Journal of neuroimmunology 116, 5–14.

Li, T., Zhai, X., Jiang, J., Song, X., Han, W., Ma, J., Xie, L., Cheng, L., Chen, H., Jiang, L., 2017. Intraperitoneal injection of IL-4/IFN-γ modulates the proportions of microglial phenotypes and improves epilepsy outcomes in a pilocarpine model of acquired epilepsy. Brain research 1657, 120–129.

Lovick, 2006. Plasticity of GABAA receptor subunit expression during the oestrous cycle of the rat: implications for premenstrual syndrome in women. Experimental Physiology 91, 655–660.

Luca, E. de, Ravasenga, T., Petrini, E.M., Polenghi, A., Nieus, T., Guazzi, S., Barberis, A., 2017. Inter-Synaptic Lateral Diffusion of GABAA Receptors Shapes Inhibitory Synaptic Currents. Neuron 95, 63-69.e5.

Luhmann, H.J., Prince, D.A., 1991. Postnatal maturation of the GABAergic system in rat neocortex. Journal of neurophysiology 65, 247–263.

MacGregor, D.G., Chesler, M., Rice, M.E., 2001. HEPES prevents edema in rat brain slices. Neuroscience letters 303, 141–144.

Mandolesi, G., Bullitta, S., Fresegna, D., Gentile, A., De, V.F., Dolcetti, E., Rizzo, F.R., Strimpakos, G., Centonze, D., Musella, A., 2017. Interferon-γ causes mood abnormalities by altering cannabinoid CB1 receptor function in the mouse striatum. Neurobiology of disease 108.

McNab, F., Mayer-Barber, K., Sher, A., Wack, A., O'Garra, A., 2015. Type I interferons in infectious disease. Nature reviews. Immunology 15, 87–103.

Meier, J., Grantyn, R., 2004. Preferential accumulation of GABAA receptor gamma 2L, not gamma 2S, cytoplasmic loops at rat spinal cord inhibitory synapses. The Journal of physiology 559, 355–365.

Miller, C.H.T., Maher, S.G., Young, H.A., 2009. Clinical Use of Interferon-γ. Annals of the New York Academy of Sciences 1182, 69–79.

Miller, M.W., 1988. Development of projection and local circuit neurons in neocortex. Cerebral cortex, vol. 7, Development and Maturation of Cerebral Cortex., 133–175.

Monteiro, S., Roque, S., Marques, F., Correia-Neves, M., Cerqueira, J.J., 2017. Brain interference: Revisiting the role of IFNγ in the central nervous system. Progress in neurobiology 156, 149–163.

Myint, A.M., Bondy, B., Baghai, T.C., Eser, D., Nothdurfter, C., Schüle, C., Zill, P., Müller, N., Rupprecht, R., Schwarz, M.J., 2013. Tryptophan metabolism and immunogenetics in major depression: a role for interferon-γ gene. Brain, behavior, and immunity 31, 128–133.

Nakamura, Y., Darnieder, L.M., Deeb, T.Z., Moss, S.J., 2015. Regulation of GABAARs by phosphorylation. Advances in pharmacology (San Diego, Calif.) 72, 97–146.

Nikodemova, M., Watters, J.J., Jackson, S.J., Yang, S.K., Duncan, I.D., 2007. Minocycline down-regulates MHC II expression in microglia and macrophages through inhibition of IRF-1 and protein kinase C (PKC)alpha/betaII. The Journal of biological chemistry 282.

Nusser, Z., Cull-Candy, S., Farrant, M., 1997. Differences in Synaptic GABAA Receptor Number Underlie Variation in GABA Mini Amplitude. Neuron 19, 697–709.

O'Connor, J.C., André, C., Wang, Y., Lawson, M.A., Szegedi, S.S., Lestage, J., Castanon, N., Kelley, K.W., Dantzer, R., 2009. Interferon-gamma and tumor necrosis factor-alpha mediate the upregulation of indoleamine 2,3-dioxygenase and the induction of depressive-like behavior in mice in response to bacillus Calmette-Guerin. The Journal of neuroscience : the official journal of the Society for Neuroscience 29.

Otis, T.S., Koninck, Y. de, Mody, I., 1994. Lasting potentiation of inhibition is associated with an increased number of gamma-aminobutyric acid type A receptors activated during miniature inhibitory postsynaptic currents. Proceedings of the National Academy of Sciences of the United States of America 91, 7698–7702.

Reetz, O., Stadler, K., Strauss, U., 2014. Protein kinase C activation mediates interferon-β-induced neuronal excitability changes in neocortical pyramidal neurons. Journal of neuroinflammation 11, 185.

Reetz, O., Strauss, U., 2013. Protein kinase C activation inhibits rat and human hyperpolarization activated cyclic nucleotide gated channel (HCN)1--mediated current in mammalian cells. Cellular physiology and biochemistry : international journal of experimental cellular physiology, biochemistry, and pharmacology 31, 532–541.

Regehr, W.G., 2012. Short-term presynaptic plasticity. Cold Spring Harbor perspectives in biology 4.

Saari, T.I., Uusi-Oukari, M., Ahonen, J., Olkkola, K.T., Koulu, M., 2011. Enhancement of GABAergic Activity: Neuropharmacological Effects of Benzodiazepines and Therapeutic Use in Anesthesiology. Pharmacol Rev 63, 243–267.

Schweizer, C., 2003. The γ2 subunit of GABAA receptors is required for maintenance of receptors at mature synapses. Molecular and Cellular Neuroscience 24, 442–450.

Seo, J.Y., Kim, D.Y., Lee, Y.S., Ro, J.Y., 2009. Cytokine production through PKC/p38 signaling pathways, not through JAK/STAT1 pathway, in mast cells stimulated with IFNgamma. Cytokine 46.

Serantes, R., Arnalich, F., Figueroa, M., Salinas, M., Andrés-Mateos, E., Codoceo, R., Renart, J., Matute, C., Cavada, C., Cuadrado, A., Montiel, C., 2006. Interleukin-1β Enhances GABAA Receptor Cell-surface Expression by a Phosphatidylinositol 3-Kinase/Akt Pathway. J. Biol. Chem. 281, 14632–14643.

Siddiqi, S.A., Mansbach, C.M., 2008. PKCζ-mediated phosphorylation controls budding of the pre-chylomicron transport vesicle. J Cell Sci 121, 2327–2338.

Stadler, K., Bierwirth, C., Stoenica, L., Battefeld, A., Reetz, O., Mix, E., Schuchmann, S., Velmans, T., Rosenberger, K., Bräuer, A.U., Lehnardt, S., Nitsch, R., Budt, M., Wolff, T., Kole, M.H.P., Strauss, U., 2014. Elevation in type I interferons inhibits HCN1 and slows cortical neuronal oscillations. Cerebral cortex (New York, N.Y. : 1991) 24, 199–210.

Sun, M.-K., Hongpaisan, J., Nelson, T.J., Alkon, D.L., 2008. Poststroke neuronal rescue and synaptogenesis mediated in vivo by protein kinase C in adult brains. PNAS 105, 13620–13625.

Tan, H.O., Christopher A. Reid, Frank N. Single, Philip J. Davies, Cindy Chiu, Susan Murphy, Alison L. Clarke, Leanne Dibbens, Heinz Krestel, John C. Mulley, Mathew V. Jones, Peter H. Seeburg, Bert Sakmann, Samuel F. Berkovic, Rolf Sprengel, Steven Petrou, 2007. Reduced cortical inhibition in a mouse model of familial childhood absence epilepsy. PNAS 104, 17536–17541.

Tayal, V., Kalra, B.S., 2008. Cytokines and anti-cytokines as therapeutics — An update. European Journal of Pharmacology 579, 1–12.

Terunuma, M., Xu, J., Vithlani, M., Sieghart, W., Kittler, J., Pangalos, M., Haydon, P.G., Coulter, D.A., Moss, S.J., 2008. Deficits in phosphorylation of GABA(A) receptors by intimately associated protein kinase C activity underlie compromised synaptic inhibition during status epilepticus. The Journal of neuroscience : the official journal of the Society for Neuroscience 28, 376–384.

Thomson, A.M., Jovanovic, J.N., 2010. Mechanisms underlying synapse-specific clustering of GABAA receptors. European Journal of Neuroscience 31, 2193–2203.

Too, L.K., Ball, H.J., McGregor, I.S., Hunt, N.H., 2014. The pro-inflammatory cytokine interferon-gamma is an important driver of neuropathology and behavioural sequelae in experimental pneumococcal meningitis. Brain, behavior, and immunity 40, 252–268.

Vetiska, S.M., Ahmadian, G., Ju, W., Liu, L., Wymann, M.P., Wang, Y.T., 2007. GABAA receptor-associated phosphoinositide 3-kinase is required for insulin-induced recruitment of postsynaptic GABAA receptors. Neuropharmacology 52, 146–155.

Vien, T.N., Moss, S.J., Davies, P.A., 2016. Regulating the Efficacy of Inhibition Through Trafficking of γ-Aminobutyric Acid Type A Receptors. Anesthesia and analgesia 123.

Vithlani, M., Hines, R.M., Zhong, P., Terunuma, M., Hines, D.J., Revilla-Sanchez, R., Jurd, R., Haydon, P., Rios, M., Brandon, N., Yan, Z., Moss, S.J., 2013. The Ability of BDNF to Modify Neurogenesis and Depressive-Like Behaviors Is Dependent upon Phosphorylation of Tyrosine Residues 365/367 in the GABA A -Receptor γ2 Subunit. J. Neurosci. 33, 15567–15577.

Wahl-Schott, C., Biel, M., 2009. HCN channels: Structure, cellular regulation and physiological function. Cell. Mol. Life Sci. 66, 470–494.

Wang, C., Constantinescu, S.N., MacEwan, D.J., Strulovici, B., Dekker, L.V., Parker, P.J., Pfeffer, L.M., 1993. Interferon alpha induces protein kinase C-epsilon (PKC-epsilon) gene expression and a 4.7-kb PKC-epsilon-related transcript. Proceedings of the National Academy of Sciences of the United States of America 90.

Widner, B., Laich, A., Sperner-Unterweger, B., Ledochowski, M., Fuchs, D., 2002. Neopterin production, tryptophan degradation, and mental depression—what is the link? Brain, behavior, and immunity 16.

Xia, Y., Haddad, G.G., 1992. Ontogeny and distribution of GABAA receptors in rat brainstem and rostral brain regions. Neuroscience 49.

Yanase, N., Hayashida, M., Kanetaka-Naka, Y., Hoshika, A., Mizuguchi, J., 2012. PKC-δ mediates interferon-α-induced apoptosis through c-Jun NH_2-terminal kinase activation. BMC cell biology 13.

Zeng, L., Webster, S.V., Newton, P.M., 2012. The biology of protein kinase C. Advances in experimental medicine and biology 740.

7 Statutory Declaration

I, Gabriel Martin Salvator Janach, by personally signing this document in lieu of an oath, hereby affirm that I prepared the submitted dissertation on the topic ‘Impact of Interferon-γ on neocortical inhibition’ / ‘Der Einfluss von Interferon-γ auf die Inhibition im Neocortex’, independently and without the support of third parties, and that I used no other sources and aids than those stated.

All parts which are based on the publications or presentations of other authors, either in letter or in spirit, are specified as such in accordance with the citing guidelines. The sections on methodology (in particular regarding practical work, laboratory regulations, statistical processing) and results (in particular regarding figures, charts and tables) are exclusively my responsibility.

Furthermore, I declare that I have correctly marked all of the data, the analyses, and the conclusions generated from data obtained in collaboration with other persons, and that I have correctly marked my own contribution and the contributions of other persons (cf. declaration of contribution). I have correctly marked all texts or parts of texts that were generated in collaboration with other persons.

My contributions to any publications to this dissertation correspond to those stated in the below declaration. All publications created within the scope of the dissertation comply with the guidelines of the ICMJE (International Committee of Medical Journal Editors; www.icmje.org) on authorship. In addition, I declare that I shall comply with the regulations of Charité – Universitätsmedizin Berlin on ensuring good scientific practice.

I declare that I have not yet submitted this dissertation in identical or similar form to another Faculty.

The significance of this statutory declaration and the consequences of a false statutory declaration under criminal law (Sections 156, 161 of the German Criminal Code) are known to me.

Date Signature

8 Declaration of Contribution

Gabriel Martin Salvator Janach contributed the following to the below listed publications:

Publication 1: Gabriel M. S. Janach, Olivia Reetz, Noah Döhne, Konstantin Stadler, Sabine Grosser, Egor Byvaltcev, Anja U. Bräuer, Ulf Strauss. Interferon-γ acutely augments inhibition of neocortical layer 5 pyramidal neurons. Journal of Neuroinflammation, 2020.

Contribution:

Co-design of the study together with Olivia Reetz and Ulf Strauss. Co-writing of the manuscript with Ulf Strauss. Parts of the Methods and Results sections were based on drafts from Olivia Reetz. Recording of evoked IPSCs (6/6), I_h in adult rats (5/8), spontaneous IPSCs in adult rats (2/8). Analysis of evoked IPSCs in late juvenile as well as I_h and spontaneous IPSCs in adult rats. Final compilation of all figures. Fig. 1 was based on a draft from Anja U. Bräuer, Figs. 2 and 6 were based on drafts from Olivia Reetz, Fig. 3 A/C was based on a draft from Konstantin Stadler and Fig. 5 A-C was based on a draft from Noah Döhne.

Publication 2: Gabriel M. S. Janach, Maximilian Böhm, Noah Döhne, Ha-Rang Kim, Marta Rosário, Ulf Strauss. Interferon-γ enhances neocortical synaptic inhibition by promoting membrane association and phosphorylation of $GABA_A$ receptors in a protein kinase C-dependent manner. Brain, Behavior, and Immunity, 2022.

Contribution:

Co-conceptualization of the study and co-writing of the manuscript with Ulf Strauss, except for Methods and Results of molecular biological experiments (biotinylation and isolation of cell surface proteins, immunoprecipitation of endogenous $GABA_AR$ γ_2 subunits and analysis of PKC-specific phosphorylation, SDS-PAGE and Western blotting). Recording of IPSCs evoked by pressure applied GABA (8/8), paired pulse stimulation experiments (5/6), miniature IPSCs for peak-scaled nonstationary noise analysis (4/6), cell attached experiments (longitudinal approach: 3/4; preincubation approach: 45/45), Wortmannin (5/8) and Calphostin C (7/7) blocker experiments as well as miniature IPSCs in female rats (5/8). Analysis of IPSCs evoked by pressure applied GABA, paired pulse stimulation experiments, miniature IPSCs for peak-scaled nonstationary noise analysis, cell attached experiments, Wortmannin and Calphostin C experiments as well as miniature IPSCs in female rats. Statistical analysis for all figures. Final compilation of all figures. Figs. 2 A/B and 4 E/F were based on drafts from Marta Rosário and Fig. 5 A/B was based on a draft from Ulf Strauss and Maximilian Böhm.

_____

Signature, date and stamp of first supervising university professor / lecturer

_____

Signature of doctoral candidate

9 Printing Copy of Publication 1

Janach *et al. Journal of Neuroinflammation* (2020) 17:69
https://doi.org/10.1186/s12974-020-1722-y

Journal of Neuroinflammation

RESEARCH Open Access

Interferon-γ acutely augments inhibition of neocortical layer 5 pyramidal neurons

Gabriel M. S. Janach[1], Olivia Reetz[1], Noah Döhne[1], Konstantin Stadler[2], Sabine Grosser[3], Egor Byvaltcev[1], Anja U. Bräuer[1,4,5] and Ulf Strauss[1*]

Abstract

Background: Interferon-γ (IFN-γ, a type II IFN) is present in the central nervous system (CNS) under various conditions. Evidence is emerging that, in addition to its immunological role, IFN-γ modulates neuronal morphology, function, and development in several brain regions. Previously, we have shown that raising levels of IFN-β (a type I IFN) lead to increased neuronal excitability of neocortical layer 5 pyramidal neurons. Because of shared non-canonical signaling pathways of both cytokines, we hypothesized a similar neocortical role of acutely applied IFN-γ.

Methods: We used semi-quantitative RT-PCR, immunoblotting, and immunohistochemistry to analyze neuronal expression of IFN-γ receptors and performed whole-cell patch-clamp recordings in layer 5 pyramidal neurons to investigate sub- and suprathreshold excitability, properties of hyperpolarization-activated cyclic nucleotide-gated current (I_h), and inhibitory neurotransmission under the influence of acutely applied IFN-γ.

Results: We show that IFN-γ receptors are present in the membrane of rat's neocortical layer 5 pyramidal neurons. As expected from this and the putative overlap in IFN type I and II alternative signaling pathways, IFN-γ diminished I_h, mirroring the effect of type I IFNs, suggesting a likewise activation of protein kinase C (PKC). In contrast, IFN-γ did neither alter subthreshold nor suprathreshold neuronal excitability, pointing to augmented inhibitory transmission by IFN-γ. Indeed, IFN-γ increased electrically evoked inhibitory postsynaptic currents (IPSCs) on neocortical layer 5 pyramidal neurons. Furthermore, amplitudes of spontaneous IPSCs and miniature IPSCs were elevated by IFN-γ, whereas their frequency remained unchanged.

Conclusions: The expression of IFN-γ receptors on layer 5 neocortical pyramidal neurons together with the acute augmentation of inhibition in the neocortex by direct application of IFN-γ highlights an additional interaction between the CNS and immune system. Our results strengthen our understanding of the role of IFN-γ in neocortical neurotransmission and emphasize its impact beyond its immunological properties, particularly in the pathogenesis of neuropsychiatric disorders.

Keywords: IFN, Neocortical neurons, Interferon receptor, HCN, Neuromodulation

Background

Interferons (IFN) are antiviral cytokines known for their multifaceted influence on the immune response. Based on their amino acid sequence, three types of IFNs are distinguished: IFN I to III. All of them possess specific receptors and signaling cascades [1].

IFN-γ is the only member of type II IFNs. It plays an important role in innate and adaptive immune response and induces antitumor mechanisms [2]. In addition to peripheral immune cells, central nervous system (CNS) cells such as microglia, astrocytes, dorsal root ganglion neurons, and cerebrovascular endothelial cells produce IFN-γ [3] under different conditions. Consecutively, IFN-γ concentration in the brain is elevated in certain pathologies, including multiple sclerosis [4], cerebral ischemia [5], and neurotrauma [6]. The concentration of IFNs in the brain is also elevated in cerebral and systemic viral infection [7, 8].

IFNs influence the CNS function in multiple ways [3, 9]. IFN-γ is involved in dendritic remodeling [10] and synaptic

* Correspondence: ulf.strauss@charite.de
[1]Charité – Universitätsmedizin Berlin, corporate member of Freie Universität Berlin, Humboldt-Universität zu Berlin, and Berlin Institute of Health, Institute of Cell Biology & Neurobiology, Charitéplatz 1, 10117 Berlin, Germany
Full list of author information is available at the end of the article

stripping by microglia [11] as well as influences the proliferation of neuronal precursor cells [12]. Dysregulation of IFN-γ production might be involved in the pathogenesis of neuropsychiatric disorders, such as depression [13] and schizophrenia [14].

The proinflammatory effects of IFN-γ are canonically mediated by binding to the multimeric IFN-γ receptor (IFN-γR), subsequently activating the Janus kinase/signal transducer and activator of transcription (JAK-STAT) pathway. Ultimately, STAT1 phosphorylation leads to the formation of STAT1-STAT1 homodimers, which regulate over 200 genes via binding of the γ-IFN activation site [15, 16]. Apart from that, IFN-γ activates alternative pathways, involving phosphatidylinositol 3-kinase (PI3-kinase) and various isozymes of protein kinase C (PKC) [17, 18]. These latter alternative pathways are also engaged in type I IFN signaling. Notably, there is evidence for activation of similar PKCs by both type I and type II IFNs in several non-neuronal cells [18, 19]. Previously, we have shown type I IFN-induced modifications of neuronal function of layer 2/3 and layer 5 pyramidal neurons that were PKC mediated. In particular, type I IFNs induced an increase in sub- and suprathreshold excitability [20, 21] due to PKC-mediated concerted action on multiple ion channels, including a decrease in hyperpolarization-activated cyclic nucleotide-gated cation (HCN) channel-mediated hyperpolarization-activated current (I_h) [20, 22]. This neuromodulatory effect of type I IFNs implies a role in the altered neuronal states during inflammation and might cause some of the side effects of IFN therapy. To what extent this can be generalized to type II IFN is currently unknown. So far, information on IFN-γ influence on intrinsic neuronal properties is sparse. Synaptic effects have been reported only for long-term application and are controversial [23–25]. Nevertheless, given the overlapping signaling pathways of type I and II IFNs, we hypothesize comparable neuromodulatory effects of these IFNs. Consequently, we here establish the presence of type II IFN receptor on layer 5 pyramidal neurons in the rat neocortex and analyze the immediate consequences of IFN-γ application on neuronal excitability, ion channel function, and synaptic transmission.

Methods

Animals and slice preparation

Male Wistar rats obtained from Janvier labs (Saint-Berthevin, France) or from the Charité central animal facility FEM (Berlin, Germany) were kept under standard laboratory specific-pathogen-free (SPF) conditions. All procedures were performed in agreement with the European Communities Council Directive of September 22, 2010 (2010/63/EU), and carried out in accordance to state of Berlin rules (registration no. T0212/14). Immunohistochemical experiments as well as RNA extraction were done in postnatal day (P)20 and P60 rats. Acute coronal brain slices for electrophysiological recordings were prepared from P10 to P84 rats mainly according to Stadler et al. [22]. Differing from the procedure used in that publication slices were cut in 2 °C cold carbogenated (95% O_2, 5% CO_2), sucrose artificial cerebrospinal fluid (sACSF) containing (in mM) 85 NaCl, 2.5 KCl, 1 NaH_2PO_4, 7 $MgCl_2$, 26 $NaHCO_3$, 50 sucrose, 10 D(+)-glucose (all from Carl Roth, Karlsruhe, Germany), and 0.5 $CaCl_2$ (Merck, Darmstadt, Germany). Slices were allowed to recover in 33 ± 1 °C warm sACSF for 30 min and subsequently stored at room temperature (RT) in a solution that contained (in mM) 92 NaCl, 2.5 KCl, 1.2 NaH_2PO_4, 30 $NaHCO_3$, 25 D(+)-glucose (Carl Roth), 5 sodium ascorbate, 20 2-[4-(2-hydroxyethyl)piperazin-1-yl]ethanesulfonic acid (HEPES), 3 sodium pyruvate (Sigma-Aldrich, Steinheim, Germany), 2 thiourea (VWR Chemicals, Radnor, PA, USA), 2 $MgSO_4$, and 2 $CaCl_2$ (Merck).

RNA extraction, cDNA synthesis and *ifngr1* amplification

Neocortex was harvested from three male Wistar rats and homogenized in TRIzol (Invitrogen, Carlsbad, CA, USA) reagent. Total RNA was extracted using the TRIzol reagent according to the manufacturer's protocol (Invitrogen). The concentration and purity of the isolated total RNA were determined by spectrophotometric analysis of 5 μg total RNA using the High-Capacity cDNA Archive Kit (Applied Biosystems, Carlsbad, CA, USA) according to the manufacturer's protocol. Control reaction was performed without MultiScribe reverse transcriptase. The quality of the amplified cDNA (with and without MultiScribe reverse transcriptase) was controlled by *β-actin* PCR. For amplification of *ifngr1* cDNA, the primers *ifngr1* 5′ (5′-aag ctt gct ctc tgt ggt aaa aaa tgc-3′) spanning bases 921–941, and *ifngr1* 3′ (5′-ctg cag tta gga cag ttc ctg ggt atc-3′), complementary to bases 1453–1473 with an amplification length from 552 bp of the *ifngr1* cDNA (GenBank accession no. NM_053783), were used. Primers for the amplification of the control gene *β-actin* were as follows: *β-actin* 5′-primer (5′-cac cac agc tga gag gga aat cgt gcg tga-3′) spanning the bases 681–710 and *β-actin* 3′-primer (5′-att tgc ggt gca cga tgg agg ggc cgg act-3′) complementary to bases 1169–1198 with an amplificate length of 520 bp for *β-actin* cDNA (GenBank accession number NM_031144.3). Due to intron inclusion, the same primers result in an amplificate length of 730 bp when genomic DNA serves as template, thus this primer combination detects possible contamination with genomic sequences.

PCR was performed in 25-μl final volume containing 1-mM deoxynucleotide triphosphates (dNTPs) (Bioline, London, UK), 2.5 units GoTaq Polymerase (Promega, Fitchburg, WI, USA), 2.5 μl 10× buffer including 2.5 M

$MgCl_2$ (Promega), 10 μM of each primer, and 1 μl of each cDNA for all molecules analyzed using a thermal cycler (Duo Cycler Software version 2.3.0.0, VWR, Radnor, PA, USA). For *ifngr1* and *β-actin*, the cycle program was 2 min 95 °C, 30 × [95 °C, 30 s; 63 °C, 30 s; 72 °C, 60 s], and 5 min 72 °C. The *ifngr1* fragment was cloned into the TA-TOPO vector (Invitrogen) and sequence of *ifngr1* cDNA confirmed.

Immunoblotting

For Western blot analysis from cytosol and membrane protein, the extract of the neocortex from individual P20 or P60 rats was subjected to 10% sodium dodecyl sulfate polyacrylamide gel electrophoresis (SDS-PAGE) under reducing conditions and then blotted to a nitrocellulose membrane (Whatman, Dassel, Germany) by semi-dry protein transfer. Blots were blocked for 1 h at RT in 5% skimmed milk (Sigma-Aldrich)/0.1% Tween/1× PBS and then incubated overnight at 4 °C with a 1:1000 dilution of rabbit-anti-IFN-γ-Rα (C-20), sc-700 (Santa Cruz Biotechnology Inc., Dallas, TX, USA), and 1:10.000 dilution of mouse-anti-β-actin, AC-74 (Sigma-Aldrich). After three washes in 1× PBST, the membranes were incubated with a 1:5000 dilution of an anti-mouse Alexa Fluor 488 or 1:10.000 anti-rabbit horseradish peroxidase-labeled antibody (GE Healthcare, Chicago, IL, USA) for 1.5 h at RT. Immunoreactive bands were detected using ECL Western blotting detection reagents (GE Healthcare). As internal loading control β-actin expression was used throughout, chemiluminescence and fluorescence images were taken using the BioRad ChemiDoc MP System (Bio-Rad Laboratories, Hercules, CA, USA).

Immunohistochemistry

Male Wistar rats were deeply anesthetized with 1.2 to 1.5 ml of a cocktail of 25 mg/ml ketamine, 1.2 mg/ml xylazine, and 0.25 mg/ml acepromazine and transcardially perfused with saline (0.9% NaCl), followed by 4% paraformaldehyde (PFA) in 0.1 M phosphate buffer (PB) (2% di-sodium hydrogen phosphate heptahydrate and 0.2% sodium di-hydrogen phosphate monohydrat (both from Carl Roth)). The brain was removed and post-fixed in the PFA/PB fixative solution overnight at 4 °C. Next, coronal sections (50 μm) of the forebrain were cut with a vibratome (Microm HM 650 V, Thermo Fisher Scientific, Waltham, MA, USA), washed in 0.1 M PB, and blocked with 0.1 M PB including 1% BSA (Serva Electrophoresis GmbH, Heidelberg, Germany) and 0.1% TritonX-100 (Sigma-Aldrich) overnight at 4 °C. Sections were subsequently incubated with anti-IFN-γ-Rα (C-20): sc-700 (1: 500) (Santa Cruz Biotechnology Inc.) and anti-MAP2 (1: 250) (Sigma-Aldrich) in blocking solution (0.1 M PB including 1% BSA) overnight at 4 °C. After several washes in 0.1 M PB, the sections were incubated with the second antibodies: Alexa 488-labeled goat anti-rabbit or Alexa 568-labeled goat anti-mouse (both 1:500) (Molecular Probes Inc., Eugene, OR, USA) in blocking solution for 2 h at RT. Sections were washed in 0.1 M PB before mounting. Confocal micrographs of fluorescent specimens were taken using an upright Leica TCS SL SP2 confocal microscope (Leica Microsystems, Wetzlar, Germany). Scanning was performed using an HCX PL APO CS 63x/NA1.4 oil objective at a resolution of 512 × 512 pixels in z-stack steps of 0.1 μm. Different wavelengths of fluorescence channels were imaged separately to rule out spill over. Images are presented as single scans and projections of stacks (27–52 sections). Images were processed in brightness and contrast using Fiji (https://fiji.sc/; RRID: SCR_002285, [26]).

Interferon

For all experiments, we used Chinese hamster ovary (CHO) derived recombinant IFN-γ (U-Cytech, Utrecht, Netherlands) in a final concentration of 1000 IU ml^{-1}. The lyophilized product was reconstituted in sterile double-distilled water, and small aliquots were stored at − 20 °C.

Patch clamp recordings

Individual slices were transferred to a submerged recording chamber containing carbogenated (95% O_2, 5% CO_2), artificial cerebrospinal fluid (ACSF) composed of (in mM) 119 NaCl, 2.5 KCl, 1 NaH_2PO_4, 1.3 $MgCl_2$, 26 $NaHCO_3$, 10 D(+)-glucose (Carl Roth), and 2.5 $CaCl_2$ (Merck).

Somatic whole-cell recordings were performed in visually identified layer 5 pyramidal neurons (mean capacitance 220.8 ± 19.7 pF, $n = 58$). The pipette solution for voltage clamp I_h recordings contained (in mM) 120 $KMeSO_4$ (ICN Biomedicals, Eschwege, Germany), 20 KCl, 4 NaCl, 14 Na-phosphocreatine (Carl Roth), 0.5 ethylene glycol-bis(2-aminoethylether)-*N*,*N*,*N*′,*N*′-tetraacetic acid (EGTA), 10 HEPES, 4 Mg^{2+}-ATP, and 0.3 GTP with 0.1 cAMP (Sigma-Aldrich) (pH 7.25, 288 mOsm). I_h was pharmacologically isolated [27] by modifying the ACSF (in mM, 10 KCl and NaH_2PO_4 omitted) and blocking confounding currents by 400 μm Ba^{2+}, 1 mM Ni^{2+} (Merck), 1 μm tetrodotoxin (TTX), 10 μm 6-cyano-7-nitroquinoxaline-2,3-dione (CNQX), 25 μm D-(-)-2-amino-5-phosphonopentanoic acid (DAP-5), 10 μm bicuculline (Tocris, Bristol, UK), 5 mM 4-aminopyridine (4-AP), and 10 mM tetraethylammonium (TEA) (Sigma-Aldrich).

All inhibitory currents were recorded in the presence of 20 μM CNQX and 25 μM DAP-5 (both from Tocris) to block ionotropic glutamate receptors. Evoked inhibitory postsynaptic currents (eIPSCs) were elicited at a somatic holding potential of − 70 mV by square pulses (100 μs, 5–40 μA) every 30 s via a glass electrode filled

with ACSF positioned approx. 100 µm laterally and 150 µm apically from the soma, using a stimulus isolator (ISO-Flex, Science Products, Hofheim, Germany). IFN-γ was applied when eIPSC amplitudes remained comparable for at least 10 min. Pipette solution for eIPSC and sIPSC recordings contained (in mM) 140 CsCl (Sigma-Aldrich), 4 NaCl, 1 $MgCl_2$ (Carl Roth), 10 HEPES, 0.1 EGTA, 0.3 GTP, 2 Mg^{2+}-ATP, and 5 QX-314 (Sigma-Aldrich) [pH 7.2, 292 mOsm]. Spontaneous IPSCs (sIPSCs) and miniature IPSCs (mIPSCs) were recorded at a holding potential of − 60 mV. For mIPSC recordings, 1 µM TTX was additionally present in the ACSF and the pipette solution contained (in mM) 130 KCl, 10 Na-phosphocreatine, 1 $MgCl_2$ (Carl Roth), 1 $CaCl_2$ (Merck), 11 EGTA, 10 HEPES, 2 Mg^{2+}-ATP, and 0.3 GTP (Sigma-Aldrich) [pH 7.2, 290 mOsm]. IPSCs were gathered from 1 to 3 min before and after application of IFN-γ as negative deflections > 5 × RMS noise.

Electrophysiological characterization of neurons was hampered in experiments on inhibition due to the specific intracellular solutions. Therefore, biocytin (0.1%, Invitrogen) filling and post hoc staining was applied to a subset ($n = 15$) to monitor accuracy of visual selection. For morphological identification, slices were fixed in 0.4% paraformaldehyde in 0.1% PB at 4 °C for 1 h. Prior to visualization of recorded neurons, slices were washed in PB and saline-buffered PB (PBS, 0.9% NaCl) subsequently blocked in PBS containing 10% normal goat serum, 0.3% TritonX-100, and 0.05% NaN_3 for at least 1 h. Slices were then incubated with fluorescent-conjugated streptavidin (Alexa Fluor-647, 1:1000, Invitrogen), in a PBS solution containing 3% normal goat serum, 0.1% TritonX-100, and 0.05% NaN3 for 24 h at 4 °C. Before slices were mounted for imaging, they have been washed in PBS and desalted in PB. Recorded neurons were imaged and identified using a laser scanning confocal microscope (FV1000, Olympus, Japan) and sample reconstruction was done using Fiji software package [26] and neuTube [28].

For current clamp measurements, pipette solution contained (in mM) 120 potassium gluconate, 10 KCl, 10 Na-phosphocreatine, 1 $MgCl_2$ (Carl Roth), 1 $CaCl_2$ (Merck), 11 EGTA, 10 HEPES, 2 Mg^{2+}-ATP, and 0.3 GTP (Sigma-Aldrich) (pH 7.2, 290 mOsm). Pipettes had a tip resistance between 2 and 5 MΩ.

Data were recorded with an EPC-10 USB double amplifier (HEKA, Lambrecht, Germany), digitized (minimum of 10 kHz, after Bessel filtering at 2.5 kHz), and stored using the PatchMaster software (HEKA).

A maximal series resistance of 20 MΩ with changes < 25% during recordings was tolerated. A fast (pipette) capacitive transient ($\tau < 1.5$ µs, 6–13 pF) was compensated. Input resistance was calculated with a linear fit of the current clamp generated I-V plot in close vicinity of the resting potential (± 50 pA). Intersection of the linear regression of the F-I relationship (estimated in the linear range) and abscissa roughly approximated the rheobase.

Statistical analysis

Data was tested for normal distribution using the Shapiro-Wilk test. In case of normal distribution, paired Student's t tests were used to test for significant differences. In case of significant deviation from normal distribution ($P > 0.05$), the non-parametric Wilcoxon signed-rank test was used. Kinetic analysis of the 10% biggest amplitudes of the mIPSCs was fitted by a single exponential equation ($y = y0 + A1(e - x/\tau1)$), and the cumulative frequency of mIPSCs and sIPSCs was analyzed using a two-sample Kolmogorov-Smirnov test. Data are presented as mean ± standard error of the mean (SEM). Results with $P < 0.05$ were regarded as statistically significant. Statistics were performed with Origin2019 (OriginLab, Northhampton, MA, USA) or Statview v.457 (Abacus Concepts Inc., CA, USA).

Results

IFN-γ receptor (IFN-γR) is expressed in neocortical layer 5 pyramidal neurons

IFN-γR expression has been confirmed for several brain regions [24, 29]. Information on the cellular localization of the receptor, however, is currently missing for many neuron types. Here we provide evidence for the expression of IFN-γR on neocortical layer 5 neurons. Using semi-quantitative RT-PCR analysis, we first assessed the transcriptional level and demonstrated that mRNA of the receptor is expressed in late juvenile and adult cortical tissue (Fig. 1a, b, left). Subsequent Western blot studies detected posttranslational expression of the ligand binding receptor α chain (IFN-γRα, also known as IFNGR1 or CD119) only in the membrane fractions derived from neocortical tissue (Fig. 1a, b, right). This suggests that interferon receptors are present on membranes of neocortical cells as astrocytes, microglia, neurons, or cerebrovascular endothelial cells. To visualize the local expression of the receptor, we used immunohistochemical staining with anti-IFN-γRα and anti-MAP2 in neocortical layer 5 of brain slices. IFN-γRα was clearly detectable in neuronal somata and weakly in dendrites, as shown by co-localization with the neuronal marker MAP2 (Fig. 1c, d). The presence of IFN-γRs in the cell membrane suggested the existence of the entire heteromeric IFN-γR at the surface of, and therefore, an influence of IFN-γ on neocortical layer 5 pyramidal neurons.

IFN-γ application leaves neuronal excitability of layer 5 pyramidal neurons unchanged

Crosstalk for type I and type II IFNs has not only been shown for the canonical pathways [31], but also for the activation of PKC [15, 19]. We have shown previously

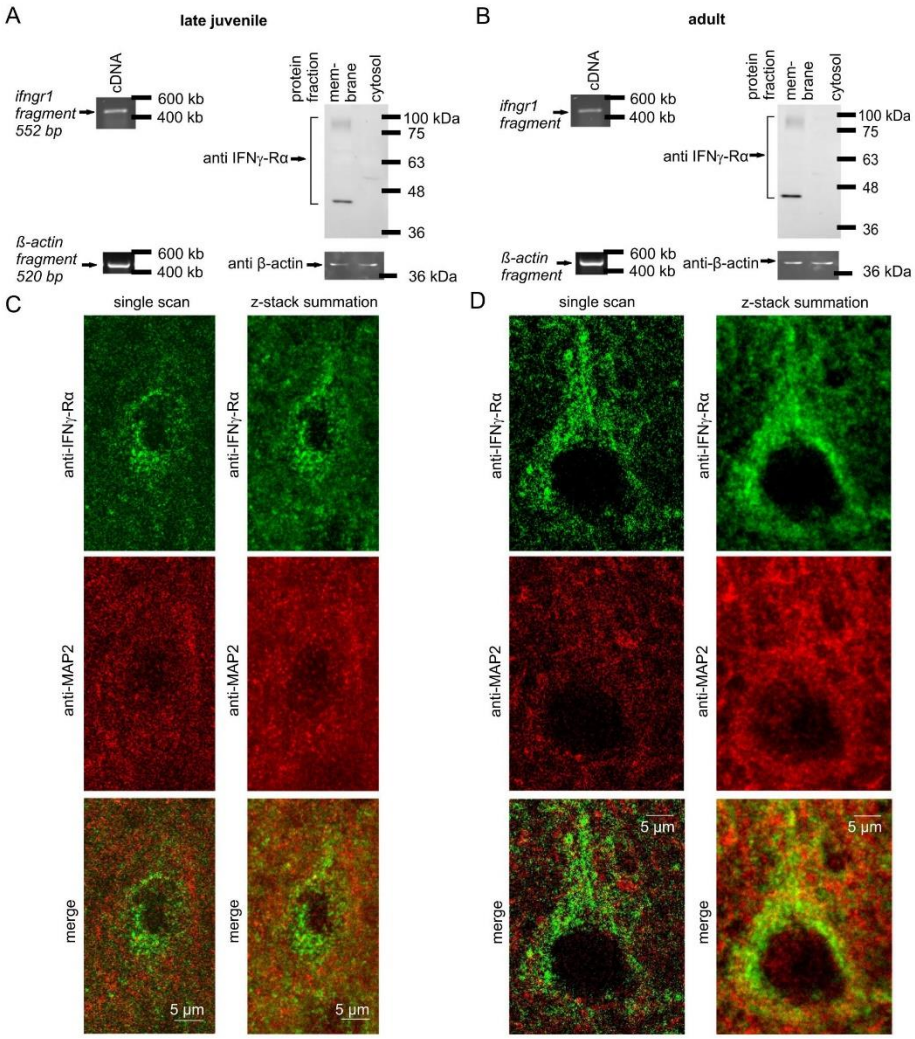

Fig. 1 Endogenous IFNγRα is expressed in neocortical layer 5 neurons of late juvenile and adult rats. **a**, **b** Semi-quantitative RT-PCR analysis and Western blots were performed on neocortical tissue of P20 (**a**, late juvenile) and P60 rats (**b**, adult). Note that PCR analysis and Western blot were done on the same animal, i.e., neocortical tissue of one hemisphere was used for PCR, while the correspondent neocortex was used for Western blotting. The results shown are representative for three independent experiments, respectively. Left panels, semi-quantitative RT-PCR analysis of *ifngr1* mRNA, showing transcriptional gene expression of IFN-γR in the neocortex. The size of the expected fragments corresponds to the expected size (552 base pairs for *ifngr1* fragment). Loading control, *β-actin* cDNA fragments (520 base pairs). Right panels, Western blot of neocortical tissue from the same animal. Detected protein bands range from 45 to 100 kDa (96 kDa predicted by the primary structure of IFNGR1). Similar protein species were previously found to specifically bind IFN-γ [30]. Therefore, we regard the bands to be either full-length or fragmented IFN-γRα that might be post-translationally modified. Alexa 488-labeled β-actin was used as loading control. For estimation of the molecular weight, the commercial weight markers Hyperladder I (for PCR; Bioline) and BlueStar Prestained Protein Marker (for Western blot; Nippon Genetics, Tokyo, Japan) were used. **c**, **d** Examples of immunohistochemical co-staining of neocortical tissue in layer 5 with anti-IFNγ-Rα (1:500) and anti-MAP2 (neuronal marker) (1:250) in P20 (**c**) and P60 (**d**) rats. Left, single scans for accurate z-localization of Alexa 488-labeled IFNγ receptors α and Alexa 568-labeled MAP2. Right, summations of z-stacks consist of 26 (**c**) or 52 single sections (**d**)

that type I IFNs boost suprathreshold excitability via activation of PKC [21]. To elucidate whether IFN-γ similarly triggers a change in excitability, we investigated the firing behavior of layer 5 pyramidal neurons before and 20 min after direct application of IFN-γ. In contrast to type I IFNs that augment the suprathreshold excitability of about 65% of layer 2/3 and layer 5 pyramidal neurons [20], IFN-γ did not change the suprathreshold excitability in layer 5 pyramidal neurons as reflected in similar F-I slope (ctrl 114 ± 11 Hz/nA vs. IFN-γ 96 ± 14 Hz/nA; $n = 9$; $P = 0.23$, paired t test) and rheobase, i.e., the minimal current amplitude for action potential induction (ctrl 194 ± 27.7 pA vs. IFN-γ 225 ± 32 pA; $n = 9$, $P = 0.40$, paired t test) (Fig. 2a, c). The resting membrane potential ($V_{m\text{-ctrl}} = -68 \pm 0.1$ mV vs. $V_{m\text{-IFN-}\gamma} = -67 \pm 0.2$ mV; $n = 9$, $P = 0.16$, Wilcoxon signed-rank test) remained constant during the experiments. Furthermore, the input resistance (R_{in}) as a measure of subthreshold excitability also remained unchanged upon IFN-γ application ($R_{in\text{-ctrl}}$ 55.7 ± 0.8 MΩ vs. $R_{in\text{-IFN-}\gamma}$ 59.7 ± 0.9 MΩ; $n = 9$, $P = 0.46$, paired t test; Fig. 2b). This precludes the possibility that we might have recorded mainly from neurons that were marginally or not affected in their suprathreshold response. In summary, the lack of effect of IFN-γ on sub- and suprathreshold excitability indicates either a failed crosstalk or additional interfering mechanisms.

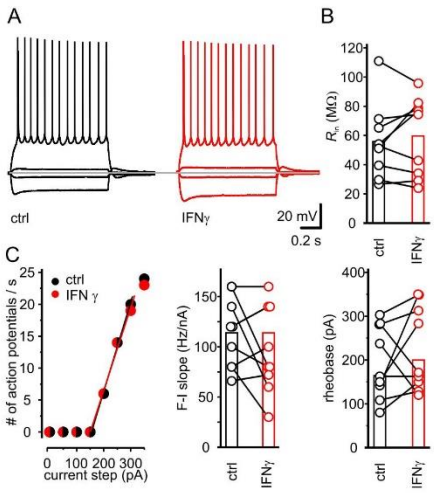

Fig. 2 IFN-γ does not acutely alter excitability of neocortical layer 5 neurons. Direct application of 1000 IU ml^{-1} IFN-γ for 20 min did neither change suprathreshold nor subthreshold excitability. **a** Example traces of a layer 5 pyramidal neuron before (black) and upon IFN-γ application (red) showing comparable firing and subthreshold behavior. Traces resemble voltage responses to rectangular current injections of − 300, − 50, 50, and 250 pA, respectively. The dotted gray line indicates a potential of − 72 mV. **b** Input resistance, as a measure of subthreshold excitability, remained unchanged upon the application of IFN-γ. **c** Action potential frequency of an example neuron plotted as a function of the input current (left). Population data reveal that neither F-I slope (middle) nor rheobase (right) was affected by IFN-γ. As two neurons showed overlapping F-I slopes, the corresponding dots in the line series are slightly dispersed from each other. Lines represent the fit through the linear part of the curve. R_s remained constant ($R_{s\text{-ctrl}} = 7.6 \pm 0.6$ MΩ vs. $R_{s\text{-IFN-}\gamma} = 7.3 \pm 0.5$ MΩ, $n = 9$; $P = 0.23$, paired t test) throughout the experiments. The average age of animals used for these current clamp experiments was P30 ± 2.8. In this and all following figures, columns indicate mean and open circles in line series resemble individual values before (black) and after (red) application of IFN-γ; $^*P < 0.05$, $^{**}P < 0.01$, $^{***}P < 0.001$

IFN-γ reduces I_h amplitude and slows its kinetics

Given the well-established PKC activation by IFN-γ [17, 18], the lack of a neuromodulatory effect might be due to a failed PKC-mediated channel modulation upon IFN-γ. As we have robust information on the effects of type I IFNs on I_h [22] mediated by the PKC pathway [21], we next analyzed the influence of IFN-γ on I_h.

Acute application of IFN-γ (1000 IU ml^{-1}) led to a reduction of I_h amplitude by about 25% from $I_{h\text{-ctrl}}$ = 881.4 ± 136.8 pA to $I_{h\text{-IFN-}\gamma} = 640.7 \pm 110.2$ pA ($n = 16$; $P < 0.001$, Wilcoxon signed-rank test). This attenuation occurred in all investigated neurons within 10 min of application (Fig. 3a, b). The reduction of I_h amplitude was associated with a depolarization of the midpoint of activation $V_{1/2}$ (Fig. 3c; $V_{1/2\text{-ctrl}} = -89.0 \pm 1.0$ mV to $V_{1/2\text{-IFN-}\gamma} = -86.2 \pm 1.2$ mV; $n = 16$, $P < 0.05$, paired t test). This shift in $V_{1/2}$ cannot account for the reduction of the peak amplitude and argues against a classical rundown. In addition, we estimated I_h amplitudes at full activation under both conditions.

In our previous study, we observed a distinct effect of type I IFNs on I_h kinetics [22]. The same effect appeared upon application of IFN-γ: the current onset was faster, i.e., the fast time constant τ_{fast} increased from $\tau_{fast\text{-ctrl}}$ = 60.9 ± 8.3 ms to $\tau_{fast\text{-IFN-}\gamma} = 82.8 \pm 13.9$ ms ($n = 16$; $P < 0.01$, Wilcoxon signed-rank test, Fig. 3d), whereas the slow time constant τ_{slow} remained unchanged ($\tau_{slow\text{-ctrl}}$ = 560.4 ± 122.7 ms vs. $\tau_{slow\text{-IFN-}\gamma} = 1096.0 \pm 403.8$ ms; n = 16, $P = 0.27$, Wilcoxon signed-rank test). Besides the activation kinetics, also the deactivation slowed down ($\tau_{ctrl} = 194.8$ ms ± 28.7 ms to $\tau_{IFN\text{-}\gamma} = 246.0$ ms ± 25.7 ms; $n = 16$, $P < 0.01$, Wilcoxon signed-rank test, Fig. 3d). The modulation of I_h by IFN-γ corresponds qualitatively and quantitatively to previously observed effects of type I IFNs on I_h [22] that were due to activation of PKC [21]. These data establish a link between IFN-γ, PKC activation, and attenuated I_h, rendering a concerted action of IFN-γ on several ionic channels likely.

Inhibitory synaptic transmission is increased in amplitude by elevated IFN-γ levels

These conflicting results—the lack of change in neuronal excitability on one, the overlap between IFN-γ and type I IFNs regarding channel modulation on the other hand—prompted us to consider other putative IFN-γ targets. Taking the role of neuronal inhibition to restrict neocortical excitability [32–34] into account, we hypothesized that IFN-γ augments GABAergic inhibition.

To investigate a possible impact of IFN-γ on GABAergic transmission, we evoked IPSCs (eIPSCs), before and 20 to 40 min after application of IFN-γ using electrical stimulation. IFN-γ increased the maximum amplitude of eIPSCs in the presence of glutamate receptor blockers by 48% (ctrl 605 ± 160 pA to IFN-γ 889 ± 263 pA; $n = 6$, $P < 0.05$, Wilcoxon signed-rank test; Fig. 4b, c). The area under the curve (AUC) that represents the total membrane charge transfer showed a trend towards increase (ctrl 3.33 ± 1.89 nA vs. IFN-γ 4.40 ± 2.48 nA; $n = 6$, $P = 0.21$, Wilcoxon signed-rank test), maybe due to bulk-induced increased uptake.

To address GABAergic transmission on the level of single synapses, we measured spontaneous IPSCs (sIPSCs) 20 to 30 min after application of IFN-γ. The amplitude of sIPSCs increased by 14.6% (from ctrl 62.4 ± 8.7 pA to IFN-γ 69.5 ± 8.8 pA; $n = 9$, $P < 0.05$, paired t test) while the frequency of sIPSCs remained unchanged (ctrl 13.7 ± 3.0 events s^{-1} vs. IFN-γ 15.7 ± 4.0 events s^{-1}; $n = 9$, $P = 0.42$, paired t test, Fig. 5a–c). Comparison of the largest (≥ 60 pA) sIPSCs that are putatively action potential driven showed comparable amplitudes (ctrl 99.0 ± 7.8 pA vs. IFN-γ 100.9 ± 6.8 pA; $n = 9$, $P = 0.16$, paired t test) or frequencies (ctrl 4.0 ± 1.1 events s^{-1} vs. IFN-γ 5.8 ± 1.3 events s^{-1}; $n = 9$, $P = 0.2$, paired t test).

Most electrophysiological recordings so far were carried out on late juvenile rats, on average aged around P20. Because we cannot exclude that developmental changes may interfere with effects of IFN-γ, we firstly used linear regression analysis on age and effect size for all electrophysiological experiments but found no correlation (probability; Pearson correlation coefficient): input resistance (p 0.69; r 0.15), rheobase (0.64; − 0.18), F-I slope (0.99; − 0.002), hyperpolarization-induced current amplitude (0.11; − 0.41), evoked IPSC amplitude (0.39; 0.44), spontaneous IPSC amplitude (0.92; 0.03), and miniature IPSC amplitude (0.22; 0.43). Secondly, because the inhibitory circuitry develops rather slow, rendering GABAergic transmission development susceptible to extrinsic influences [35], we investigated whether the synaptic effect of IFN-γ persists in adult rats. In detail, we recorded sIPSCs at P60 and found—similar to juvenile rats—an amplitude increase of sIPSCs by 15.7% (from ctrl 45.4 ± 4.4 pA to IFN-γ 52.2 ± 5.2 pA; $n = 8$, $P < 0.05$, paired t test) while frequencies remained comparable (ctrl 42.1 ± 9.2 events s^{-1} vs. IFN-γ 48.7 ± 12.6 events s^{-1}; $n = 8$, $P = 0.18$, paired t test, Fig. 5d–f). Here, the amplitude of the largest (≥ 60 pA) sIPSCs increased by 11.8% (from ctrl 88.8 ± 3.3 pA to IFN-γ 99.3 ± 5.3 pA; $n = 8$, $P < 0.05$, paired t test) whereas their frequency remained unchanged (ctrl 12.1 ± 4.3 events s^{-1} vs. IFN-γ 18.4 ± 7.1 events s^{-1}; $n = 8$, $P = 0.07$, paired t test).

Finally, we recorded miniature IPSCs (mIPSCs) in the presence of glutamate receptor blockers and TTX to analyze the effects of IFN-γ on inhibitory transmission, while excluding any action potential driven responses. After 20 min of application, IFN-γ increased the amplitude of mIPSCs by 20% from ctrl 13.8 ± 1.2 pA to IFN-γ 16.5 ± 1.5 pA ($n = 10$; $P < 0.01$, paired t test) without any

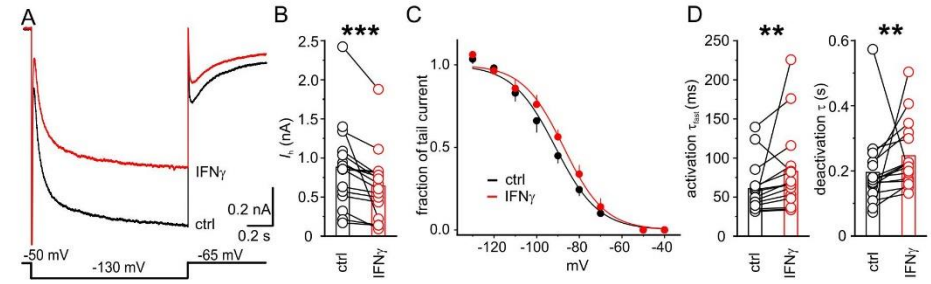

Fig. 3 I_h is inhibited by IFN-γ in neocortical layer 5 neurons. **a** After 10 min, 1000 IU ml^{-1} IFN-γ decreased maximum amplitude of I_h and slowed its activation and deactivation as exemplified by traces of pharmacologically isolated and offline leak subtracted I_h before (black) and upon (red) direct IFN-γ application. I_h was elicited by the voltage step shown at the bottom. **b** IFN-γ reduced the I_h amplitude in all investigated neurons. **c** For the graph steady-state activation, curves were constructed from average relative tail currents (SEM given as bars) upon returning to − 65 mV from I_h activation, plotted against preceding activating voltages before (black) and after the application of IFN-γ (red). Fits of Boltzmann function are superimposed. Note that $V_{1/2}$ after IFN-γ is depolarized and cannot explain the decrease in maximum I_h. **d** Application of IFN-γ decelerated the fast component of activation (quantified by an increase of τ_{fast}, left) and I_h deactivation as indicated by increased deactivation times (right). R_s remained constant ($R_{s\text{-ctrl}}$ 9.7 ± 0.7 MΩ vs. $R_{s\text{-IFN-}\gamma}$ 10.0 ± 0.7 MΩ, $n = 16$; $P = 0.3$, paired t test) throughout the experiments. Average age of animals for this series of experiments P35.6 ± 11.0

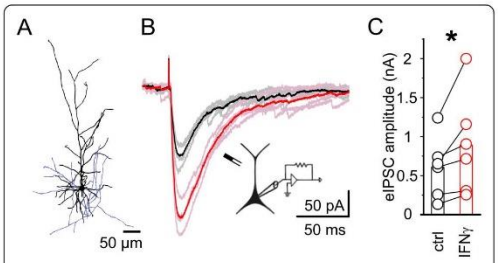

Fig. 4 IFN-γ increases the amplitude of evoked IPSCs in neocortical layer 5 pyramidal neurons. Electrically evoked IPSCs were recorded in the presence of CNQX and DAP5 to block ionotropic glutamate receptors. **a** Exemplary layer 5 pyramidal neuron stained with biocytin and reconstructed to ensure neuronal identity when electrophysiological characterization was impaired by recording conditions. Soma and dendrites are represented in black, the axon in blue. **b** Example traces of IPSCs evoked before (gray) and after 30 min of IFNγ application (1000 IU ml^{-1}; rose). Averaged traces are shown in black (before IFN-γ application) and red (after IFN-γ application). A scheme of the experimental setup, including the apicolaterally positioned bipolar stimulation electrode, is depicted below. **c** Maximum amplitudes of all eIPSCs increased under the influence of IFN-γ. Analysis of eIPSC amplitudes was performed before and 20 to 40 min after the application of IFN-γ. Holding current (507.9 ± 189.0 pA vs. 1285.9 ± 626.0 pA, $n = 6$; $P = 0.22$, Wilcoxon signed-rank test) and R_s ($R_{s\text{-ctrl}} = 9.2 \pm 2.1$ MΩ vs. $R_{s\text{-IFN-γ}} = 9.4 \pm 2.2$ MΩ, $n = 6$; $P = 0.7$, Wilcoxon signed-rank test) remained comparable. Average rat age P23.7 ± 0.8

effect on the frequency (ctrl 8.2 ± 1.0 events s^{-1} vs. IFN-γ 8.7 ± 1.7 events s^{-1}; $n = 10$, $P = 0.85$, Wilcoxon signed-rank test; Fig. 6a–c). Kinetic analysis of the 10% biggest amplitudes indicated no changes of the decay time (Fig. 6d, e).

These results provide evidence for an acute augmentation of GABAergic transmission by IFN-γ.

Discussion

Our main finding is that short-term IFN-γ application provokes complex changes in neuronal function of neocortical layer 5 pyramidal neurons, enabled by the presence of type II IFN receptors on these neurons. In detail, IFN-γ, when acutely released, augments inhibitory currents in neocortical layer 5 pyramidal neurons. Augmented perisomatic inhibition links our seemingly conflicting other findings: on the one hand, the decrease and slowing of I_h mimics the effect we previously found for type I IFNs [22], which indicates a comparable, PKC-mediated mechanism [21]. On the other hand, the therefore expected increase in neuronal sub- and suprathreshold excitability (as seen in the majority of neurons upon type I IFNs [20]) was entirely absent.

Our newly found short-term effects of IFN-γ on GABAergic responses in neocortical pyramidal neurons in acute slice preparations add to the knowledge on

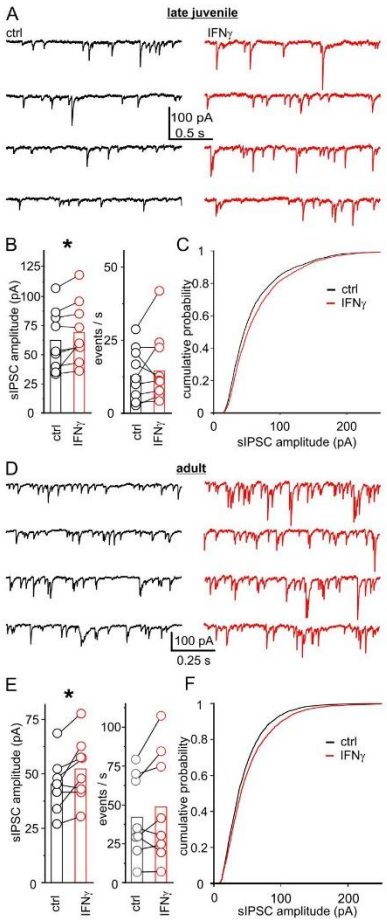

Fig. 5 IFN-γ increases the amplitude of spontaneous IPSCs in neocortical layer 5 pyramidal neurons of late juvenile and adult rats. Spontaneous IPSCs were recorded in the presence of CNQX and DAP5 to block ionotropic glutamate receptors. **a**, **d** Example traces of sIPSCs of late juvenile (**a**) and adult (**d**) rats before (black) and after application of IFN-γ (1000 IU ml^{-1}; 20 min; red). **b**, **e** IFN-γ application (20 to 30 min) increased sIPSC amplitudes of pyramidal neurons of late juvenile (**b**) and adult (**e**) rats (left) but left sIPSC frequency (right) unchanged. **c**, **f** Cumulative sIPSC amplitudes in neurons of late juvenile (**c**) and adult (**f**) rats after application of IFN-γ (red) were shifted to bigger amplitudes when compared with control (black). Holding current (for late juvenile rats 325.7 ± 91.9 pA vs. 412.5 ± 72.5 pA, $n = 9$; $P = 0.13$, Wilcoxon signed-rank test/for adult rats 135.5 ± 28.2 pA vs. 135.0 ± 19.5 pA, $n = 8$; $P = 0.97$, paired t test) and R_s (for late juvenile rats $R_{s\text{-ctrl}} = 9.2 \pm 2.1$ MΩ vs. $R_{s\text{-IFN-γ}} = 9.4 \pm 2.2$ MΩ, $n = 9$; $P = 0.7$, Wilcoxon signed-rank test/for adult rats $R_{s\text{-ctrl}} = 7.1 \pm 1.0$ MΩ vs. $R_{s\text{-IFN-γ}} = 7.0 \pm 0.5$ MΩ, $n = 8$; $P = 0.8$, paired t test) remained comparable. Mean age of animals P19.0 ± 1.0 (late juvenile) and P60.0 ± 0.6 (adult)

long-term IFN-γ effects on inhibition. In line with our findings of an augmented inhibition, layer 1 interneurons respond to meningeal IFN-γ release and increase tonic inhibition in layer 2 projection neurons [36]. Further support of our findings comes from other brain regions such as the hippocampus, where IFN-γ augmented synaptic inhibition as shown in the brain slices of late juvenile rats by an increase in frequency of spontaneous and miniature IPSCs [37] or in culture at peak synaptogenesis by increased spontaneous IPSC frequency and miniature IPSC amplitude [23], both at later time points, i.e., at hours to days after IFN-γ exposure. The latter authors linked their findings to increased neuronal activity, an interaction that recently has been deciphered [38]. Such a mechanism is not likely to account for our findings because we blocked glutamatergic transmission with CNQX for AMPA and DAP-5 for NMDA receptors in our experiments. However, in contrast to these rather supporting findings on IFN-γ-induced augmentation, there is also evidence for an attenuation of inhibition. IFN-γ reduced or even depolarized GABAergic activity in neurons in the dorsal horn of the spinal cord [39] and increased IFN-γ levels diminished inhibition by reducing frequency but not amplitude of spontaneous and miniature inhibitory postsynaptic current (IPSC) [40] in hippocampal CA1 neurons. Adding another layer of complexity, the IFN-γ-induced reduction in GABA release has been shown to increase hippocampal excitability [40, 41], and IFN-γ may induce increase in hippocampal excitatory synaptic activity and AMPA receptor clustering without obvious changes in GABAergic transmission [25]. These inconsistent findings in diverse regions of the central nervous system certainly demand further studies of localized and age-dependent neuronal IFN-γ effects.

Although the similarity of the effects of IFN-γ and type I IFNs on I_h suggests a comparable mechanism of acute action, i.e., PKC mediation, the obvious differences in influencing neuronal excitability together with the diverse effects of mere IFN-γ application in different preparations and brain regions described previously provoke several speculations. The most parsimonious hypotheses are (1) subcellular receptor location: IFN-γ receptors may preferentially interact with inhibitory $GABA_A$ receptors at the soma of pyramidal neurons whereas type I IFN receptors might rather modulate dendritic conductances. A partial overlap may explain the lack of suprathreshold effects in a small subset (14/39) of IFN-β treated pyramidal neurons [20]. (2) Different subcellular PKC subtype or intracellular PKC target distribution [42]. (3) Differential action on resident interneuron subclasses, depending on their ion channel composition. (4) IFNs as cytokines rarely act alone; thus, effects should be considered in conjunction with other cytokines present or even induced in the local environment. For instance, IFN-γ may evoke either TNFα production in glial cells that, in turn, could influence (excitatory) synaptic function [43] or CX3CL1 [44, 45]. Interestingly, the latter mimics the here described IFN-γ effect, i.e., it augmented sIPSC amplitudes but not frequencies when acutely applied [46]. However, this effect was specific for serotonergic neurons, and CX3CL1 induction by IFN-γ was not described to be in the time frame of

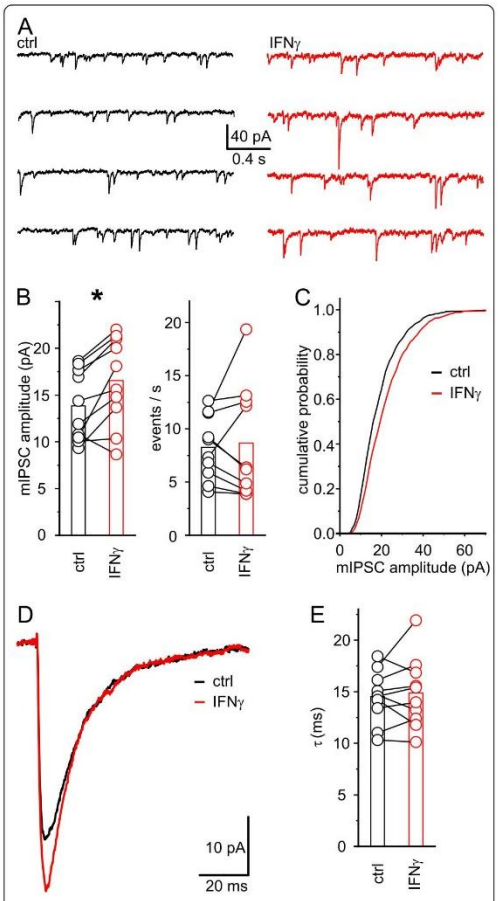

Fig. 6 IFN-γ increases mIPSC amplitudes in neocortical layer 5 neurons. **a** Example traces of mIPSCs recorded in the presence of CNQX, DAP5, and TTX before (black) and upon application of IFN-γ (1000 IU ml^{-1}; 20 min; red). **b** Mean mIPSC amplitudes (left) increased upon application of IFN-γ, while mIPSC frequency (right) remained unaltered. **c** Cumulative relative frequency graph of mIPSC amplitudes for an example neuron shows an increase in amplitudes after application of IFN-γ (red) in comparison to the initial state (black). **d** Example trace of a single mIPSC before (black) and upon application of IFN-γ (red). **e** IFN-γ did not influence mIPSC decay time. R_s remained constant ($R_{s\text{-}ctrl}$ 14.1 ± 0.7 MΩ vs. $R_{s\text{-}IFN\text{-}\gamma}$ 14.5 ± 0.8 MΩ; $n = 10$; $P = 0.55$, paired t test) throughout the experiments. Average rat age P16.1 ± 1.9

the effects we observe, yet. (5) Finally, although our (specifically due to the time course) and several other studies are in favor of a direct neuromodulatory effect of cytokines, we cannot entirely exclude the possibility that a variable (micro-)glial influence affects short- or long-term neuromodulation [47], in particular, because IFN-γ induced CX3CL1 release [44, 45] that might have an impact on GABAergic networks, at least in development [48].

Our experiments suggest that early enhancement of GABAergic inhibition may protect against pro-excitatory events, as previously proposed by [36]. However, further studies are needed here because the significance of the results beyond the level of the brain slice still needs to be clarified. Pro- and anti-excitatory incidents might be simultaneously induced by IFN-γ as HCN1 reduction has been shown to be sufficiently counteracted by GABAergic enhancement [34]. Dampening neuronal activity might even counteract the morphological changes indicative for upcoming degeneration as dendritic beads initiated by Ca^{2+} permeable receptor complexes of IFN-γR and GluR1 [24] or be beneficial before IFN-γ forces neurons to instruct inhibitory synapse loss in viral *déjà vu* disease [11]. Although our experiments in acute brain slices do not provide data on chronic impact, initial augmentation of GABAergic inhibition might lead to a rearrangement that finally results in the chronic outcomes described by others (see above). Whatever the exact mechanisms are, our finding might show the onset of the suggested neuroprotective role. This would be in line with findings that GABAergic activity was enhanced in surviving neurons in primary cortical cultures following rabies or influenza A infection [49, 50].

Recent research points to a role of IFN-γ (and therewith putatively changes in inhibition) in the pathophysiology of other diseases besides viral infections. IFN-γ was reported to be involved in depressive behavior in humans [51], and intraventricular delivery of IFN-γ caused a depressive and anxiety-like behavior in mice due to dysfunction of the cannabinoid receptor CB1Rs that (if functioning) reduces GABA transmission in the striatum [52]. Our findings on an altered synaptic transmission by IFN-γ add a new aspect on the role of pro-inflammatory cytokines in epilepsy. So far, IL-1β, TNFα, and IL-6 are regarded as major pro-epileptic players [42]. In contrast, IFN-γ-induced augmentation of inhibition might rather constrain seizures, although its absence in development seems to diminish seizures later in life [53].

Conclusion

The data improve our understanding of the role of IFN-γ as a neuromodulatory cytokine [3] and reveal potential mechanisms of altered behavior and perception during early states of infectious diseases. Our data once more emphasize that immune and nervous system do act autonomously but mutually affect each other's function. Knowledge on IFN-γ-induced neuromodulation is important because it is of clinical relevance, due to IFN-γ presence in the CNS under pathological conditions and even beyond, since it might influence social behavior [36].

Abbreviations

4-AP: 4-Aminopyridine; ACSF: Artificial cerebrospinal fluid; ATP: Adenosine triphosphate; BSA: Bovine serum albumin; cAMP: Cyclic adenosine monophosphate; cGMP: Cyclic guanosine monophosphate; CHO: Chinese hamster ovary; CNQX: 6-Cyano-7-nitroquinoxaline-2,3-dione; CNS: Central nervous system; DAP-5: D-(-)-2-amino-5-phosphonopentanoic acid; EGTA: Ethylene glycol-bis(2-aminoethylether)-*N,N,N',N'*-tetraacetic acid; HCN: Hyperpolarization activated cyclic nucleotide gated; HEPES: 2-[4-(2-Hydroxyethyl)piperazin-1-yl]ethanesulfonic acid; IFN: Interferon; I_h: Hyperpolarization activated cyclic nucleotide gated nonselective cationic current; IPSC: Inhibitory postsynaptic current (e - evoked, s - spontaneous, m-miniature); JAK: Janus kinase; P: Postnatal day; PB: Phosphate buffer; PBS: Saline-buffered phosphate buffer; PCR: Polymerase chain reaction; PKC: Protein kinase C; RT: Room temperature; SDS-PAGE: Sodium dodecyl sulfate polyacrylamide gel electrophoresis; STAT: Signal transducer and activator of transcription; TEA: Tetraethylammonium; TTX: Tetrodotoxin

Acknowledgements

We thank Julia Koenig, Rike Dannenberg, and Jennifer Sevecke-Rave for excellent technical assistance, Dr. Pierluca Coiro for preparing RT-PCR/immunohistochemistry, and Dr. Petra Bolte (Core Facility Fluorescence Microscopy, Oldenburg) for helping with the image analysis.

Authors' contributions

GMSJ, OR, and US designed the study and wrote the manuscript. GMSJ, OR, ND, KS, EB, and US performed and analyzed the electrophysiological experiments. SG and AUB were responsible for the morphological and molecular biological experiments. All authors revised and approved the final manuscript.

Funding

We acknowledge support from the German Research Foundation (DFG) and the Open Access Publication Funds of Charité – Universitätsmedizin Berlin. The project was supported by the German Research Council DFG (STR865/3-1). OR was temporarily in receipt of a grant from the Sonnenfeld-Stiftung, which also sponsored some technical equipment for US and AUB.

Availability of data and materials

The datasets used and/or analyzed during the current study are available from the corresponding author on reasonable request.

Ethics approval and consent to participate

All procedures were performed in agreement with the European Communities Council Directive of September 22nd 2010 (2010/63/EU) and carried out in accordance with the state of Berlin rules (registration no. T0212/14).

Consent for publication

Not applicable

Competing interests

The authors declare that they have no competing interests.

Author details

[1]Charité – Universitätsmedizin Berlin, corporate member of Freie Universität Berlin, Humboldt-Universität zu Berlin, and Berlin Institute of Health, Institute of Cell Biology & Neurobiology, Charitéplatz 1, 10117 Berlin, Germany. [2]Industrial Ecology Programme, NTNU - Norwegian University of Science and Technology, Trondheim, Norway. [3]Charité – Universitätsmedizin Berlin, corporate member of Freie Universität Berlin, Humboldt-Universität zu Berlin, and Berlin Institute of Health, Institute of Integrative Neuroanatomy, Berlin, Germany. [4]Research Group Anatomy, School of Medicine and Health Sciences, Carl von Ossietzky University Oldenburg, Oldenburg, Germany. [5]Research Center for Neurosensory Science, Carl von Ossietzky University Oldenburg, Oldenburg, Germany.

Received: 26 August 2019 Accepted: 20 January 2020
Published online: 22 February 2020

References

1. Owens T, Khorooshi R, Wlodarczyk A, Asgari N. Interferons in the central nervous system: a few instruments play many tunes. Glia. 2014;62:339–55.
2. Schroder K, Hertzog PJ, Ravasi T, Hume DA. Interferon-gamma: an overview of signals, mechanisms and functions. J Leukoc Biol. 2004; 75:163–89.
3. Monteiro S, Roque S, Marques F, Correia-Neves M, Cerqueira JJ. Brain interference: revisiting the role of IFNγ in the central nervous system. Prog Neurobiol. 2017;156:149–63.
4. Traugott U, Lebon P. Interferon-gamma and Ia antigen are present on astrocytes in active chronic multiple sclerosis lesions. J Neurol Sci. 1988; 84:257–64.
5. Li HL, Kostulas N, Huang YM, Xiao BG, van der Meide P, Kostulas V, et al. IL-17 and IFN-gamma mRNA expression is increased in the brain and systemically after permanent middle cerebral artery occlusion in the rat. J Neuroimmunol. 2001;116:5–14.
6. Lau LT, Yu AC. Astrocytes produce and release interleukin-1, interleukin-6, tumor necrosis factor alpha and interferon-gamma following traumatic and metabolic injury. J Neurotrauma. 2001;18:351–9.
7. Heremans H, Billiau A, De Somer P. Interferon in experimental viral infections in mice: tissue interferon levels resulting from the virus infection and from exogenous interferon therapy. Infect Immun. 1980; 30:513–22.
8. Frei K, Leist TP, Meager A, Gallo P, Leppert D, Zinkernagel RM, et al. Production of B cell stimulatory factor-2 and interferon gamma in the central nervous system during viral meningitis and encephalitis. Evaluation in a murine model infection and in patients. J Exp Med. 1988;168:449–53.
9. Reyes-Vázquez C, Prieto-Gómez B, Dafny N. Interferon modulates central nervous system function. Brain Res. 2012;1442:76–89.
10. Monteiro S, Ferreira FM, Pinto V, Roque S, Morais M, de Sá-Calçada D, et al. Absence of IFNγ promotes hippocampal plasticity and enhances cognitive performance. Transl Psychiatry. 2016;6:e707.
11. Di Liberto G, Pantelyushin S, Kreutzfeldt M, Page N, Musardo S, Coras R, et al. Neurons under T cell attack coordinate phagocyte-mediated synaptic stripping. Cell. 2018;175:458–71 e19.
12. Sun L, Tian Z, Wang J. A direct cross-talk between interferon-gamma and sonic hedgehog signaling that leads to the proliferation of neuronal precursor cells. Brain Behav Immun. 2010;24:220–8.
13. Schmidt FM, Lichtblau N, Minkwitz J, Chittka T, Thormann J, Kirkby KC, et al. Cytokine levels in depressed and non-depressed subjects, and masking effects of obesity. J Psychiatr Res. 2014;55:29–34.
14. Arolt V, Rothermundt M, Wandinger KP, Kirchner H. Decreased in vitro production of interferon-gamma and interleukin-2 in whole blood of patients with schizophrenia during treatment. Mol Psychiatry. 2000;5:150–8.
15. Platanias LC. Mechanisms of type-I- and type-II-interferon-mediated signalling. Nat Rev Immunol. 2005;5:375–86.
16. Boehm U, Klamp T, Groot M, Howard JC. Cellular responses to interferon-gamma. Annu Rev Immunol. 1997;15:749–95.
17. Deb DK, Sassano A, Lekmine F, Majchrzak B, Verma A, Kambhampati S, et al. Activation of protein kinase C delta by IFN-gamma. J Immunol. 2003;171:267–73.
18. Srivastava KK, Batra S, Sassano A, Li Y, Majchrzak B, Kiyokawa H, et al. Engagement of protein kinase C-theta in interferon signaling in T-cells. J Biol Chem. 2004;279:29911–20.
19. Hald A, Andrés RM, Salskov-Iversen ML, Kjellerup RB, Iversen L, Johansen C. STAT1 expression and activation is increased in lesional psoriatic skin. Br J Dermatol. 2013;168:302–10.
20. Hadjilambreva G, Mix E, Rolfs A, Müller J, Strauss U. Neuromodulation by a cytokine: interferon-beta differentially augments neocortical neuronal activity and excitability. J Neurophysiol. 2005;93:843–52.
21. Reetz O, Stadler K, Strauss U. Protein kinase C activation mediates interferon-β-induced neuronal excitability changes in neocortical pyramidal neurons. J Neuroinflammation. 2014;11:185.
22. Stadler K, Bierwirth C, Stoenica L, Battefeld A, Reetz O, Mix E, et al. Elevation in type I interferons inhibits HCN1 and slows cortical neuronal oscillations. Cereb Cortex. 2014;24:199–210 Oxford University Press.
23. Brask J, Kristensson K, Hill RH. Exposure to interferon-gamma during synaptogenesis increases inhibitory activity after a latent period in cultured rat hippocampal neurons. Eur J Neurosci. 2004;19:3193–201.
24. Mizuno T, Zhang G, Takeuchi H, Kawanokuchi J, Wang J, Sonobe Y, et al. Interferon-gamma directly induces neurotoxicity through a neuron specific, calcium-permeable complex of IFN-gamma receptor and AMPA GluR1 receptor. FASEB J. 2008;22:1797–806.
25. Vikman KS, Owe-Larsson B, Brask J, Kristensson KS, Hill RH. Interferon-gamma-induced changes in synaptic activity and AMPA receptor clustering in hippocampal cultures. Brain Res. 2001;896:18–29.
26. Schindelin J, Arganda-Carreras I, Frise E, Kaynig V, Longair M, Pietzsch T, et al. Fiji: an open-source platform for biological-image analysis. Nat Methods. 2012;9:676–82.
27. Strauss U, Kole MH, Bräuer AUA, Pahnke J, Bajorat R, Rolfs A, et al. An impaired neocortical Ih is associated with enhanced excitability and absence epilepsy. Eur J Neurosci. 2004;19:3048–58.
28. Feng L, Zhao T, Kim J. neuTube 1.0: a new design for efficient neuron reconstruction software based on the SWC format. eNeuro. 2015;2. ENEURO. 0049-14.2014.
29. Robertson B, Kong G, Peng Z, Bentivoglio M, Kristensson K. Interferon-gamma-responsive neuronal sites in the normal rat brain: receptor protein distribution and cell activation revealed by Fos induction. Brain Res Bull. 2000;52:61–74.
30. Aguet M, Dembić Z, Merlin G. Molecular cloning and expression of the human interferon-gamma receptor. Cell. 1988;55:273–80.
31. Gough DJ, Messina NL, Hii L, Gould JA, Sabapathy K, Robertson APS, et al. Functional crosstalk between type I and II interferon through the regulated expression of STAT1. PLoS Biol. 2010;8:e1000361.
32. Fellous JM, Rudolph M, Destexhe A, Sejnowski TJ. Synaptic background noise controls the input/output characteristics of single cells in an in vitro model of in vivo activity. Neuroscience. 2003;122:811–29.
33. Chance FS, Abbott LF, Reyes AD. Gain modulation from background synaptic input. Neuron. 2002;35:773–82.
34. Chen X, Shu S, Schwartz LC, Sun C, Kapur J, Bayliss DA. Homeostatic regulation of synaptic excitability: tonic GABA(A) receptor currents replace I(h) in cortical pyramidal neurons of HCN1 knock-out mice. J Neurosci. 2010;30:2611–22.
35. Micheva KD, Beaulieu C. Development and plasticity of the inhibitory neocortical circuitry with an emphasis on the rodent barrel field cortex: a review. Can J Physiol Pharmacol. 1997;75:470–8.
36. Filiano AJ, Xu Y, Tustison NJ, Marsh RL, Baker W, Smirnov I, et al. Unexpected role of interferon-γ in regulating neuronal connectivity and social behaviour. Nature. 2016;535:425–9 Nature Publishing Group.
37. Flood L, Korol SV, Ekselius L, Birnir B, Jin Z. Interferon-γ potentiates GABAA receptor-mediated inhibitory currents in rat hippocampal CA1 pyramidal neurons. J Neuroimmunol. 2019;337:577050.
38. Flores CE, Nikonenko I, Mendez P, Fritschy J-M, Tyagarajan SK, Muller D. Activity-dependent inhibitory synapse remodeling through gephyrin phosphorylation. Proc Natl Acad Sci U S A. 2015;112:E65–72 National Acad Sciences.
39. Vikman KS, Duggan AW, Siddall PJ. Interferon-gamma induced disruption of GABAergic inhibition in the spinal dorsal horn in vivo. Pain. 2007;133:18–28.
40. Zhu PJ, Huang W, Kalikulov D, Yoo JW, Placzek AN, Stoica L, et al. Suppression of PKR promotes network excitability and enhanced cognition by interferon-γ-mediated disinhibition. Cell. 2011;147:1384–96.
41. Müller M, Fontana A, Zbinden G, Gähwiler BH. Effects of interferons and hydrogen peroxide on CA3 pyramidal cells in rat hippocampal slice cultures. Brain Res. 1993;619:157–62.
42. Vezzani A, Viviani B. Neuromodulatory properties of inflammatory cytokines and their impact on neuronal excitability. Neuropharmacology. 2015;96:70–82.
43. Beattie EC, Stellwagen D, Morishita W, Bresnahan JC, Ha BK, von Zastrow M, et al. Control of synaptic strength by glial TNFalpha. Science. 2002;295:2282–5.
44. Imaizumi T, Matsumiya T, Fujimoto K, Okamoto K, Cui X, Ohtaki U, et al. Interferon-gamma stimulates the expression of CX3CL1/fractalkine in cultured human endothelial cells. Tohoku J Exp Med. Tohoku University Medical Press. 2000;192:127–39.
45. Yoshida H, Imaizumi T, Fujimoto K, Matsuo N, Kimura K, Cui X, et al. Synergistic stimulation, by tumor necrosis factor-alpha and interferon-gamma, of fractalkine expression in human astrocytes. Neurosci Lett. 2001;303:132–6.
46. Heinisch S, Kirby LG. Fractalkine/CX3CL1 enhances GABA synaptic activity at serotonin neurons in the rat dorsal raphe nucleus. Neuroscience. 2009;164:1210–23.

47. Ta T-T, Dikmen HO, Schilling S, Chausse B, Lewen A, Hollnagel J-O, et al. Priming of microglia with IFN-γ slows neuronal gamma oscillations in situ. Proc Natl Acad Sci U S A. 2019;116(10):4637–42.
48. Bertot C, Groc L, Avignone E. Role of CX3CR1 signaling on the maturation of GABAergic transmission and neuronal network activity in the neonate hippocampus. Neuroscience. 2019;406:186–201.
49. Ladogana A, Bouzamondo E, Pocchiari M, Tsiang H. Modification of tritiated gamma-amino-n-butyric acid transport in rabies virus-infected primary cortical cultures. J Gen Virol. 1994;75(Pt 3):623–7.
50. Brask J, Owe-Larsson B, Hill RH, Kristensson K. Changes in calcium currents and GABAergic spontaneous activity in cultured rat hippocampal neurons after a neurotropic influenza A virus infection. Brain Res Bull. 2001;55:421–9.
51. Schmidt FM, Schröder T, Kirkby KC, Sander C, Suslow T, Holdt LM, et al. Pro- and anti-inflammatory cytokines, but not CRP, are inversely correlated with severity and symptoms of major depression. Psychiatry Res. 2016;239:85–91.
52. Mandolesi G, Bullitta S, Fresegna D, Gentile A, De Vito F, Dolcetti E, et al. Interferon-γ causes mood abnormalities by altering cannabinoid CB1 receptor function in the mouse striatum. Neurobiol Dis. 2017;108:45–53.
53. Getts DR, Matsumoto I, Müller M, Getts MT, Radford J, Shrestha B, et al. Role of IFN-gamma in an experimental murine model of West Nile virus-induced seizures. J Neurochem. 2007;103:1019–30.

Publisher's Note

10 Printing Copy of Publication 2

Janach, G.M.S., Böhm, M., Döhne, N., Kim, H.-R., Rosário, M., Strauss, U., 2022. Interferon-γ enhances neocortical synaptic inhibition by promoting membrane association and phosphorylation of GABAA receptors in a protein kinase C-dependent manner. Brain, behavior, and immunity 101, 153–164.

https://doi.org/10.1016/j.bbi.2022.01.001

11 Curriculum Vitae

My curriculum vitae does not appear in the electronic version of my dissertation for reasons of data protection.

12 Complete List of Publications

Janach, G.M.S., Olivia Reetz, Noah Döhne, Konstantin Stadler, Sabine Grosser, Egor Byvaltcev, Anja U. Bräuer, Ulf Strauss, 2020. Interferon-γ acutely augments inhibition of neocortical layer 5 pyramidal neurons. J Neuroinflammation 17, 1–12.

Janach, G.M.S., Böhm, M., Döhne, N., Kim, H.-R., Rosário, M., Strauss, U., 2022. Interferon-γ enhances neocortical synaptic inhibition by promoting membrane association and phosphorylation of GABAA receptors in a protein kinase C-dependent manner. Brain, behavior, and immunity 101, 153–164.

Döhne, N., Falck, A., Janach, G.M.S., Byvaltcev, E., Strauss, U., 2022. Interferon-γ augments GABA release in the developing neocortex via nitric oxide synthase/soluble guanylate cyclase and constrains network activity. Front. Cell. Neurosci. 16, 413

13 Acknowledgements

First and foremost, I want to express my gratitude towards Prof. Dr. Ulf Strauß, who crossed my way by fortunate coincidence, for scientific supervision and support on the way towards becoming an independent researcher, for great freedom in the establishment of experimental methods and for teaching me how to solve theoretical and practical problems in the laboratory on my own. I would also like to thank him for long days and nights in- and outside of the lab, his humor and many fruitful conversations, not only about neuroscience and our studies, but also about humanities, politics and the art of shaping one's life.

I would like to thank Janna Lehnhoff for introducing me to the fascinating world of patch-clamp, teaching me how to handle almost every machine in the lab and for her value-free support on the way towards the conscious decision of taking responsibility for my own animals.

I am grateful for meeting Noah Döhne, who not only improved our research with excellent experimental skills and thoughtful remarks, but also has become one my closest friends during these years.

I am very thankful to Olivia Reetz for the transfer of her project and help on the hunt for data thought to be lost. Further, I would like to thank all co-authors for their contributions to our research projects, Julia König, Rike Dannenberg as well as Denis Lajkó for excellent technical assistance, the Promotionskommission for accepting me in the first cohort of the MD/PhD programme and the Berlin Institute of Health for temporary funding.

I want to thank my close ones in this life for love and laughter, the artists of Samariterstraße for inspiration and balance, and Ms. Fedtke and Mr. Zamani for being honorable friends as well as great teachers in the field of applied neurosciences. All of you helped in building and maintaining the level of frustration tolerance, that is inevitable for every electrophysiologist.

Special thanks goes to my mother for being her, for financial backing without which these years of research would not have been possible and for the mental support of my decisions, irrespective of their nature.

Finally, I am grateful to the forest, the stars, and the sea for reminding me of relativity in times of crisis.

„When they said *repent*,
I wonder what they meant.”
Leonard Cohen